DESIGN AND VALIDATION OF A LOW-COST BIOREACTOR SYSTEM FOR THERAPEUTIC MESENCHYMAL STROMAL CELL EXPANSION

By

MORGAN MANTAY

(Under the Direction of Cheryl Gomillion)

ABSTRACT

The use of stem cells for clinical applications has increased as biomedical researchers develop cell-based therapeutic approaches for use in tissue regeneration and/or the treatment of medical conditions such as diabetes or other diseases. Large numbers of stem cells are required as research progresses from the laboratory to clinical trials and on to subsequent industrial scale-up for large-scale manufacturing for distribution. There are a wide range of bioreactors available on the market for anchorage-dependent stem cell expansion, however, to increase accessibility and affordability of cell therapies, it is critical to consider the bioprocesses associated with culturing to support cell expansion and quality. In this work, we aimed to design a low-cost bioreactor system for as mesenchymal stromal cell (MSC) expansion that yields clinically relevant numbers of cells with reduced labor, while maintaining cell potency and immunomodulatory capabilities essential for successful clinical application.

KEYWORDS: Bioreactor Design; Mesenchymal Stromal Cells; Cell Therapy Manufacturing

DESIGN AND VALIDATION OF A LOW-COST BIOREACTOR SYSTEM FOR THERAPEUTIC MESENCHYMAL STROMAL CELL EXPANSION

By

MORGAN MANTAY

B.S. Engineering, University of Georgia, 2017

A Thesis Submitted to the Graduate Faculty of the University of Georgia in Partial Fulfillment of the Requirements for the Degree

MASTER OF SCIENCE

ATHENS, GEORGIA

2019

DESIGN AND VALIDATION OF A LOW-COST BIOREACTOR SYSTEM FOR THERAPEUTIC MESENCHYMAL STROMAL CELL EXPANSION

By

MORGAN MANTAY

Major Professor: Cheryl Gomillion

Committee Members: James Kastner

Yajun Yan

Electronic Version Approved:

Suzanne Barbour

Dean of the Graduate School

The University of Georgia

August 2019

DEDICATION

I would like to dedicate this to all of the people who have continued to support my passions along this journey.

ACKNOWLEDGEMENTS

I would like to acknowledge:

My advisor and my mentor, Dr. Cheryl Gomillion for the last two years under her direction. You have helped me grow tremendously and I could not imagine a better advisor for me. Thank you for all of the patience you have given me; for the countless answers to my countless questions; for the tough love; for the laughter; and for the best two years of following my passion that I could have asked for. Yes, there were times I failed. I failed many times. But that's alright. You helped me see that there will be days you win and then there will be days you learn. Thank you so much for the opportunity to work in your lab.

Dr. Yajun Yan and Dr. Jim Kastner for serving on my committee. I enjoyed both of your guidance during my undergraduate and graduate career at the University of Georgia.

Mr. Terry Walsh and Mr. Bryce Schuebert from the College of Engineering for their help in the preliminary design of the bioreactor. Mr. Carlos Barrow from the Instrument Design & Fabrication Shop for his help in building the bioreactor. Optech for building our custom media reservoirs.

And finally, my lab mates, both present and graduated. You have brought me so much laughter. I am so glad to have you as my friends and for all of the support these last two years.

TABLE OF CONTENTS

Page

LIST OF TABLES

Page

LIST OF FIGURES

Page

CHAPTER 1

INTRODUCTION

Stem cells, or stromal cells, derived first from mouse embryos in 1981, and later from human embryos in 1998, are vital for research focused on human development and regenerative medicine [1]. Embryonic stem cells are derived from the inner cell mass of an embryo, also known as a blastocyst, and from there, those cells have the ability to specialize into adult cell types such as muscle, fat, liver or skin [2]. This ability of specialization into all tissues, totipotency, is limited to embryonic stem cells; however, niche populations of adult stem cells reside in tissues, which can be activated for regeneration due to an injury [1, 3]. Mesenchymal stromal cells (MSCs), named for the mesoderm, are a type of adult stem cell that exist in mesenchymal tissues, connective tissues, such as muscle, bone, cartilage, and fat [4, 5]. MSCs are considered to be multipotent, the ability to differentiate and regenerate specific connective tissues; but it has been reported that these cells have the capability to specialize broadly such as neurons and epithelial cells [4, 6-8].

Stem cells have the great potential to open doors for biomedical research, specifically in the fields of tissue engineering and cell therapy. At present, various aspects of stem cells are investigated through numerous research studies, from manipulation of cells for expansion and differentiation for cell therapies and tissue regeneration, to understanding how cell cycle development or mutation can lead to diseases and medical conditions like cancer and diabetes [9-13]. The success of these research endeavors relies on a single commonality – having a sufficient number of stem cells for research, and ultimately, clinical application. A large number of stem

cells are necessary research studies, which will subsequently lead to clinical trials and afterward, industrial scale-up for large-scale manufacturing for the distribution of therapies. To increase the accessibility and affordability of these cell therapies, it is critical for researchers to simultaneously consider the bioprocesses that have to be included to make this a reality without delay.

The objective of this work was to design, fabricate and evaluate a modular bioreactor system for the expansion of anchorage-dependent cells, such as MSCs, by exploring the recent advances of culture platforms for the manufacturing of cells for MSC-based therapies. This system has the potential to improve certain aspects of the cellular products and minimize the obstacles that must be overcome in order to maximize MSC efficiency. Incorporating a mathematical model to predict key culture parameters will allow for the opportunity to improve experiment design as well as modeling of certain aspects of cell culture mechanisms that would be difficult to measure through experiment alone in numerous hypothetical scenarios. Thus, MATLAB was used to develop code for a mathematical model for this work.

CHAPTER 2

LITERATURE REVIEW

2.1 STEM CELLS

According to the National Institutes of Health (NIH), stem cells are unspecialized cells that exist within the human body that, after exposure to a physical stimulation or environmental cue, can differentiate, or specialize, into a more specific type of cell [1]. These specific types of cells can include bone cells, skin cells, fat cells, muscle cells, or neurons, even if they have been dormant for a long time. Depending on their location in the body, stem cells can have a range of activity from being regularly active, dividing and specializing in keeping the body healthy and strong or only activating under certain conditions such as an injury [1]. Examples include the neural stem cells located in the subventricular zone and the subgranular zone in the brain, which supports continuous neurogenesis and the directed migration of mesenchymal stromal cells and other kinds of epithelial cells to begin tissue repair on a scraped knee [14, 15]. Researchers are interested in using stem cells in regenerative medicine to replace damaged tissues and organs due to their biological characteristics of giving rise to either more or the same undifferentiated cell for extended periods of time and their ability to specialize, or differentiate, into a specific cell type [16]. For example, if a researcher was working to develop a bone or cartilage graft, they could utilize unspecialized stem cells and develop strategies for their use in personalized medical treatments for patients with extensive orthopedic injuries resulting in bone or cartilage loss (Figure 1), particularly if the tissue has limited regeneration potential [17]. Stem cells could, therefore, offer

an alternative to traditional therapeutic approaches and help restore the normal function of damaged tissue [18]. However, this need for stem cells brings up the question of where researchers can acquire stem cells for designing these types of cell therapies.

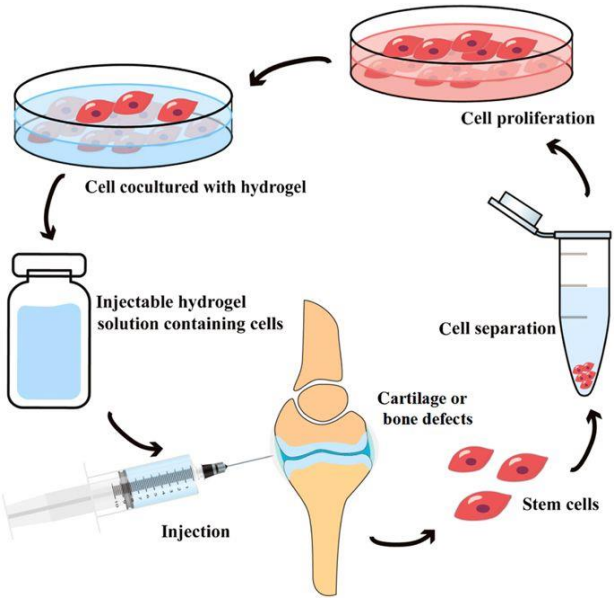

Figure 1. Potential use of stem cells for treatment of orthopedic injuries [19].

2.1.1 STEM CELL SOURCES

There are three potential sources for stem cells available. Embryonic stem cells are cells derived from the inner cell mass of the blastocyst from human embryos (Figure 2) that were donated, with the informed consent of the donor, for research purposes following an *in vitro* fertilization procedure [1]. Human embryonic stem cells (hESCs) are unique because of their ability to expand and divide to an almost unlimited magnitude and to differentiate into any cell type found in the human body [20, 21]. The use of hESCs and their properties has created concern regarding their potential to form tumors from rapid and uncontrollable expansion, immune rejection from the host, and differentiation into unwanted cell types after transplantation into a patient [21].

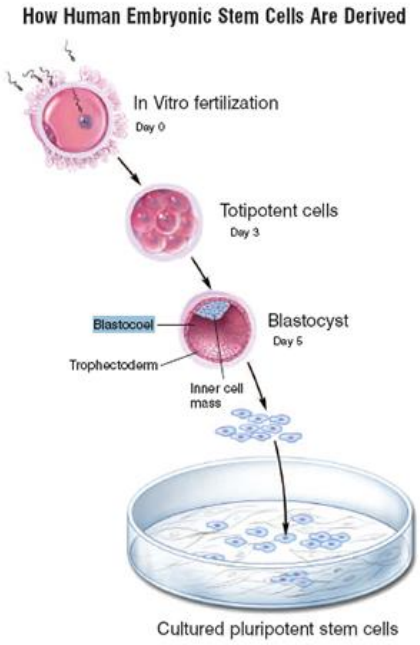

Figure 2. Derivation of human embryonic stem cells [22].

Also, there are ethical or moral concerns surrounding the use of hESCs, which has led to the prohibition of research utilizing hESCs in some countries or heavily regulated research in other countries [23]. In the United States (U.S.), it could be suggested that the polarization around embryonic stem cell research is linked to the Supreme Court decision that legalized abortion via a woman's right to privacy in *Roe v. Wade* in 1973 [24]. The limitations of federal funding after that would be the beginning of delineation between public medical research that was federally funded research and medical research supported via private funding sources [24].

In 1999, in response to a query posed by the NIH, the Office of the General Counsel of the U.S. Department of Health and Human Services (DHHS) "concluded that the then current law prohibiting the use of DHHS appropriated funds for human embryo research would not apply to research using stem cells 'because such cells are not a human embryo within the statutory definition'" in the Rabb Letter [24, 25]. The Rabb Letter said that human pluripotent stem cells

are not considered to be a human embryo, having the potential to become an organism, by definition, as they are just cells [24].

As an alternative to embryonic stem cells, adult stem cells, found in adult tissues throughout the human body, have been widely investigated. Adult stem cells have the capacity to differentiate into multiple cell types, a property called multipotency; however, unlike embryonic stem cells, adult stem cells are limited in the number of cell types that they can differentiate into [26]. Human mesenchymal stromal/stem cells (hMSCS) are a commonly used adult stem cell source in biomedical research. In addition to being classified as multipotent, hMSCs maintain properties such as immunomodulation and self-renewal, which make them attractive candidates for cell therapies and regenerative medicine [27, 28]. Adult stem cells can be found in many accessible body tissues, and hMSCs can be derived explicitly from bone marrow (Figure 3), adipose tissue, and blood, as well as from the umbilical cord blood, placenta, and other connective tissues [28, 29].

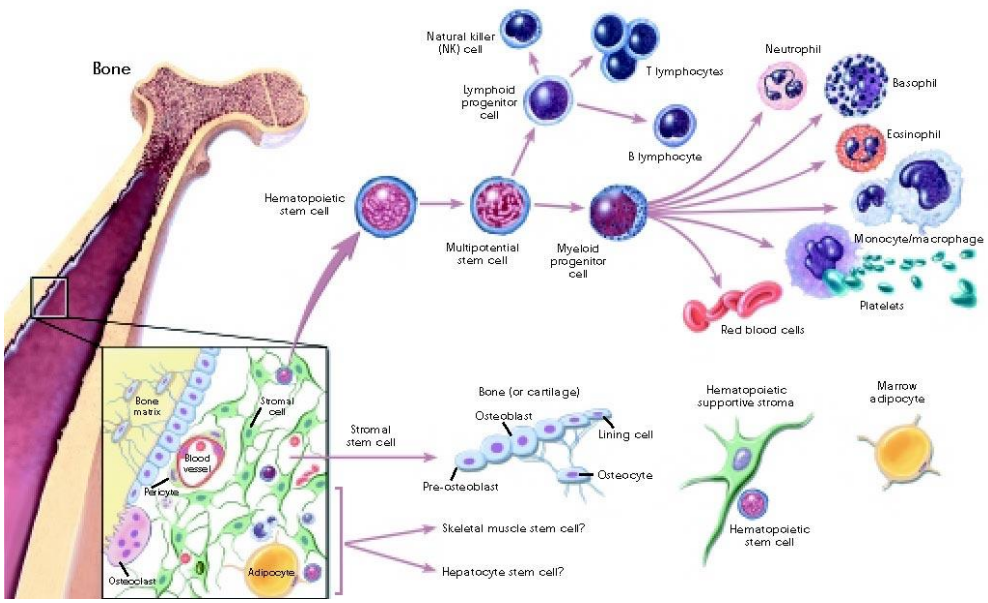

Figure 3. Differentiation of stem cells found in the bone marrow [30].

Most recently, human induced pluripotent stem cells (iPSCs) were reported to have been created, or reprogrammed in 2006 by Dr. Shinya Yamanaka [31], and have become a widely sought alternative to embryonic stem cells. These iPSCs were skin fibroblasts, reprogrammed to resemble embryonic stem cells with their beneficial properties of self-renewal and pluripotency. Specifically, several transcription factors: *Oct4*, *Sox2*, *c-myc*, and *Klf4* were targeted for reprogramming human somatic (i.e., adult) cells to form iPSCs [31]. This modification can be done to reprogram various types of cells, such as more easily accessible types including skin cells, fat cells, and blood cells. iPSCs are considered to be "pluripotent" because they can specialize, or differentiate, into the three germ layers like embryonic stem cells (Figure 4), which means they can give rise to all of the cells in the human body [32]. However, several drawbacks and limitations exist for iPSCs, particularly related to production efficiency and application. Specifically, the efficiency for different cell types regarding transduction with retroviruses is varied, and the transcription of the retroviral construct is lost after the cell becomes an iPSC. There is also a chance that the transgenes may reactivate in the cells later derived from the iPSC line. Another concern is that the genes used to induce the pluripotent state can also lead to tumor development [33].

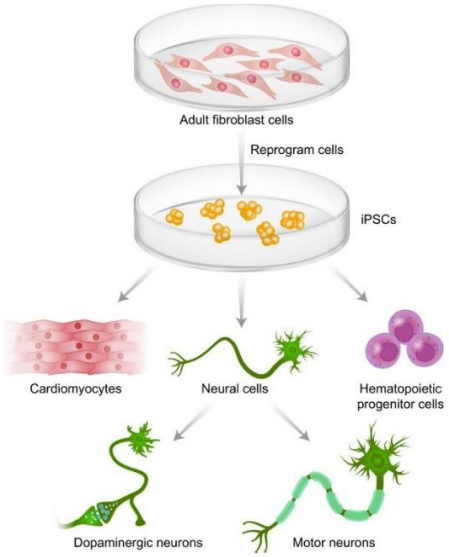

Figure 4. Induced pluripotent stem cell maturation [34].

When considering which class of stem cell is used, the source of donor tissue origin should also be considered. Cells may be obtained from autologous or allogeneic sources, meaning from their own body or a properly matched donor, respectively. As previously mentioned, there is a stigma around hESCs due to ethical concerns about the cell source; additionally, there are other concerns such as spontaneous tumor formation from uncontrolled proliferation and the risk of differentiating into undesired stem cell types [21, 35]. Another risk is that hESCs are obtained from an allogenic source, or a donor, and there is the possibility of the patient's immune system rejecting the cell therapy, and they would, therefore, be required to take immunosuppressant drugs [36]. The use of iPSCs and MSCs have the potential for autologous treatments, as cells could be obtained from a patient biopsy, and would thus, not be rejected upon implantation into that patient. The advent of autologous therapies could decrease the cost of therapies and stem cell transplants because the patient will not be required to take immunosuppressant drugs indefinitely, however, achieving clinically relevant numbers of these cells is a current challenge for widespread use of autologous cell therapies. Here, the remainder of the discussion in this review will focus on hMSC-based applications.

2.1.2 ACHIEVING CLINICALLY RELEVANT CELL NUMBERS

The investigation of hMSCs for clinical applications has the been extensive due to their self-renewal and multipotency, but also due to other characteristics, such as immunomodulatory, anti-inflammatory, neuroprotective, and angiogenic properties. Thus, clinical applications for MSCs have ranged from tissue regeneration applications to cell therapy for treatment of cancer and chronic diseases, including cardiovascular disease, autoimmune diseases, and neurodegenerative diseases, which have been reviewed extensively by others [37-42]. For these

applications in the clinic, the number of cells required will vary; however, it is expected that the magnitude of cells required will be significant, thereby making it necessary to have sufficient culturing methods for achieving the required numbers of cells.

The culture environment for expansion and differentiation of hMSCs is essential, as these cells are extremely sensitive to biochemical and biophysical cues, and culture conditions such as the presence of signaling molecules can affect their expansion potential and differentiation [43]. For example, in the body, mechanical stimulation as bone remodeling occurs aids in bone cell differentiation and maturation, which supports the maintenance of structural integrity; thus, designing a physiologically relevant environment for cell culture can improve cell expansion and differentiation outcomes [44, 45]. In addition, hMSCs in culture are often in contact with various substrates for which properties such as the surface stiffness, topography or chemistry can influence cell behavior by inducing a response that results in the hMSC differentiation to a specific lineage of cells [46]. Researchers have studied how critical culture parameters can influence hMSC expansion, as reaching clinically relevant numbers can be challenging since a significant number of cells will be needed for therapeutic treatments (whether single or multiple dosages). Clinically, there is a very low retrieval percentage (~0.01%) of hMSCs acquired from bone marrow biopsies [4, 47], making the expansion of these cells *ex vivo* essential. Long-term culturing outside of the body, however, can be difficult and influence the efficacy of the resulting cells. Specifically, the limitations of long-term culture include senescence in hMSCs, which can result in a decrease in the proliferation potential of cells, changes in hMSC phenotype, or a decrease in differentiation potential [27, 48]. Therefore, it is important to consider how to manipulate cell culture conditions to appropriately mimic physiological environments to improve expansion and yields for achieving clinically relevant numbers.

Table 1 describes several therapeutic targets for which researchers have applied MSCs and the proposed range of cells (per kg of the patient) required for that treatment. Because the MSCs are the actual therapeutic, it is important to develop large, *healthy* populations for clinical treatments; thus, the scale-up production of hMSCs must also adhere to good manufacturing practices (GMP) [49]. The range of cells required for a dose depends on the therapeutic application and the weight of the patient (at least 200×10^6 cells). As previously mentioned, there is a low retrieval rate of MSCs from bone marrow, in part, because they are a smaller proportion of cells in the marrow. As a result, interest has grown for the use of other more accessible sources for stem cells, such as adipose-derived stromal cells (ADSCs) where the percentage of stem cells obtained from biopsies can range from 1% to 10% [50, 51]. In order to meet the demands of clinically relevant numbers, cell expansion platforms for large-scale culturing of MSCs must be considered.

Table 1. Ranges of hMSCs used for clinical cell therapies.

Therapeutic Target	**Range of Cells**	**Reference**
Acute Respiratory Distress Syndrome (ARD)	3×10^6 cells/kg	[52]
Amyotrophic Lateral Sclerosis (ALS)	11-12 $\times10^5$ cells/patient 2×10^5 cells/kg	[53, 54]
Diabetes (Type 1)	2.1 – 3.6 ×106 cells/kg	[55]
Multiple Sclerosis	$1 – 2\times10^6$ cells/kg	[56, 57]
Idiopathic Parkinson's Disease (iPD)	1×10^6, 3×10^6, 6×10^6, or 10×10^6 cells/kg	[4]
Spinal Cord Injury	8×10^6, 40 $\times10^6$, or 50 $\times10^6$ cells/patient *depending on location and time point of clinical trial*	[58]

2.2 CELL EXPANSION PLATFORMS

Various culturing vessels and systems exist for cell expansion, as shown in Figure 5. These culturing platforms include both static and dynamic systems, which are applicable for anchorage-dependent cells, such as MSCs. The selection of a static or dynamic system for culturing can depend upon the specific purpose of the culture, whether intended for expansion, differentiation, or conditioning of the cells for *in vivo* applications. A summary of selected culture systems will be discussed in further detail in this review.

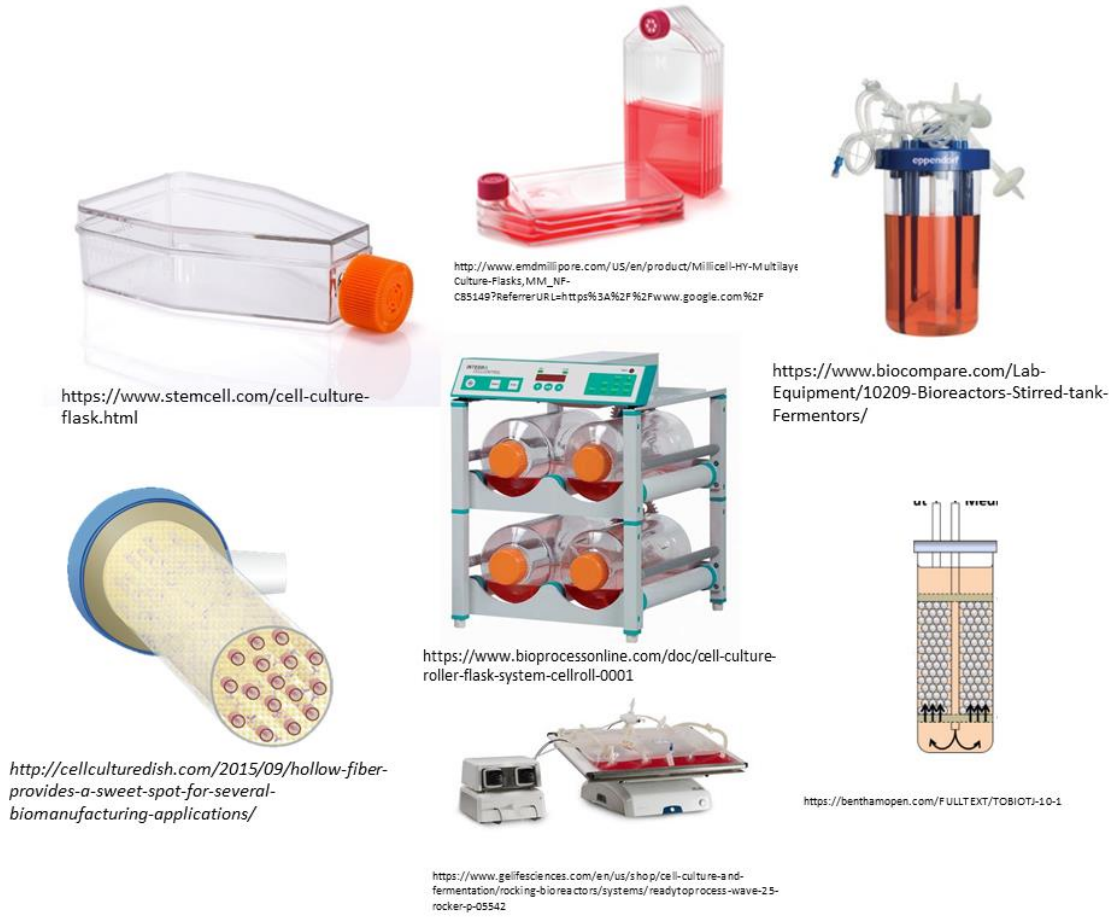

Figure 5. Examples of various cell culturing systems.

2.2.1 STATIC CULTURE SYSTEMS

hMSCs are classified to be anchorage-dependent, meaning that they need to adhere to a surface to properly proliferate and expand. It is possible for hMSCs to aggregate together, cluster, or stick to each other, if the surface is not sufficient, and in these cases, cell proliferation will be limited [59]. The expansion potential of these cells can be limited by the amount of surface area available. In the past, the expansion of hMSCs was most commonly performed in monolayer culture using tissue culture-treated flasks because the surface was adequate for cell attachment. However, the quantity of cells generated was limited by the surface area of the flasks used, and there were issues with long-term culture expansion due to senescence [60]. This indicated a need for developing more complex culturing systems for clinically relevant numbers. From there, multi-layered vessels or flasks were developed, but have still been limited in many ways, primarily due to insufficient yields for industrial level scale-up and a lack of automation in place to supply late-stage clinical trials [36, 60, 61]. Alternative expansion strategies have, thus, been sought to circumvent these limitations of conventional two-dimensional (2D) monolayer flasks, and dynamic three-dimensional (3D) or bioreactor culture systems have been investigated, since they more accurately mimic an environment more akin to what the cells experience *in vivo* and should, therefore, be more optimal for culturing [36].

2.2.2 DYNAMIC CULTURE SYSTEMS

Since the 1980's when tissue engineering applications were suggested, researchers have sought ways to overcome several of the obstacles that prevent or limit the attainment of clinically relevant stem cell populations needed for therapeutic applications, and researchers today are still working to achieve these sufficient population densities [62, 63]. The development of dynamic

culture systems, such as various forms of bioreactors, has been essential for scale-up production of mammalian cells and will be further detailed in this review.

Bioreactors are defined as a vessel or container used for biochemical and biological processes/production. They are particularly advantageous tools in the industry because they can allow for monitoring of parameters and control of the environment in which the reaction occurs [64]. Bioreactors are useful because of their potential for automation, application to large scale-up production, and reproducibility of the desired product from batch-to-batch. The classical uses of bioreactors include fermentation, wastewater treatment, pharmaceutical production, and recombinant protein production [65]. There are also bioreactors specifically designed to tackle these processes efficiently; the selection of the most appropriate bioreactor type is critical to developing an efficient manufacturing process.

The specific type of bioreactor selected will depend on whether or not the process is a batch production or a continuous production, or a static or dynamic culture system [66]. A batch production is defined as a reactor that is filled or charged with reagents that will be left inside the vessel as the reaction is carried out with no inflow or outflow until the reaction is complete [67]; whereas a continuous production refers to a vessel that has a continuous inflow of reagents and a continuous outflow of product, as it is assumed to be appropriately mixed while operating at steady-state [67]. Essentially, batch production is much more reminiscent of a fermentation process where the cells and their nutrients are kept in one vessel, and new media and supplements might be added to keep the cells expanding until the product the cells produce has been maxed out.

A continuous production is similar in the sense that the vessel contains the cells and there is an inflow of nutrients, but there is also an outflow, which will remove inhibitory byproducts that might harm the cells if the concentrations get too high. There has been a shift to more designs that

favor continuous manufacturing, as there are many advantages such as assumed steady-state operations; a homogeneous or heterogeneous environment; a constant volume and density; cost-efficiency; isothermal conditions; automation; product consistency; and the ability to monitor critical culture parameters [66, 68].

These “critical culture parameters” can be defined as aspects of the cell culturing process that is vital to maintaining healthy cells. This could include, for example, a proper amount of fresh media to provide appropriate nutrients to the cells. Continuous manufacturing processes allow for these parameters to be easily adjusted, as they can be monitored in real-time through appropriate sensors measuring pH or carbon dioxide levels from the cell expansion process. The live feedback attained will then allow for immediate adjustments. Therefore, the selection of the appropriate bioreactor design for parameters such as oxygen gradients, shear stress, metabolic byproduct concentration, pH concentration, temperature, and carbon dioxide concentration, is vital [68]. A vast majority of technology used in the biopharmaceutical field is for fed-batch processes, but with the field swiftly evolving there is a need to adopt different technologies for manufacturing more complex products such as cell therapies [69]. In the case of cell therapy production, there are many different approaches to solve the current limitations of supplying enough hMSCs for therapies, and various culturing vessels have been investigated for expansion of these cells. The following sections will overview various bioreactors (summarized in Table 2) and their applications for human stem cell culture.

Table 2. Comparison of selected culturing systems

Features	Flask	Spinner Flask	Continuous Perfusion Bioreactor	Packed / Fixed-Bed Bioreactor	Hollow Fiber Bioreactor
Culture Automation	No	Yes	Yes	Yes	Yes
System Type	Open	Closed	Closed	Closed	Closed
Contamination Risk	High	Low	Low	Low	Low
Homogeneity	No	Yes	Moderate	Depends	Moderate
Shear Stress	No	High	Moderate	Moderate	High
Oxygen Transfer	No	High	Moderate	Moderate	High
Cell Harvesting Difficulty	Easy	Difficult	Difficult	Difficult	Easy

2.2.2.1 SPINNER FLASKS

A dynamic culture system, such as a continuous stirred tank bioreactor (or spinner flask if little or no monitoring system incorporated), makes for an attractive solution to traditional static culture systems because it is simple, easy to scale-up, provides excellent gas exchange to cell cultures and monitoring critical culture parameters is straightforward [70]. Most importantly, the properties of stem cells cultured under 3D dynamic conditions can be altered and controlled for specific applications [71].

There are three possible types of culture systems within a suspension stirred tank reactor: cell aggregates, cells encapsulated in microcarriers, and cells seeded onto coated microcarriers [72-76]. Stem cell aggregate culture is when the anchorage-dependent stem cells will adhere to one another when there is no suitable other alternative present to support cell adhesion [77]. It is difficult to control the expansion scale-up of stem cell aggregate culture because it is almost

impossible to control the aggregate size. In addition, aggregate culture can also damage the final stem cell product, as the increase in aggregate size and density can result in a decrease of mass transport of nutrients to the center, limiting cell growth and potentially damaging the stem cells [78].

Microcarrier based culture relies on a high surface-area-to-volume ratio to produce a high density of stem cells in the final product. Thus, the smaller the microcarrier, then the higher the potential surface area present, which increases the potential growth area [79]. This characteristic makes microcarriers ideal for process scale-up as higher densities can be achieved in a reduced medium volume, which can lower the cost of expansion production [80].

Microcarriers can be made from ceramics, and synthetic or natural polymers depending on the needed characteristics, length of culture and time and application. Initially, synthetic microcarriers made from glass or polymers, such as polystyrene, and polylactic acid, allowed for sufficient mechanical strength and consistency in the microcarrier properties from batch-to-batch. However, these types of microcarriers maintained limited cell attachment proficiency due to the lack of sites for anchorage-dependent cells to adhere to [81, 82]. This limitation has been overcome by preparing microcarriers either by coating with extracellular matrix proteins or a hydrogel mixture containing appropriate ligands or by chemically enhancing the surface to promote cell adhesion for cell expansion purposes [83, 84]. Natural biomaterials for microcarriers are widely available and inexpensive. Natural materials such as gelatin, collagen, cellulose, pectin, alginate, and chitosan also have excellent biocompatibility as they do not induce an adverse biological response from the stem cells, and have been used for microcarrier based applications with stem cells [81, 82, 85, 86]. Further, microcarriers are advantageous because properties such as their surface chemistry, topography, porosity, geometric shape, matrix coating, and mechanical

characteristics can be augmented to control stem cell attachment for expansion better and to potentially enhance the phenotype expression of stem cells [86-89].

2.2.2.2 PERFUSION BIOREACTORS

Although microcarriers present a 3D shape, cells grown in microcarrier culture are still similarly cultured as cells grown in monolayer, which does not accurately represent the natural environment found inside the body [90]. Perfusion bioreactors feature a vessel where the media is directed to flow through a construct that is either porous or 3D, which can help overcome the expansion bottlenecks seen in monolayer cell culture methods by increasing oxygen and nutrient transport in the system [91, 92]. Studies have shown that cell metabolism is crucial to stem cells retaining pluripotency, or multipotency depending on the source, and perfusion bioreactors can provide a constant flow of fresh media that removes inhibitory metabolic byproducts, resulting in a stable metabolic system for high-density expansion [93].

Perfusion bioreactors are selected when there is a specific cell phenotype of interest to amplify with external cues or for conditioning cells for clinical applications. Schröder, *et al*. designed a novel bioreactor system for the purpose of conditioning the chondrocyte cells used in autologous chondrocyte implants (ACI). The flow of the media was used to provide hydrostatic pressure to the cells for potentially increased protein production and gene expression [94]. The bioreactor was designed to condition the chondrocytes to decrease the chances of graft hypertrophy and the unintended development of a different type of cartilage, where the estimated pressure loads on cartilage of 0.1 – 0.2 MPa were achievable in the system [95].

Beşkardeş, *et al.* used a perfusion bioreactor set-up to explore how co-cultures of osteoblasts and osteoclasts interacted in a dynamic environment since bone is continuously metabolically active, and bone remodeling is controlled through the interaction of bone-resorbing

osteoclasts and bone-forming osteoblasts [96]. As biomechanical stimulation is necessary for bone remodeling, the limitations of a two-dimensional static culture will influence cell viability, nutrient flow, and cell density, however, dynamic culture can provide appropriate stimulation to upregulate differentiation to bone and resulting bone function long-term [45].

Perfusion bioreactors present a lot of potential as they can be automated for low labor-cost and are a closed system, which decreases the risk of contamination. This design can support long-term cell culturing of tissue constructs or expansion of cells on porous scaffolds with a continuous inlet flow of nutrients and oxygen, while continuously removing byproducts and waste. However, the dynamic environment can expose the cells growing along the scaffold to higher shear stress with the possibility of potentially causing cell damage. Further, the pressure gradient created in perfusion bioreactors is not necessarily accurate to *in vivo* environments [97].

2.2.2.3 PACKED BED BIOREACTORS

Packed bed bioreactors (PBRs) are cylindrical vessels that contain a layer or packing of material, such as microcarriers, that support cell adhesion and facilitate the circulation of media through the "packed bed" to provide the necessary nutrients, oxygen delivery and removal of metabolic byproducts [65, 67]. PBRs belong in the same family of dynamic culture systems such as the spinner flask and perfusion bioreactors, and as such, offer many of the same advantages. Most importantly, however, PBRs offer a controlled environment for stem cell expansion in a small volume, which is cost-effective in terms of materials and medium [65]. This vessel type is also beneficial for anchorage-dependent, or immobilized, stem cells because it offers a low shear stress environment [43]. It is important to consider how the vessel's culture system can affect the cells as shear stress has been studied to observe its effects such as reduction or alteration of the

stem-like properties and differentiation lineage and the overall quality of the final stem cell population after expansion [98, 99]. The most significant limitation of PBRs for MSCs is the maximum media flow rate [100]. Literature studies have shown that this mechanical stress can be beneficial if adequately regulated; for example, shear stress can upregulate MSCs predetermined lineage preference to osteogenesis if the shear stress reaches 0.015 Pa [101].

Osiecki, *et al.* developed a scalable packed bed style bioreactor for the isolation and subsequent expansion of MSCs [100]. The design in this study featured a plasma-treated and fused bed of polystyrene beads, the same material as tissue culture plastic in flasks, encased in a shell that was gas permeable to enhance gas exchange [100]. The MSCs were expanded in the system, but had a lower growth rate than the control flasks and an uneven distribution of the cells due to the seeding methods; however, the cells did retain their osteogenic potential [100]. This is an example of how beneficial a packed bed style bioreactor can be, as it is a closed system that can be automated and can overcome nutrient gradients with a high enough flow rate. Unfortunately, cell harvesting can be very difficult as the system has to be flushed with a trypsin-EDTA solution to cleave the cells from the culturing surface. This can be insufficient, thus resulting in lower cell yields for this type of bioreactor system.

2.2.2.4 HOLLOW FIBER BIOREACTORS

Hollow fiber bioreactors are perfusion-like bioreactors that present an opportunity to produce a high density of cells before MSCs cross the threshold for expansion before losing key stem cell characteristics such as potency [102]. Hollow fiber bioreactors are glass tubes containing one or a bundle of polymer fibers that culture medium is perfused through [103]. The hollow fibers can be used for different transports, such as supplying fresh nutrients and oxygen or removing

spent medium and cell products [103-105]. The set-up of hollow fiber bioreactors creates a closed environment comparable with *in vivo* conditions and a large surface area for anchorage-dependent stem cells, which satisfies one of the key necessities of dynamic culture [106]. Hollow fiber bioreactors have been used for stem cell expansion, cell product formation, and vector production, with the intent of finding a culturing platform to integrate at the industry level of scale-up [107-110].

Cipriano, *et al*. evaluated how hollow fiber bioreactors could improve the metabolic functions of the MSC-derived hepatocyte-like cells (HLCs) by comparing the 3D culturing environment to control two-dimensional (2D) monolayer culture [111]. The perfused environment and the 3D culturing environment will mimic the natural gradient environment found in the body, and in this study, the specifically mimic the liver which could upregulate certain gene expressions and develop a more heterogeneous cell population [111, 112].

This version of a perfused culturing system has been proposed for organ or tissue construct development due to the increased mass transfer, high cell density expansion or producing cell-compounds like monoclonal antibodies; where the geometry of the hollow fiber bioreactor is important [113-116]. Additionally, there may be phenotype changes to the cells in 3D culturing, desired or undesired; therefore, the selection of the culturing system will depend on the scientific application [111].

2.3 FUTURE DIRECTIONS

When developing strategies for therapeutic application of cells, it is essential to consider the source of the stem cells and the culturing techniques for expansion in order to meet the increasing demand for large populations of healthy and potent stem cells. With regard to

anchorage-dependent culture, bioreactor culturing platforms should be selected based on the intended use; for example, cell expansion or cell conditioning. Continuous flow systems with perfused media have the advantage of providing fresh nutrients, but the seeding technique and the cell harvesting technique are crucial to retrieving the expanded cells without damaging them. A potential solution to this would be to design a vessel with a removable insert where the culturing surface is loosely packed, making it easier to wash and harvest with trypsin-EDTA solutions. Additional alternative improvements for future bioreactor designs may include in-line monitoring of novel biomarkers or metabolites more closely associated with stem cell function; however, research towards these improvements is ongoing.

CHAPTER 3

EXPANSION AND EVALUATION OF MESENCHYMAL STROMAL CELLS UNDER DYNAMIC CULTURING CONDITIONS

3.1 INTRODUCTION

3.1.1 BACKGROUND

Currently, there are many different, commercially available options for culturing anchorage-dependent cells. In a typical lab setting, culture flasks are commonly used to expand cells, but these vessels have a high contamination risk because they are open, there is a labor-cost associated with cell maintenance and media changes, and there is unbalanced transport of nutrients [117]. Bioreactors, on the other hand, have become an integral part of the scale-up production process by allowing for an automated option to researchers where culture parameters can be controlled, and robust and well-defined populations of cells for research can be provided [118]. Large numbers of cells are required for *in vitro* experiments to evaluate strategies for developing therapies before moving into clinical trials. There are different types of bioreactors available, which are used for various forms of dynamic culture available for stem cell culturing, such as suspension culture in either a spinner flask or a wave bioreactor, a perfusion bioreactor, or a packed-bed style bioreactor.

We propose designing a modular bioreactor system for the expansion of anchorage-dependent cells, such as mesenchymal stromal cells (MSCs). The material selected for fabrication of the bioreactor vessel is a polycarbonate, Lexan™, which is affordable and allows for easy

observation of the system while in use. Modular capabilities of the bioreactor were implemented via the fabrication of two different cell culturing inserts to support different forms of culturing using monolayer or microcarriers. Here, a series of proof-of-concept experiments were performed to evaluate how well this design can support monolayer culture of MSCs and to assess the effects of this dynamic culturing approach on the stem-like properties of the resulting cells (determined by evaluating osteogenic potential).

3.1.2 HYPOTHESIS

The focus of this phase of the project was to establish a modular bioreactor system capable of supporting rapid stem cell expansion under defined conditions. The effects of the dynamic culture environment on the cell growth rate, cell viability, metabolic byproduct production, and expanded mesenchymal stromal cell potency were then evaluated using various assays. We hypothesized that the dynamic bioreactor conditions will mimic the *in vivo* environment of the body and increase the expansion potential and the potency of MSCs, thus improving the efficacy of cell culturing platforms.

3.1.3 OBJECTIVES

There were two phases for this work, with objectives for each phase as follows:

1. Bioreactor design and fabrication
    a. Build a “novel” bioreactor
    b. Perform proof-of-concept testing
2. Dynamic culture evaluation

a. Explore effects on stem cell growth and differentiation from monolayer culture in bioreactor vessel
b. Examine metabolic products from a continuous bioreactor system
c. Perform an economic analysis of the system compared to traditional methods

3.2 MATERIALS & METHODS

3.2.1 BIOREACTOR VESSEL DESIGN AND SYSTEM ASSEMBLY

AutoCAD software was used to design bioreactor features and generate a rendering of the modular bioreactor (Figure 6). A custom-built cylindrical bioreactor vessel was designed to provide housing and support for cell culturing inserts (monolayer and microcarrier supports) while permitting continuous perfusion of culture medium through the vessel. Fabrication of the custom vessel was completed by the University of Georgia Instrument Design & Fabrication Shop (Athens, GA). The bioreactor vessel was fabricated from a cylindrical Lexan™ tube with two pieces, a top and bottom, cut to fit together with an O-ring to create a pressure seal. There are four small pegs near the base of the vessel bottom to secure each culturing platform inside the chamber. The vessel inlet and outlet caps were also made from Lexan™ and are threaded with removable O-rings for maintenance of sterility. Barbed hose attachments (Cole-Parmer, Vernon Hills, IL) are placed at the ends for attachment of tubing to connect the system. The top cap has two additional barbed hose attachments for the gas exchange tubing. The bioreactor chamber rests on a PVC stand allowing for the connection of the inlet and outlet to the system. The chamber and the caps are sterilizable with ethanol and UV light.

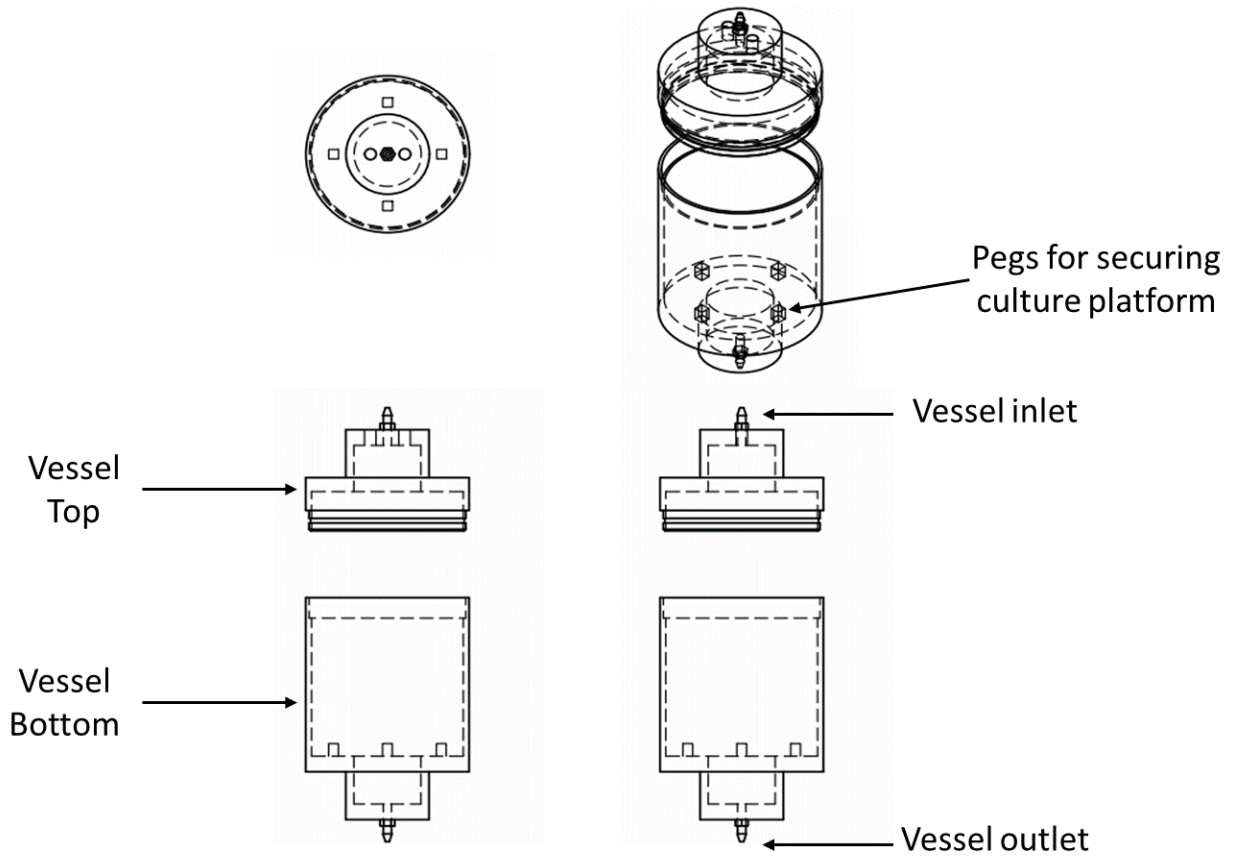

Figure 6. AutoCAD drawing of the bioreactor vessel.

Two cell culture inserts were designed and fabricated to support either monolayer culture or microcarrier-based culture (Figure 7A). The monolayer culture insert is made from Lexan™ and has approximately the same growth area as a standard T-75 culture flask (Falcon, Corning, Corning, NY), with 75 cm^2 of growth area for anchorage-dependent cell culture. There is an attachable stem for the installation and removal of the insert from the bioreactor. The 3D microcarrier culture insert is made from Delrin® plastic (U.S. Plastic Corp, Lima, OH) and has openings to allow for drainage of spent media through the system (Figure 7B). There is a removable handle on the insert for the installation of a nylon mesh to contain the microcarriers and for removal of the insert from the bioreactor. Both inserts are sterilizable with ethanol and UV.

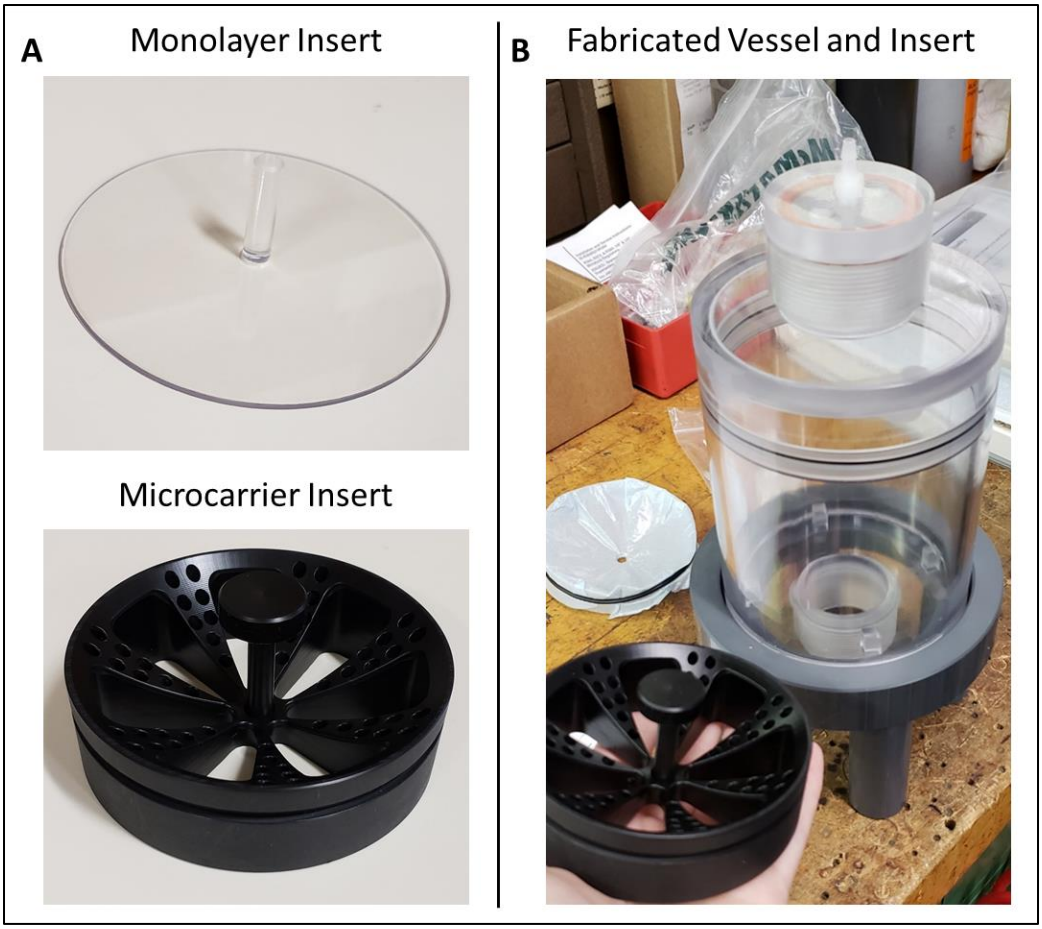

Figure 7. A) Bioreactor cell culture inserts for monolayer and microcarrier cultures. B) Assembled bioreactor vessel and inserts post-fabrication.

To complete the bioreactor system set-up, a single-channel MasterFlex L/S Digital Miniflex peristaltic pump (Cole-Parmer) was selected. Two variations of bioreactor assembly for short-term and long-term closed/recirculation cell culture are detailed in Figure 8A. For short-term culture, the bioreactor set-up consists of the peristaltic pump and the custom vessel with monolayer culturing platform, as previously described. The inlet and outlet caps made are connected via barbed hose attachments using platinum-cured, L/S 16, silicone tubing with an inner diameter of 3.1 mm (Cole Parmer) with high gas permeability to facilitate gas exchange. The long-term bioreactor system set-up consists of the peristaltic pump and custom culture vessel with a 3D

microcarrier platform, as previously described. The inlet and outlet are connected using the same platinum-cured silicone tubing, and an additional media reservoir (Figure 8B) is located in-line. The media reservoir was constructed to support long-term recirculation culture within the bioreactor system since it allows for media exchange by removing the spent media and replenishing with fresh media inside the reservoir. The media reservoir, as shown in Figure 8C, is a glass media bottle (Corning) modified with the addition of two barbed hose attachments to connect the media reservoir to the system with platinum-cured silicone tubing. Both the tubing and media reservoir can be sterilized by autoclaving. The entire bioreactor system, once assembled, was kept inside a standard cell culture incubator at 37°C and 5% CO_2 (Steri-cycle i160 CO_2 incubator, Thermo Fisher Scientific, Waltham, MA) for culturing experiments.

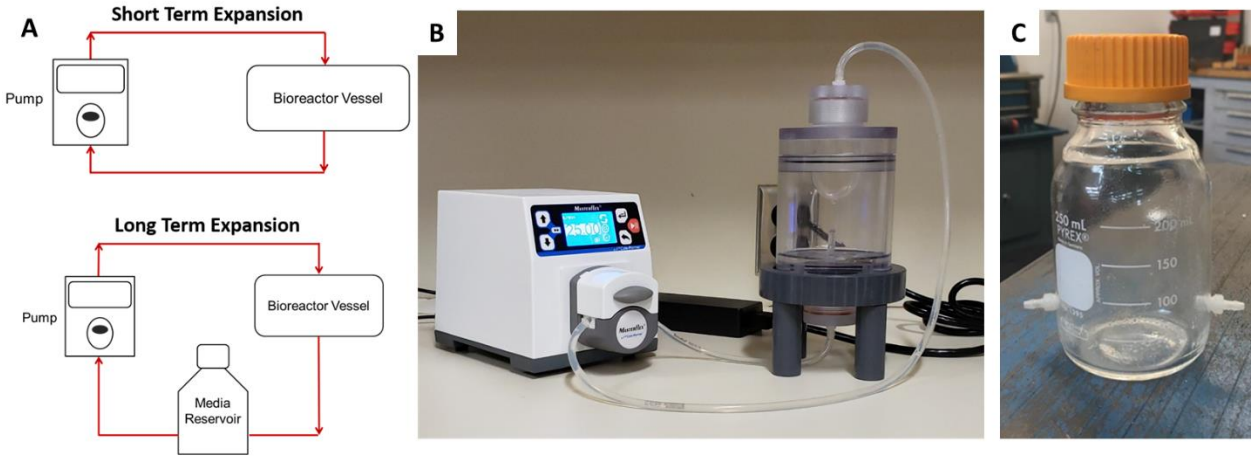

Figure 8. Schematic representation of the modular bioreactor system. A) Proposed system set-up for short-term expansion in the bioreactor and proposed set-up for long-term cell expansion, which includes a media reservoir for media replenishment. B) Picture of the assembled bioreactor system, including the peristaltic pump. C) The media reservoir.

3.2.2 BIOREACTOR ASSEMBLY VALIDATION

The bioreactor system was assembled, and preliminary evaluation performed to check for fluid leaks. The bioreactor vessel was first assembled without the pump, filled with water and left

overnight to see if the vessel was airtight. Upon review, PTFE thread sealant tape (Grainger Industrial Supply, Lake Forest, IL) was applied to the threaded outlet to prevent liquids in the bioreactor vessel from leaking out and to maintain sterility. An additional pass with methylene chloride was also performed to ensure that the Lexan™ pieces were sufficiently bonded together to create an air-tight seal. The system was assembled with the pump, and the water leak test was repeated with the pump running.

3.2.3 MONOLAYER CULTURE INSERT PREPARATION

Prior to cell culturing experiments, the Lexan™ inserts were plasma treated and sterilized. A Plasmod Oxygen Plasma Cleaner (Tegal Corporation, Petaluma, CA) was used to remove organic particulate on the monolayer insert and to oxidize the surface. The Lexan™ inserts were treated for 2 minutes with oxygen plasma ignited at 50 W following the manual. After plasma cleaning, the inserts were soaked in a 70% v/v ethanol solution for additional protonation.

3.2.4 PRELIMINARY CELL ATTACHMENT EVALUATION

Cell attachment to the monolayer Lexan™ insert was evaluated using a commercially available murine bone marrow-derived mesenchymal stromal cell line (D1 cells, ATCC, Manassas, VA). D1 cells were seeded in suspension for the bioreactor system at a high density of 400,000 cells/cm^2 to ensure maximum attachment potential on the monolayer insert. Cells at the same density were also seeded in a T-75 flask (Falcon, Corning) for a static control for comparison. The cells were cultured in low-glucose Dulbecco's Modified Eagle Medium (DMEM, Gibco, Waltham, MA) containing 10% fetal bovine serum (FBS, Atlanta Biologics, Atlanta, GA) and 1% U/mL penicillin/ streptomycin antibiotics (Gibco), denoted as DMEM-Complete. The bioreactor

system was assembled with the culturing set-up for monolayer experiments, as shown in Figure 9. The assembled bioreactor was then placed inside an incubator at culture conditions of 37°C and 5% CO_2 for the duration of the study.

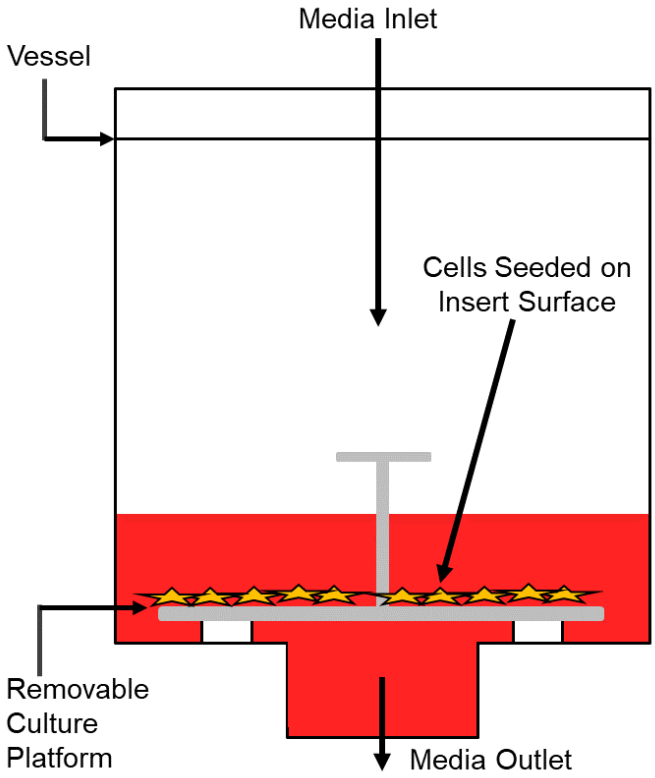

Figure 9. Schematic demonstrating set-up of bioreactor vessel for monolayer cell culture experiments.

The cells were cultured for 24 hours and then evaluated using a LIVE/DEAD® Viability/Cytotoxicity Kit (Molecular Probes, Eugene, OR) to qualitatively assess cell adhesion. Briefly, a LIVE/DEAD® working solution was prepared by adding 20 µL of 2mM ethidium homodimer (EthD-1) stock solution to 10 mL of PBS and vortexed to mix. After, 5 µL of 4 mM calcein AM solution was added to the mixture and vortexed to mix. The insert was removed from the culture vessel, and the cell monolayer was carefully rinsed with phosphate-buffered saline (PBS) (Gibco). The working solution was added to the monolayer an incubated at room

temperature in the dark for 45 minutes. This LIVE/DEAD® assay was repeated for the flask for comparison, and both samples were evaluated for cell viability by visualizing samples using an EVOS FLc Cell Imaging System (Thermo Fisher Scientific) equipped with phase and fluorescence light for capturing images. This experiment was also repeated to evaluate cells after 4 days in culture to evaluate proliferation and compare the confluency of cells in both the flask and the bioreactor to the initial attachment time point.

3.2.5 SHORT-TERM MSC EXPANSION VIA DYNAMIC BIOREACTOR CULTURE

D1 cells were cultured in DMEM-Complete and grown to confluence. Cells were seeded in both the bioreactor system and a 2D control T-75 flask at a density of 400,000 cells/mL at Day 0. The closed vessel was added to the closed-loop bioreactor system via attachment with silicone tubing and placed into an incubator at standard culture conditions of 37°C and 5% CO_2 with the pump that was previously assembled prior to seeding. The peristaltic pump was turned on after allowing the cells 24 hours to attach to the Lexan™ insert. The inlet flow from the pump was set to 1 mL/min to limit the potential of a high flowrate from dislodging the D1 cells until Day 3. A summary of all culture conditions is provided in Table 3.

Table 3. Comparison of culturing conditions.

	Static	**Dynamic**
Cell seeding density	400,000 cells/cm^2	400,000 cells/cm^2
Temperature	37°C	37°C
Humidity (CO_2)	5%	5%
Medium flow rate	N/A	1 mL/min
Medium volume	12 mL	110 mL

3.2.6 SHORT-TERM HARVEST AND EFFICIENCY EVALUATION

Media samples were collected from both the bioreactor system and the static T-75 flask before the harvesting cells for further analysis. The T-75 flask was rinsed with PBS and replaced with an equivalent volume of 0.05% trypsin-EDTA (Gibco). The flask was incubated (5% CO_2 and 37°C) for 5 minutes. The trypsin was neutralized with an equal volume of DMEM-Complete medium, and contents were transferred to a 15-mL conical tube. Similarly, the Lexan™ insert was removed from the bioreactor vessel and washed with PBS. The PBS was removed, and 0.05% trypsin-EDTA was used to cleave the cells. The insert was left in the biosafety cabinet to incubate for 5 minutes at room temperature. The trypsin was neutralized with an equal volume of DMEM-Complete medium and transferred to a 50-mL conical tube. Both tubes were centrifuged to collect the cells. The resulting supernatant was removed, and a known volume fresh medium was used to resuspend the cell pellets before counting, which was performed using a hemocytometer and Trypan Blue exclusion dye (Gibco). The described experiment and subsequent analyses were performed for three trials.

3.2.7 METABOLIC ANALYSES

The collected media samples from the static and bioreactor cultures were evaluated to assess cell metabolism. Lactic acid and glucose levels were measured using a YSI Biochemistry Analyzer 2900 (YSI, Yellow Springs, OH). The YSI Biochemistry Analyzer 2900 uses an immobilized enzyme electrode to measure the concentrations of compounds such as glucose and lactate from samples, with comparisons made within the unit to appropriately calibrated standards for both glucose and lactate.

Levels of hydrogen peroxide, a reactive oxygen metabolic byproduct, were measured using a Hydrogen Peroxide (H_2O_2) Colorimetric/Fluorometric Assay Kit from BioVision, Inc. (San Francisco, CA). Briefly, a 10 mM H_2O_2 and 0.1 mM H_2O_2 standards were used to create a standard curve. To create the colorimetric assay solution, 46 µL Assay Buffer, 2 µL OxiRed™ Probe solution, and 2 µL Horse Radish Peroxidase (HRP) solution were mixed for a total of 50 µL. The Reaction Mix was pipetted to each well, and the plate was incubated at room temperature for 10 minutes. A Biotek 800TS microplate reader (Biotek, Winooski, VT) plate reader was used to measure the OD at 570 nm.

3.2.8 EVALUATION OF MSC OSTEOGENIC POTENTIAL

Resulting cells expanded in the dynamic bioreactor set-up were evaluated post-expansion using a series of functional analyses to assess their bone differentiation potential, as shown in the study timeline of Figure 10. Cells cultured under static conditions were also evaluated for comparison. The harvested cells were seeded at a density of 80,000 cells/cm^2 into 24-well plates (Falcon, Corning), with two plates for each culture condition: static or dynamic. Cells were cultured with either DMEM-Complete growth medium, as previously defined, for 14 days or with osteogenic differentiation medium. The osteogenic differentiation medium consisted of high glucose-DMEM (Gibco) containing 10% FBS, 1% penicillin/streptomycin (Gibco), 50 µg/mL ascorbic acid (#A-8960, Sigma-Aldrich, St. Louis, MO), and 4 mM beta-glycerophosphate (β-GP, #G-5422, Sigma-Aldrich). The media was refreshed every 2-3 days, and samples were collected at Day 7 and Day 14 for analysis.

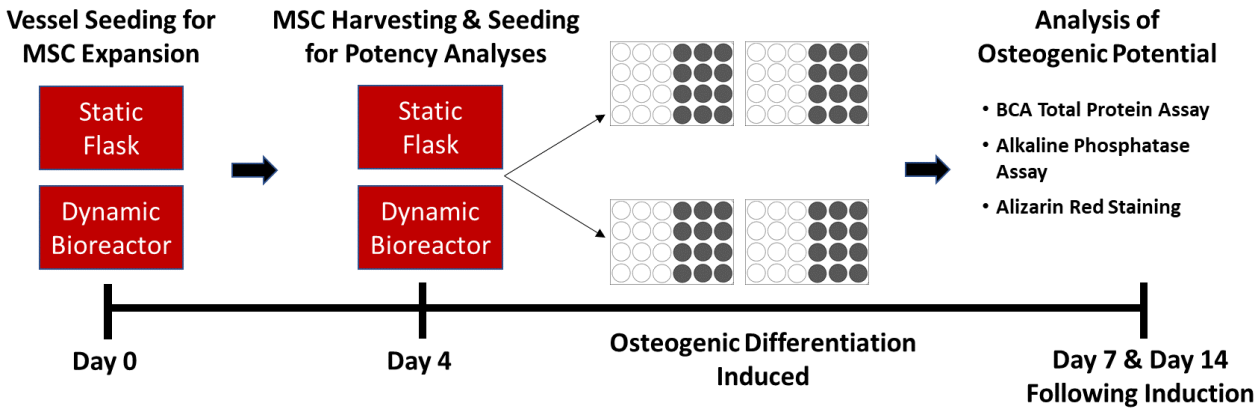

Figure 10. Schematic demonstrating timeline used for conducting experiments.

3.2.9 PROTEIN ANALYSIS

Protein samples were collected at Day 7 and Day 14 post-differentiation. Briefly, M-PER Mammalian Protein Extraction Reagent (Thermo Fisher Scientific) was used to extract protein samples, according to the manufacturer's instructions for monolayer culture. Total protein concentration was determined using the Pierce BCA Protein Assay (Thermo Fisher Scientific). Standards and working reagent required for the assay were prepared according to the manufacturer's instructions in order to create a precise standard curve to compare the unknown protein quantities. After samples and standards were plated, the working reagent was added, and the plates were shaken for 30 seconds on a rocker to mix the solutions before being incubated for 30 minutes at 37°C. The plates were allowed to cool to room temperature before the absorbance was read at 562 nm with a Biotek 800TS microplate reader.

Alkaline phosphatase (ALP) protein activity was determined using an Alkaline Phosphatase Assay Kit (BioVision Inc.). A set of standards was prepared for the standard curve following the manufacturer's instructions. The standards were pipetted into individual wells in duplicates. A volume of 50 µL of each test sample was pipetted into individual wells in duplicates, along with 50 µL of 5mM p-nitrophenyl phosphate (pNPP) solution. ALP conversion was activated

with 10 μL of ALP enzyme, and the plate was incubated in the dark at room temperature for 1 hour. The conversion was stopped by adding 20 μL of Stop Solution to each well, and then plates were placed on a shaker briefly to mix gently. The absorbance of the samples was read at 405 nm with a plate reader. The amount of pNPP created by ALP was calculated with the standard curve, and the ALP activity was calculated following the manufacturer's instructions. ALP concentration was then normalized to total protein content determined via BCA assay.

3.2.10 MINERALIZATION ASSESMENT

Following culturing in osteogenic medium for 14 days, cells were evaluated for mineral formation as an indicator of differentiation. Calcium deposits in the well plates were stained with 500 μL of 2% Alizarin Red working solution made by dissolving 2 g Alizarin Red S (#A-5533, Sigma-Aldrich) in 100 mL H_2O. Stained cells were then washed with water four times and visualized by phase microscopy. To quantify mineralization, the wells were destained with 10% acetic acid (Thermo Fisher Scientific), and the destained solution was collected. The absorbance of the destained solutions was measured using a Biotek 800TS microplate reader (Biotek, Winooski, VT) by reading at 405 nm. Absorbance of the destained solution was normalized to total protein content.

3.2.11 STATISTICAL ANALYSIS

Statistical analysis was performed using GraphPad Prism 6 (GraphPad Software Inc.). Experimental data was tested for statistical significance using an unpaired t-test, one-way ANOVA, two-way ANOVA, and the Tukey post-hoc test. A difference of $p < 0.05$ was noted to be statistically significant. Data is expressed as mean and standard deviation.

3.3 RESULTS

3.3.1 BIOREACTOR ASSEMBLY VALIDATION

The bioreactor assembly revealed that PTFE thread sealant tape would be required for the threading on the outlet cap to prevent the cell medium from leaking out. Without the PTFE tape, the bioreactor would be an open system and would compromise sterility. Several spots along the areas where the custom cut Lexan™ had been bonded together needed an additional pass with methylene chloride to ensure the air-tight seal. Overnight leak tests with the pump running increased confidence in the ability of the system to run without oversight as the result was a successful run with no leaks. A non-stick pan was purchased to place beneath the bioreactor stand as a precaution for the incubation of the assembled unit.

3.3.2 PRELIMINARY CELL ATTACHMENT EVALUATION

The ability of the plasma-treated Lexan™ insert to support anchorage-dependent cell culture was assessed. Qualitative evaluation of cell attachment with LIVE/DEAD® staining showed that after 24 hours of culture, green-stained cells were visibly present for both the flask and the bioreactor insert. Cell attachment was relatively the same for both the flask and insert culture, with little to no dead cells observed (Figure 11). At Day 4, assessment of the cell attachment showed increased cell growth, when compared to 24 hours, as more green-stained cells were observed for both the flask and the bioreactor insert. Qualitative comparison of the flask to the bioreactor insert showed greater confluency for the bioreactor than for the flask cultures at Day 4 (Figure 12).

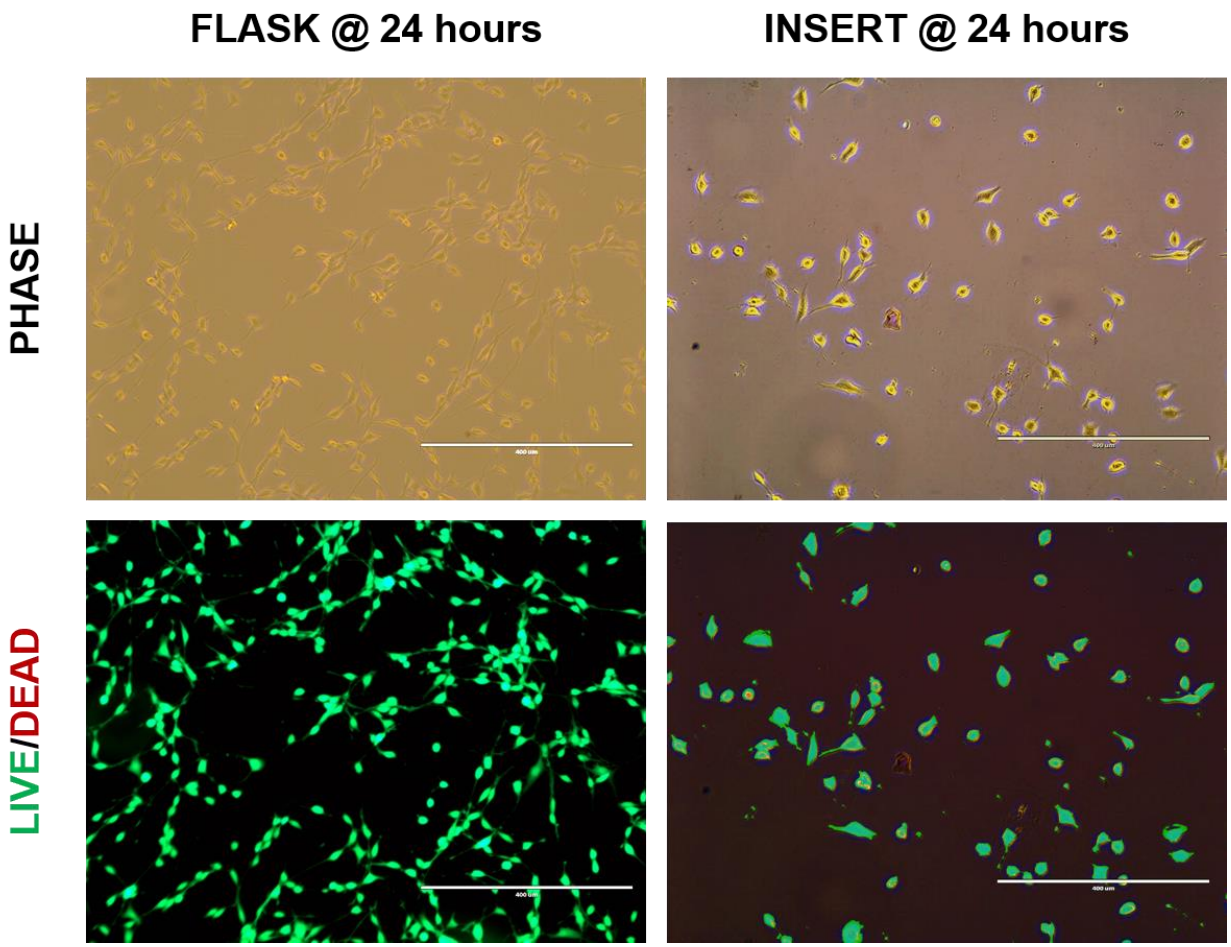

Figure 11. Representative images of cells cultured for 24 hours in a static control flask (left) or on the Lexan™ bioreactor insert (right). Cells stained using a LIVE/DEAD® Viability assay indicate live, viable cells with green fluorescence and dead cells with red fluorescence. The top row shows D1 cells under transmitted light, and the bottom row shows cells with GFP and Texas Red overlay to visualize stained cells. All images captured using 10× objective magnification.

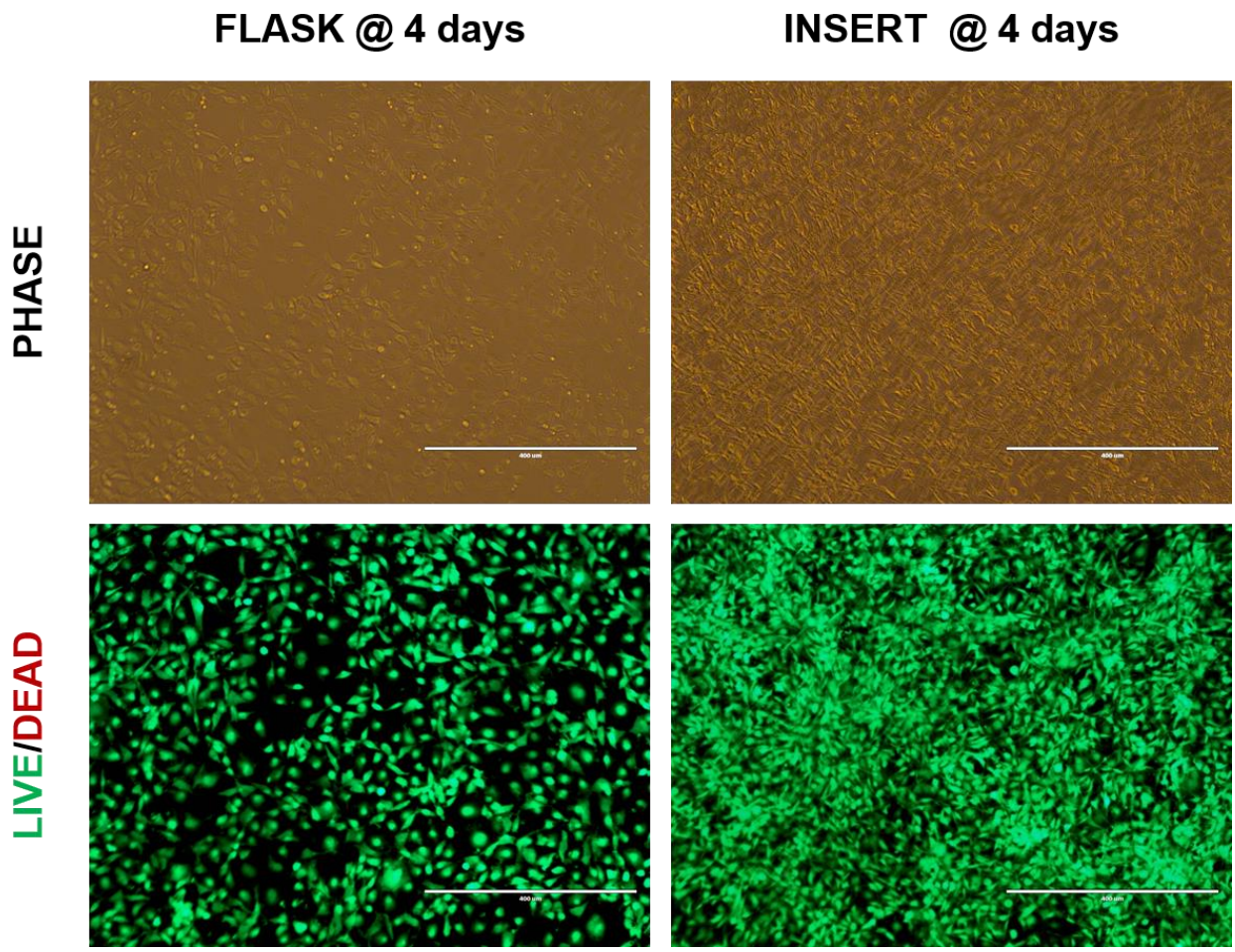

Figure 12. Representative images of cells cultured for 4 days in a static control flask (left) or on the Lexan™ bioreactor insert (right). Cells stained using a LIVE/DEAD® Viability assay indicate live, viable cells with green fluorescence and dead cells with red fluorescence. The top row shows D1 cells under transmitted light, and the bottom row shows cells with GFP and Texas Red overlay to visualize stained cells. All images captured using 10× objective magnification.

3.3.3 SHORT-TERM HARVEST AND EFFICIENCY EVALUATION

Cell proliferation was observed to evaluate culture efficiency after allowing cells to remain in culture for 4 days. Cells were harvested and counted to determine cell yield for three individual trials, as shown in Table 4. The average cell yields for the static flask and bioreactor culture were determined to be 11×10^6 and 14.8×10^6, respectively, as shown in Table 4 and Figure 13. Evaluation of the cell yields showed that the bioreactor yielded a higher number of cells, on average, than the

traditional flask; however, no statistical significance was observed when the conditions were compared with an unpaired t-test ($p > 0.05$).

Table 4. Comparison of cell yields for each culturing vessel.

	Static	**Dynamic**
Trial 1	5,850,000	13,392,500
Trial 2	9,150,000	16,950,000
Trial 3	11,425,000	17,462,500
Trial 4	12,500,000	11,400,000
Average	11,025,000	14,801,250

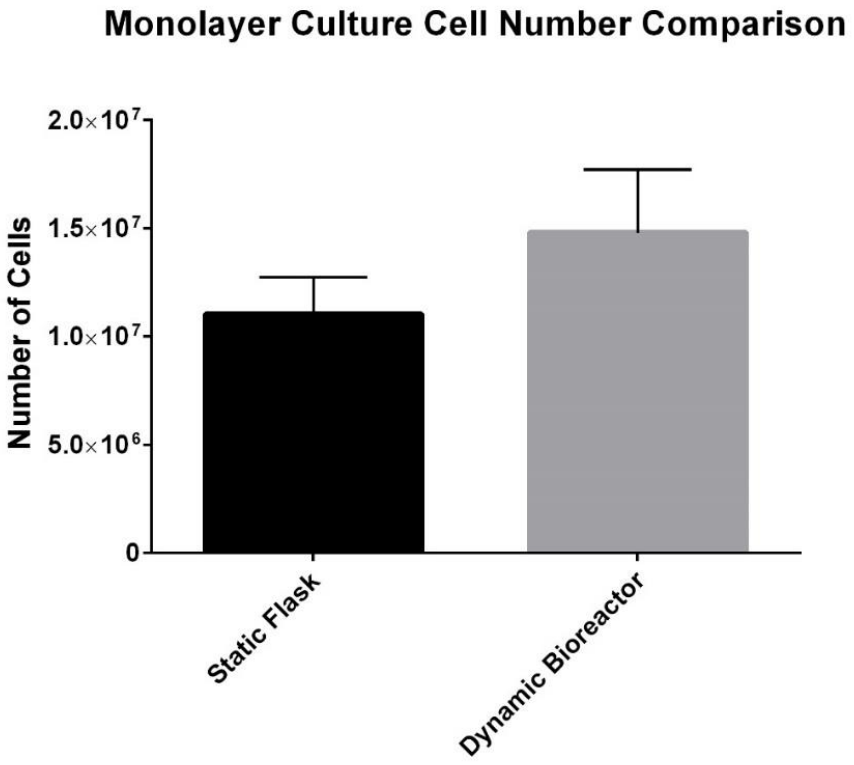

Figure 13. Monolayer cell yields after 4 days of culturing in the control T-75 tissue culture flask and the bioreactor Lexan™ insert.

The doubling time (DT) of the cells was also calculated using the following equation and then averaged:

$$Doubling\ time = DT = (t - t_0) \times \frac{\log 2}{(\log N - \log N_0)}$$

where N_0 = initial cell number seeded, t_0 = specific starting time, and N = number of cells at a given time, t [119]. The average DTs are shown in Figure 14. The DT for the bioreactor culture was shorter than the DT for the static flask culture, however, there was no statistical difference observed for the conditions ($p > 0.05$).

Figure 14. Doubling times were calculated using the previously described equation. There was no statistical significance observed.

3.3.4 METABOLIC ANALYSES

Media samples were collected on the final day of culturing from both the flask and the bioreactor vessel and analyzed to assess the metabolism of the cells in the different culture conditions by measuring the concentrations of glucose and lactate in the media. These "conditioned media" samples were then compared to the standard culture growth media without any cells. At Day 4 of culture, all of the glucose was depleted from the media in the static flask (Figure 15A), and the lactate levels were high in comparison to the baseline control media sample (Figure 15B) Alternatively, for the bioreactor culture, at Day 4, while there was an increase in lactate observed due to production by the cells, there was glucose still present in the media, with a significantly higher concentration noted ($p < 0.05$).

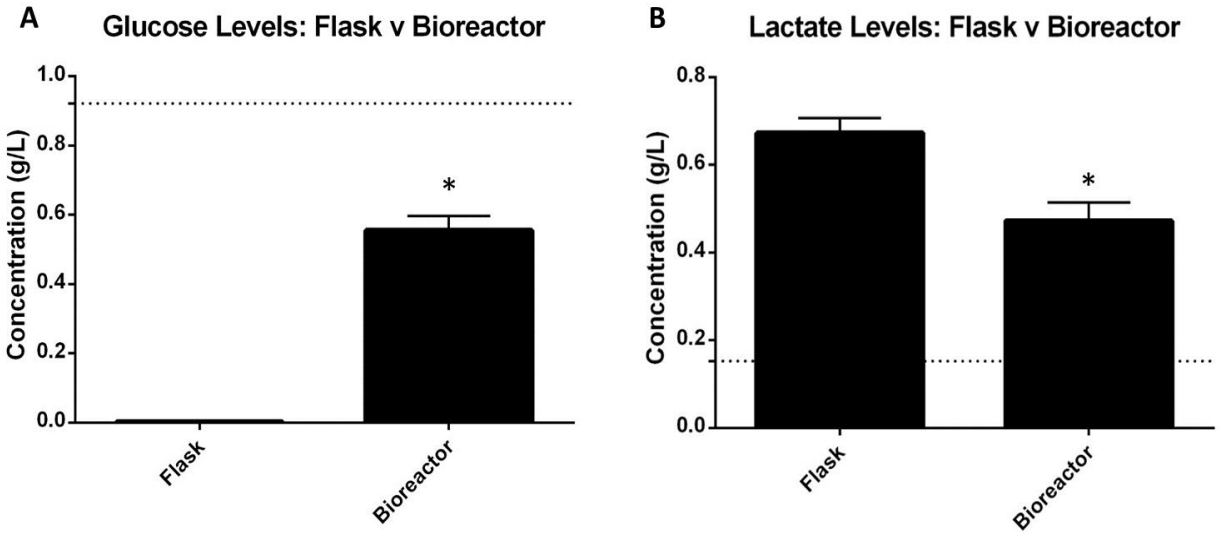

Figure 15. A) Comparison of the glucose levels measured in the conditioned media from the static flask culture and the dynamic bioreactor vessel system. B) Comparison of the lactate concentration measured for the conditioned media of the static flask system and the dynamic bioreactor vessel system. The dotted line for each graph indicates the level of glucose or lactate measured for a control media sample without cells. Statistical significance indicated with an asterisk (*).

Quantification of hydrogen peroxide, a reactive oxygen metabolic byproduct, was determined using the aforementioned assay kit. Comparison of the measured hydrogen peroxide

levels for media from the static flask to that from the bioreactor showed no statistical difference ($p > 0.05$) between the levels of hydrogen peroxide for media from either vessel (Figure 16).

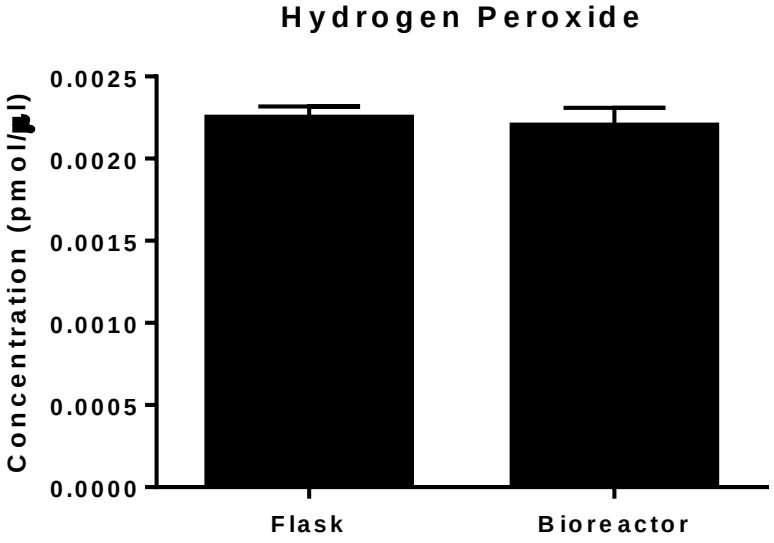

Figure 16. Comparison of the hydrogen peroxide levels measured for cells in the static flask and the bioreactor.

3.3.5 EVALUATION OF MSC OSTEOGENIC POTENTIAL

The MSCs expanded in the bioreactor or in the static flask were seeded into well plates after expansion to assess their potential differentiation to bone. Cells were either cultured using DMEM-Complete growth medium or osteogenic differentiation medium and assessed on Day 7 and Day 14, and assays were performed to measure total protein, ALP activity, and mineral formation.

3.3.6 PROTEIN ANALYSIS

In order to evaluate the density of cells seeded to assess osteogenic potential at Day 7 and Day 14 of culture, protein samples were collected at each respective day for all culture conditions. BCA protein assay was used to determine the total protein concentration. Total protein was

relatively comparable for all conditions at Day 7. However, there was significantly higher protein ($p= 0.0153$) measured for the cells from dynamic bioreactor culture in differentiation medium than those cultured in control medium (Figure 17A). Similarly, at Day 14, total protein was comparable for most conditions, however, the cells cultured in differentiation medium had significantly higher protein measured for both cells from the static flask ($p= 0.0041$) and the dynamic bioreactor ($p= 0.0017$), when compared to their respective controls cultured in control medium (Figure 17B).

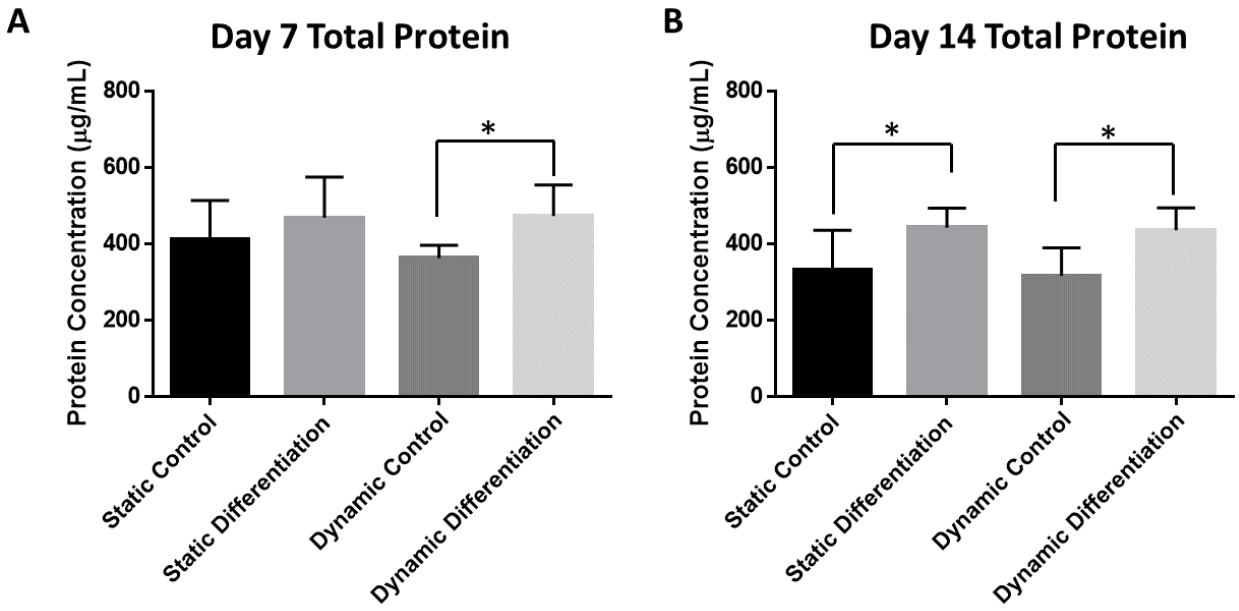

Figure 17. Comparison of average total protein measured using BCA assay at Day 7 (A) and Day 14 (B) for cells cultured with or without osteogenic media after harvesting from flask or bioreactor culture for three trials. Statistical significance indicated with an asterisk (*).

ALP protein activity was determined using an ALP Assay Kit and then normalizing the obtained values to the total protein concentration for each respective well (determined with BCA assay). As shown in Figure 18, a slight increase in ALP activity was observed from Day 7 to Day 14 for most conditions. ALP activity was highest at Day 14 for samples treated with control medium from the flask and bioreactor in Trials 2 and 3. Comparison of samples treated with control

medium from the flask and bioreactor showed significantly higher ($p < 0.05$) ALP activity than their respective cells cultured in osteogenic medium for those trials (Figure 18B). Further, when averaged to compare differentiated cells from the flask and bioreactor across all trials, there was no significant difference observed between the groups, although the bioreactor ALP was slightly higher.

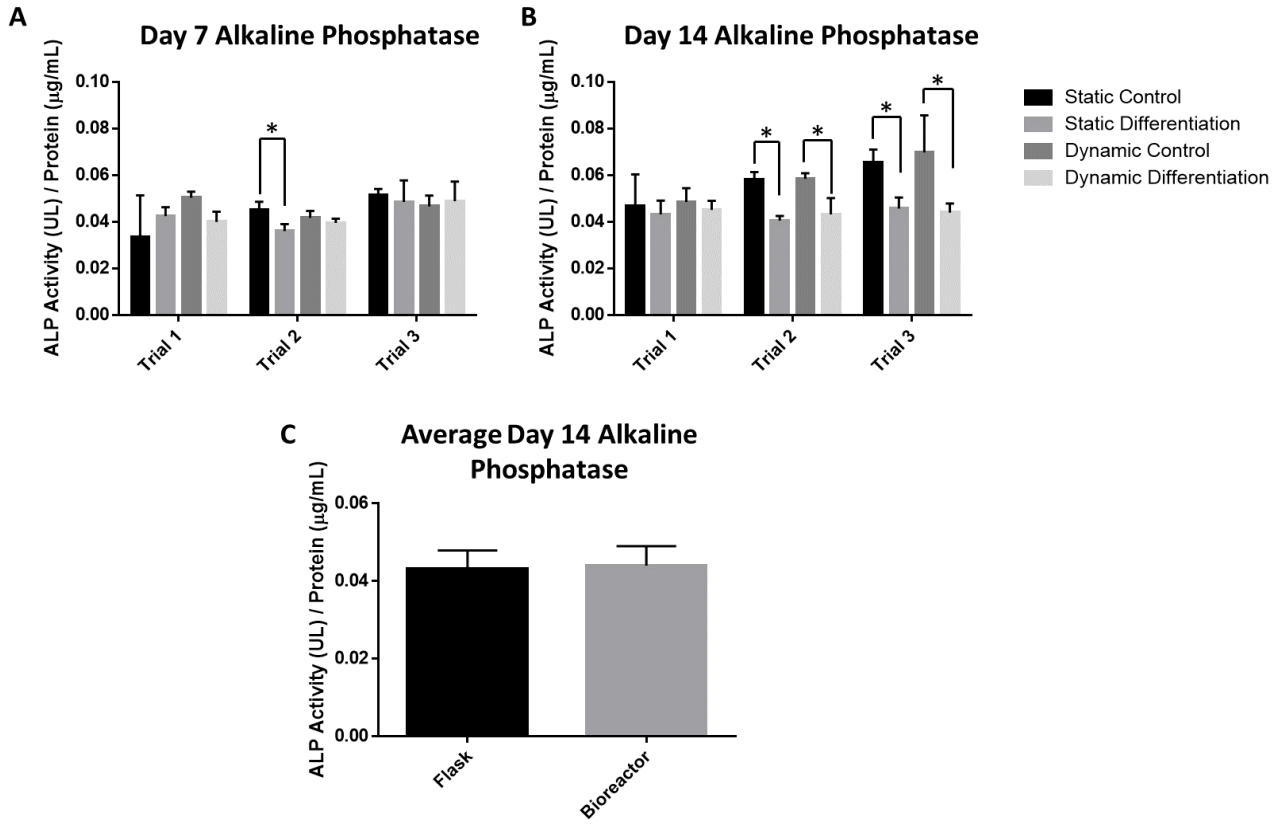

Figure 18. Comparison of ALP activity values normalized to total protein for each trial at Day 7 (A) and Day 14 (B). Average values for the differentiated cells from the flask and bioreactor were compared (C).

3.3.7 MINERALIZATION ASSESSMENT

At Day 7, microscopic evaluation showed that cells cultured in the control DMEM-Complete medium appeared very similar to the cells receiving osteogenic differentiation media,

with little to no mineralization observed for any of the cells (Figure 19). At Day 14, no mineralization was observed for cells cultured with DMEM-Complete growth medium, however, visible calcium formation was observed for cells from the static flask and the bioreactor that were cultured in osteogenic differentiation medium, as shown by the red-stained mineral nodules for those conditions (Figure 20).

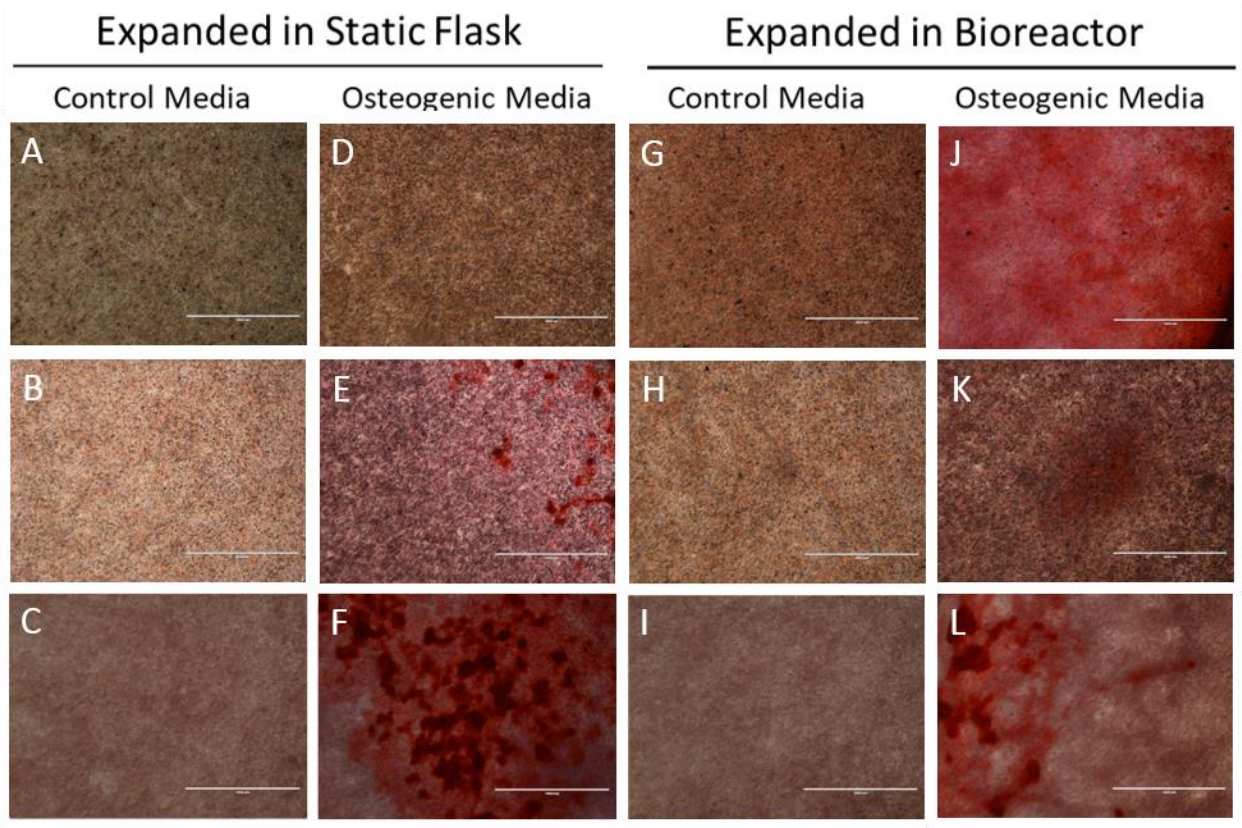

Figure 19. Alizarin Red staining on Day 7 for cells cultured from the control flask (A, B, & C) in control media without osteogenic additives and the cells cultured from the control flask in osteogenic differentiation media (D, E, & F). Cells at Day 7 from the bioreactor (G, H, & I) in control media without osteogenic additives and the cells from the bioreactor exposed to osteogenic differentiation media (J, K, & L). All images captured at 4X objective magnification. Scale bar = 1000µm.

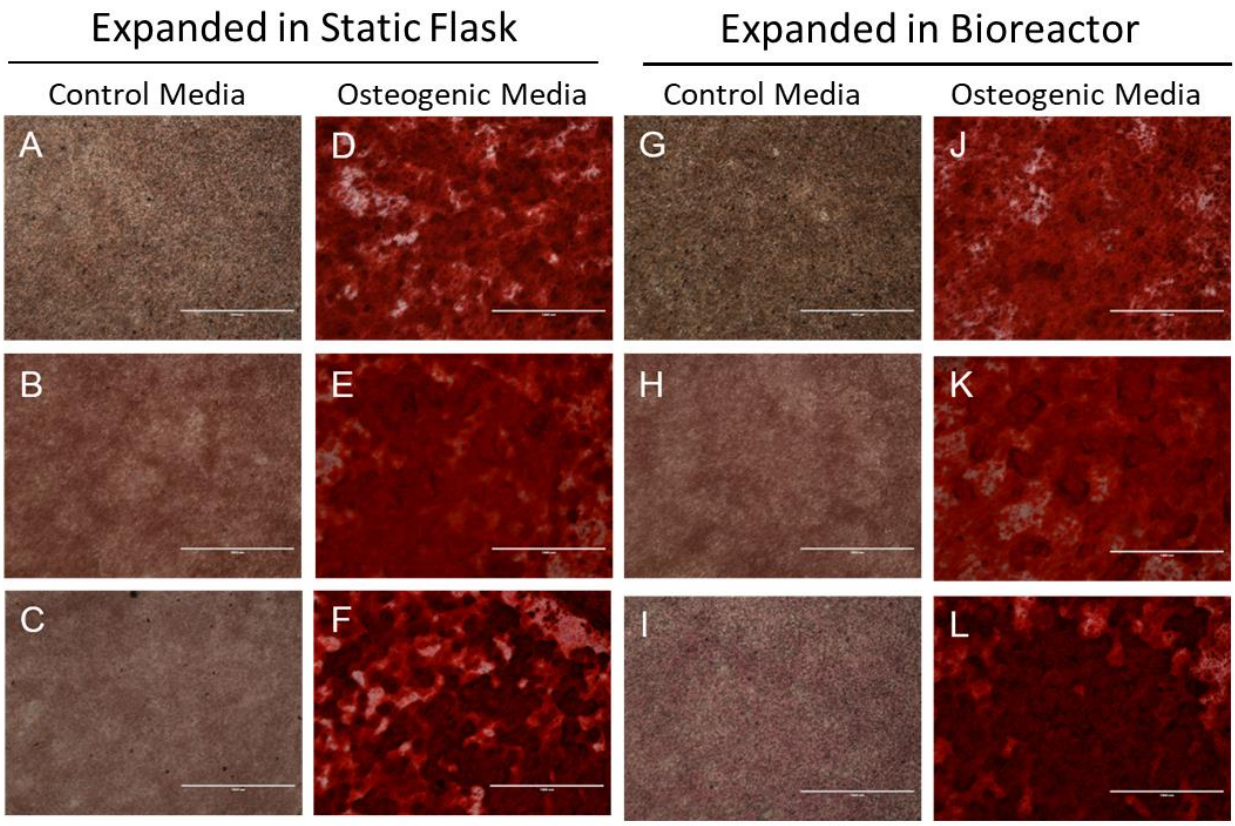

Figure 20. Alizarin Red staining on Day 14 for cells cultured from the control flask (A, B, & C) in control media without osteogenic additives and the cells cultured from the control flask in osteogenic differentiation media (D, E, & F). Cells at Day 14 from the bioreactor (G, H, & I) in control media without osteogenic additives and the cells from the bioreactor exposed to osteogenic differentiation media (J, K, & L). All images captured at 4X objective magnification. Scale bar = 1000µm.

The amount of Alizarin Red staining of calcium deposits was quantified by destaining each sample with acetic acid and measuring the absorbance of each sample at Day 7 and Day 14. The absorbance values from the Alizarin Red were then normalized to the average total protein concentration for that condition. The results for each of the three trials is shown in Figure 21A&B. At Day 7, there was little Alizarin Red staining measured for any of the conditions (Figure 21A). By Day 14, there was significantly higher ($p < 0.05$) Alizarin Red measured for cells from the flask and bioreactor that were cultured in osteogenic media, as compared to Day 7 (Figure 21B). The

average quantity of Alizarin Red was then determined for all trials and the resulting quantity of Alizarin Red for cells obtained from the flask and bioreactor and cultured in osteogenic media were compared. Samples identified as outliers, specifically from wells that exhibited extreme cellular contraction during culturing, were excluded from the analyses of all trials. As shown in Figure 21C, while the cells harvested from the flask had higher mineralization based on Alizarin Red staining, there was no statistical difference observed when compared to the cells harvested from the bioreactor and then differentiated ($p < 0.05$).

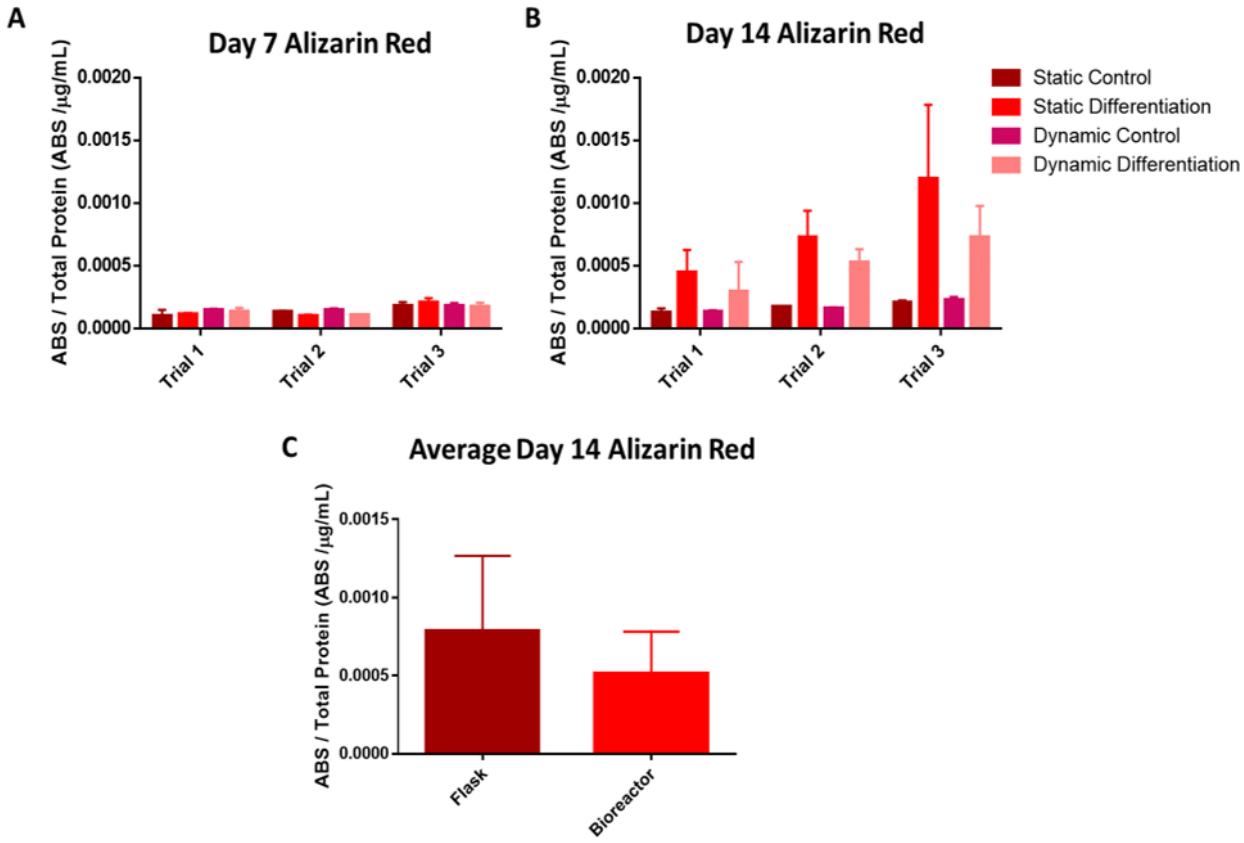

Figure 21. Comparison of the Alizarin Red destained solution normalized to total protein for each trial at Day 7 (A) and Day 14 (B). Average values for the differentiated cells from the flask and bioreactor were compared (C). Statistical significance indicated with an asterisk (*).

3.4 DISCUSSION

MSCs respond actively to their environment and designing an environment than mimics the *in vivo* environment of the human body, literature has shown that such dynamic environments can result in the production of bioactive factors and impact the expansion and differentiation potential of stem cells [43, 120, 121]. Bioreactors can be automated to tweak said characteristics and it is of great interest to researchers to explore such operating conditions to optimize the and standardize said culturing conditions [61]. Here, the experiments detailed in this chapter focused on proof-of-concept to demonstrate the feasibility of the designed bioreactor to support MSC expansion under dynamic conditions. While two variations for culturing were developed using a monolayer or microcarrier insert, specifically, for this phase of work, the focus was developing a protocol for monolayer cell culturing inside this custom-built closed-loop perfusion flow bioreactor system to determine effects on cell yield and metabolic products present in the spent culture medium.

When developing the design for the bioreactor system, several characteristics and features were desired such as a closed system that will not be opened to prevent contamination; a well-mixed system for the prevention of concentration gradients; and an environment that will improve biofactor production that could increase the potency of the MSC population (shown in table 2) [48, 122, 123]. The original design proposed (shown in Appendix Figure A1) consisted of a rectangular chamber made of Lexan™ that featured thin culturing plates that would fit into the contoured bottom of the vessel. The culturing plates had the potential to support hydrogel layers, with small arms to secure in place. The flow of the media would pass over the culturing plate horizontally and remove all spent media and refresh with new media. This design was ultimately rejected because of the potential “dead spots” or accumulation areas of spent media and dead cells that

could not be removed from the system in the corners of the vessel, as the corners made the vessel less streamline.

The working design, as shown in Figure 6, which was ultimately fabricated for experimental *in vitro* testing is cylindrical and vertical with a smooth design that allows for the flow of media. As opposed to the square design, this shape presents less area for accumulation of waste products that could not be removed from the vessel. Further, this design was easier to machine, with fewer total parts, which was easier for assembly in the lab and increased potential of cost-effective manufacturing.

The material selected for the monolayer cell culture inserts, Lexan™, is a polycarbonate that does not typically support adhesion essential for anchorage-dependent cell culture because of its smooth surface and low surface charge [124]. Therefore, surface treatment was necessary to modify the surface characteristics of the Lexan™ for cell culturing. Plasma treatment was performed in order to etch away the biological particles on the surface, and deposit charged molecules along the material surface, thus changing the surface chemistry to a more hydrophilic surface [125]. In addition, the cell culture inserts were soaked in ethanol for sterilization and further surface preparation. The structure of ethanol will donate additional protons to the surface of the insert via hydroxylation which increases the hydrophilic property of the surface and increasing wettability [126]. Typical tissue culture-treated plastics for cell culture are commonly plasma treated, thus, the combination of plasma treatment and the ethanol wash yielded a surface on the Lexan™ inserts comparable to standard culture-treated flasks on the market, which were used as our controls for comparison within experiments [127].

Once the bioreactor system was prepared for monolayer culture experiments, a cell line for the proof-of-concept testing needed to be selected. The selected cells, D1 cells, are murine bone

marrow-derived MSCs with demonstrated multipotent potential, including favorable osteogenic potential [128, 129]. Additionally, this cell line has a fast growth rate compared to the growth rate of human bone marrow-derived MSCs, and prior experience working with them showed these cells to be hearty, which would serve well for the proof-of-concept testing [130, 131]. Because stem cells are anchorage-dependent, proper cell attachment to the culture substrate is essential for growth and subsequent proliferation [59]. In order to evaluate the efficiency of the treatment of the Lexan™ inserts, a preliminary evaluation of cell attachment was performed after 24 hours and a follow-up evaluation to assess proliferation was conducted after 4 days of culturing in the bioreactor. Preliminary evaluation of cell attachment to the treated inserts was performed using a LIVE/DEAD® assay for qualitative assessment. The LIVE/DEAD® assay contains two probes: calcein AM and ethidium homodimer-1 (EthD-1). The calcein AM dye will fluoresce green after permeating the membrane of live cells. The EthD-1 will fluoresce red in dead cells after binding to exposed nucleic acids of the dead cells with a broken membrane because EthD-1 cannot penetrate the intact membrane of live cells.

As shown in Figure 11, at the 24-hour time point, both the flask and the Lexan™ insert exhibited green fluorescing live cells and no red fluorescing dead cells. When anchorage dependent cells die, cell detachment is observed, so it was expected to see little to no red fluorescence. At the 4-day time point, the Lexan™ insert exhibited a high density of green fluorescing cells compared to that of the cells seen in the flask at the same time point (Figure 12). This visually indicates that the dynamic environment of the bioreactor did not impede the proliferation of the D1 cells, thus indicating the selected culture conditions (i.e., flow rate, seeding density, culture time, etc.) were sufficient for cell expansion in the bioreactor. Additional

experiments were then performed to quantitatively assess the expansion capacity of the bioreactor system.

As previously described in the short-term expansion of the materials and methods, the T-75 flask and the Lexan™ insert of the bioreactor system were seeded with the same density of cells, 400,000 cells/cm^2 and cultured for four days (n = 4). The cells were harvested and counted manually by Trypan Blue exclusion with a hemocytometer. The cell yield comparison can be seen in Fig 13, where the bioreactor system had a higher cell count, on average, of 14.8×10^6 cells, as compared to the flask with an average of 11×10^6 cells. The data was then used to calculate the doubling time of the cells and the results were similar (Figure 14), with the doubling time for the D1 cells cultured in the bioreactor system at approximately 52.5 hours, as compared to approximately 67.4 hours in the flask. While there was no statistical difference in cell yield or doubling time, these results do confirm that the dynamic environment did not decrease the expansion potential of the stem cells compared to the control at these conditions. Further studies using a greater number of replicates may be needed to determine statistical significance, and additional studies could be performed to determine effects of flow rate on cell yields to see if bioreactor culture results in increased cell numbers over time.

MSCs secrete bioactive molecules such as cytokines and chemokines, growth factors such as vascular endothelial growth factor (VEGF), extracellular matrix (ECM) proteins and metabolites in conditioned media, spent media [132, 133]. It has been reported that conditioned media can be beneficial in stem cell expansion and differentiation by exposing the target cell population to specific metabolites, ECM proteins and growth factors [120, 134]. Thus, media samples were collected at the end time point of the short-term expansion from the bioreactor vessel and static flask and used to evaluate the metabolic activity of the cells in the two culturing systems.

Glucose and lactate are related through the cell metabolic cycle such that, as glucose in culture media is consumed, lactate is produced as a waste product [135]. Levels of glucose and lactate in spent media from the vessels were determined and compared to those measured for fresh media not in contact with cells. After 4 days of culturing, the concentration of glucose in the flask was almost completely depleted, while the bioreactor vessel media still maintained more than half the initial concentration (Figure 15). Since there is a greater volume of media in the bioreactor vessel than the flask, the bioreactor can support longer term culturing with less maintenance (i.e., media replenishment not required as frequently). Comparison of the lactate levels were as expected; the flask had higher levels of lactate than the bioreactor vessel because the greater volume of media in the vessel essentially diluted the lactate (Figure 15), resulting in a more balanced state for the cells. This is an additional advantage for the bioreactor system as the dilution of lactate will decrease its concentration and the resulting pH of the media will not decrease as quickly. Culture media has buffers present to balance the pH but metabolite production, the increase in the concentration of H+ ions in the media, can acidify the media and damage the cells [136].

The media samples were also tested for the presence of hydrogen peroxide (H_2O_2), which is a reactive oxygen species (ROS) that is a metabolic byproduct of stem cells. Hydrogen peroxide is produced when oxygen is partially, or incompletely, reduced which can have a negative impact on cell culture quality [137]. ROS accumulation can cause damage within the cells and induce a loss of function and rapid aging which will decrease the potency of stem cells [138]. Hydrogen peroxide is produced during cell metabolism of healthy cells and has also been reported to play a role in controlling inflammation as a signaling molecule [139-141]. Comparison of the hydrogen peroxide data showed a very small difference, not statistically significant, between the two culturing conditions during the short-term expansion, thus indicating similar levels of metabolic

activity (Figure 16) irrespective of culture environment. However, while the concentrations have a small difference, the volumes of the culturing system are much different. The greater volume of the bioreactor system will dilute the concentration of hydrogen peroxide, so the amount is higher. This is correlates with the slightly higher cell yield from the bioreactor system.

Cells cultured during the short-term expansion were harvested and seeded for further culturing to examine how the dynamic culture could have impacted the potency, or differentiation potential, of the D1 cells. Literature has shown that MSCs respond actively to their environment and will secrete various growth factors for proliferation, angiogenesis, and to reverse the effects cell damage from mechanical stimulation, radiation or hypoxia [142]. Thus, it was important to determine if a continuous flow of media would diminish or enhance the stem like properties of the cultured cells [120]. As proof-of concept, we evaluated the cells for their osteogenic potential, with assays performed at Day 7 and Day 14 post-differentiation.

Initial evaluation of total protein content was performed to determine cell density for each condition. The measured protein levels were mostly comparable across all conditions at Day 7 and Day 14, which was as expected since the same initial seeding density was used for all wells. For differentiation to occur, cells must have progressed past the proliferation stage to allow proper cell signaling to occur, thus, our reason for using a high seeding density (close to confluence) for seeding. Since the cells were seeded at a high density, continued culture of cells in the control media resulted in a slight decrease of protein production over time from Day 7 to Day 14 and when compared to the respective cells cultured in differentiation medium. This was not surprising given the limited surface area available for continued proliferation in the multi-well plates that was likely observed for cells in the DMEM-Complete medium, as opposed to the cells cultured in differentiation media that were no longer proliferating. When a cell population reaches a high

density, and runs out of space to expand, they cells will halt proliferation which can lead to a mutation that could lead tumor formation from uncontrolled division or cell death from glucose starvation [143, 144]. These findings are indicative that cells cultured in the bioreactor maintain proliferation potential post-expansion.

Protein samples were further analyzed to assess ALP activity. ALP is important for bone formation and is a biomarker to track the process of mineralization, and it is closely associated with bone metabolism [144, 145]. From Day 7 to Day 14, there was a slight increase in ALP for most conditions, and the highest at Day 14 samples cultured with control medium exhibited the highest levels of ALP for certain trials. However, when averaged across trials, there was no significant difference observed between the groups, although the bioreactor ALP was slightly higher. This outcome was not entirely as expected, given the association of ALP with bone metabolism, where ALP was expected to increase as osteogenesis progressed. In this work, however, cells were cultured in osteogenic media for 14 days, whereas many *in vitro* studies have used culture periods of 21 to 28 days for bone cell differentiation [45]. If the cells had differentiated for longer, there may have been a larger difference in ALP concentration and activity between the two culturing conditions observed, however the potential for bone differentiation was still affirmed as no inhibition or reduction was observed.

Mineralization was also assessed to evaluate bone-related function for the cells in culture. As expected, at Day 7 there was little to no mineralization observed for any conditions as shown by Alizarin Red images and subsequent quantification. After 14 days of exposure to osteogenic differentiation media, the mineralization was observed for cells from the static flask and dynamic bioreactor. Quantification of the destained Alizarin Red solution showed greater apparent mineralization for the static flask cells, although not a significant difference. Closer evaluation of

the samples in this work showed that for the D1 cells harvested from the bioreactor and then differentiated, cells began to contract and pull away from the edges of the well plate (Figure 22), which resulted in reduced density of cells comprising the confluent monolayer, and subsequently an apparent reduction in formed mineral for differentiated cells. This contraction could be attributed to behavior of the D1 cells, where despite being given osteogenic differentiation media that should halt cell division, they still proliferate, run out of surface area to expand and contract from the surface of the culture substrate. While this contraction resulted in lower Alizarin Red staining, the cells from the bioreactor were still able to differentiate, indicating that potency of cells expanded in the bioreactor was maintained.

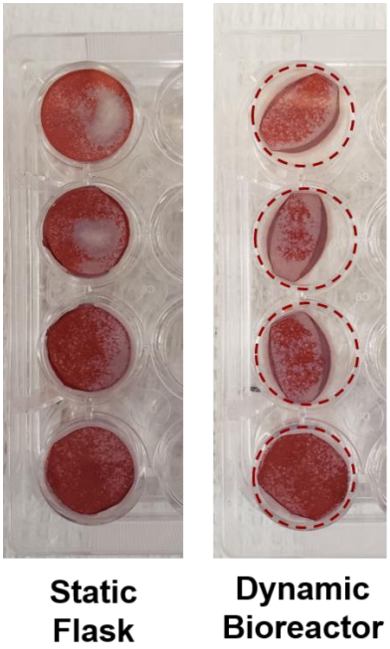

Figure 22. Photograph comparison of the Alizarin Red on day 14 of osteogenic differentiation. The cells from the flask (left) exhibited negligible contraction and the cells from the bioreactor system (right) exhibited noticeable retraction. The edge of the well on the right plate has been outlined in red dashes.

The final portion of the bioreactor validation consisted of an economic analysis. Table 5 compiles the materials and their cost for the bioreactor vessel fabrication and the bioreactor system

set-up. The largest portion of the cost went to labor for manufacturing which totaled $765.00 while the materials cost $267.64. The peristaltic pump was the most expensive portion of the bioreactor system at $1,750.00. All of the purchases for the bioreactor system are considered to be a one-time purchase that will have a long life of use unlike the flasks used in culture, which are one-use only that cost $92.30 for a 60-case. In our lab, typically more than one person at a time is running experiments so materials like culturing flasks and pipette tips can get used up quickly and require re-ordering. A list of materials commonly used in cell culture was tabulated in Table 6 to help calculate the culturing cost comparison seen in Table 7. It cost significantly less to culture cells in a flask than in the bioreactor system the first time after assembling the bioreactor system, $49.01 to $2,815.07. However, the next time the culturing systems are compared, the cost of manufacturing and the system components like the pump do not have to be re-manufactured or re-purchased which brings down the overall cost to only $50.12 as seen in Table 8. After 232 rounds of experiments, the flask system will cost more to continue using. The cost may be high for the initial manufacturing of the system but the experiments that follow only cost $2.65 more than culturing in a flask.

Table 5. Bioreactor fabrication component list

Bioreactor Fabrication				
Item	**Description**	**Ordered**	**Units**	**Amount**
Lexan™ Polycarbonate Sheet	0.060"(1.5mm) x 12" x 12" Lexan™ Polycarbonate Sheet	6		$ 20.46
Lexan™ Polycarbonate Sheet	0.354"(9.5mm) x 24" x 24" Clear Lexan™ 9034 Polycarbonate Sheet	1		$ 77.41
Impact Resistant Polycarbonate	Impact Resistant Polycarbonate			$ 38.36
Polyvinyl Chloride (PVC) Rod		1.5	lb.	$ 6.66
PVC Sheet		0.5		$ 2.50
Barbed Hose Attachment	Cole-Parmer NPT Male Adapter to Hose Barb, 1/16" NPT to 1/8" ID, PVDF	10	pack	$ 22.25
Miscellaneous	Small parts and materials			$ 100.00
Labor	Instrument Design & Fabrication Shop: CB & JA			$ 765.00
	Bioreactor System			
Peristaltic Pump	Masterflex L/S Digital Miniflex Pump, Single-Channel, 300 rpm, 90 to 260 VAC	1		$ 1,750.00
Tubing	Masterflex L/S Platinum-Cured Silicone Tubing, L/S 16, 25 ft	25	feet	$ 75.00
			TOTAL	$2,857.64

Table 6. Monolayer cell culture experiment material list

Experiment Materials				
Item	**Description**	**Ordered**	**Units**	**Amount**
	DMEM Complete Media Materials			
DMEM low-glucose media	Gibco™ DMEM, Low Glucose, Pyruvate	10	pack	$ 32.96
Fetal Bovine Serum	Fetal Bovine Serum Premium	500	ml	$ 578.00
Penicillin/Streptomycin	Gibco™ Penicillin-Streptomycin	100	ml	$ 23.25
500 ml filter system	Corning® 500 mL Vacuum Filter/Storage Bottle System	12	case	$ 162.56
	Culturing			
T-75 Flask	Falcon™ Tissue Culture Treated Flasks	60	case	$ 92.30
2 ml pipette	Fisherbrand™ Sterile Polystyrene Disposable Serological Pipets with Magnifier Stripe	500	pack	$ 109.77
5 ml pipette	Fisherbrand™ Sterile Polystyrene Disposable Serological Pipets with Magnifier Stripe	200	pack	$ 56.10
10 ml pipette	Fisherbrand™ Sterile Polystyrene Disposable Serological Pipets with Magnifier Stripe	200	pack	$ 61.39
25 ml pipette	Fisherbrand™ Sterile Polystyrene Disposable Serological Pipets with Magnifier Stripe	200	pack	$ 134.93
Glass pipette	Fisherbrand™ Disposable Borosilicate Glass Pasteur Pipets	1140	case	$ 96.52
PBS	Gibco™ DPBS without Calcium and Magnesium	500	ml	$ 22.67
Trypsin 0.05% EDTA	Gibco™ Trypsin-EDTA (0.05%), Phenol red	500	ml	$ 43.90
15 ml conical tube	Corning® 15mL PP Centrifuge Tubes, Bulk Packed with CentriStar™ Cap	500	case	$ 209.20
50 ml conical tube	Corning® 50mL PP Centrifuge Tubes, Conical Bottom with CentriStar™ Cap	500	case	$ 302.75
			TOTAL	$ 1,614.35

Table 7. Monolayer cell culture system comparison, first round

Culturing Cost				
Item	**Control Monolayer Cost**		**Control Monolayer Cost**	
	Amount	**Control Monolayer Cost**	**Amount**	**Bioreactor Monolayer Cost**
Cell Culture Set-up				
Culture Vessel	1	$ 1.54	1	$ 1,002.24
Peristaltic Pump	0	$ -	1	$ 1,750.00
Tubing	0	$ --	46 inches	$ 11.50
DMEM Complete Media				
DMEM Complete Media	150 ml	$ 23.91	150 ml	$ 23.91
DMEM, low glucose	*133.5 ml*		*133.5 ml*	
Fetal bovine serum	*15 ml*		*15 ml*	
Penicillin/Streptomycin	*1.5 ml*		*1.5 ml*	
Filtration Unit	1	$ 13.55	1	$ 13.55
Culturing Materials				
2 ml pipette	2	$ 0.44	2	$ 0.44
5 ml pipette	10	$ 2.81	5	$ 1.40
10 ml pipette	10	$ 3.07	15	$ 4.60
25 ml pipette	2	$ 1.35	5	$ 3.37
Glass pipette	10	$ 0.85	10	$ 0.85
PBS	5 ml	$ 0.23	15 ml	$ 0.68
Trypsin 0.05% EDTA	5 ml	$ 0.44	15 ml	$ 1.32
15 ml conical tube	2	$ 0.84	0	$ -
50 ml conical tube	0	$ -	2	$ 1.21
TOTAL		$ 49.01		$ 2,815.07

Table 8. Monolayer cell culture system comparison, second round

Culturing Cost				
	Control Monolayer Cost		**Control Monolayer Cost**	
Item	**Amount**	**Control Monolayer Cost**	**Amount**	**Bioreactor Monolayer Cost**
Cell Culture Set-up				
Culture Vessel	1	$ 1.54	1	$ 1,002.24
Peristaltic Pump	0	$ -	1	$ 1,750.00
Tubing	0	$ --	46 inches	$ 11.50
DMEM Complete Media				
DMEM Complete Media	150 ml	$ 23.91	150 ml	$ 23.91
DMEM, low glucose	*133.5 ml*		*133.5 ml*	
Fetal bovine serum	*15 ml*		*15 ml*	
Penicillin/Streptomycin	*1.5 ml*		*1.5 ml*	
Filtration Unit	1	$ 13.55	1	$ 13.55
Culturing Materials				
2 ml pipette	2	$ 0.44	2	$ 0.44
5 ml pipette	10	$ 2.81	5	$ 1.40
10 ml pipette	10	$ 3.07	15	$ 4.60
25 ml pipette	2	$ 1.35	5	$ 3.37
Glass pipette	10	$ 0.85	10	$ 0.85
PBS	5 ml	$ 0.23	15 ml	$ 0.68
Trypsin 0.05% EDTA	5 ml	$ 0.44	15 ml	$ 1.32
15 ml conical tube	2	$ 0.84	0	$ -
50 ml conical tube	0	$ -	2	$ 1.21
TOTAL		$ 47.47		$ 50.12

3.5 CONCLUSION

A continuous perfused flow bioreactor was designed and evaluated. Cells grown in the bioreactor system averaged a higher yield than the cells grown in the flask, but no statistical difference was observed between growth rates. The dynamic culture of the bioreactor system did not have a negative impact on the growth rate compared to the growth rate in the control. Media analysis revealed that the flask was depleted of glucose in the media, and the lactate levels were high. The bioreactor system diluted the lactate concentration due to the volume difference and there was still glucose for continued culturing time. Further media analysis examined the hydrogen

peroxide concentration in the media of both culturing systems; the flask had a higher concentration but not statistically significant, which indicates relatively similar metabolism for both culture vessels.

The osteogenic potential was tested by seeding the cells cultured in both systems in well-plates and culturing with either control growth medium or osteogenic differentiation medium. Evaluation of total protein showed cells from the bioreactor remained their proliferation capacity after expansion. Further, ALP analysis and Alizarin Red staining indicated that MSC potency was maintained for cells expanded in the bioreactor, although additional experiments with longer culture periods, increased number of trials and perhaps adjusted flow rates are essential to determine if properties of MSCs expanded in the dynamic bioreactor can be enhanced as compared to traditional static culture systems.

Future work will include evaluation of cells using the designed microcarrier culture platform for increased cell expansion, as shown below.

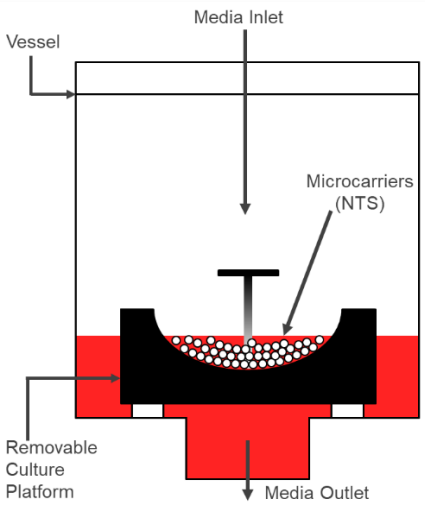

Figure 23. Schematic demonstrating set-up of bioreactor vessel for microcarrier cell culture experiments.

CHAPTER 4

MATHEMATICAL MODEL

4.1 INTRODUCTION

4.1.1 BACKGROUND

Cell culture and tissue growth are complex phenomena that contain many bioprocesses that are difficult to isolate and analyze through experimentation alone. Mathematical models and computer simulations offer researchers the opportunity to run a multitude of hypothetical scenarios. This allows for rapidly and in a cost-effective evaluation of system designs and can lead to bioreactor design optimization.

With proof-of-concept bioreactors like the one described in this thesis, it is important to develop math models to modify and optimize the design for future iterations. The concentration of nutrients in the growth medium such as glucose, waste products from cell metabolism such as lactate, which could acidify the medium, and other important nutrients for cell culturing like oxygen could be monitored with inline sensors. However, a math model in a proof-of-concept system, with experimental data to validate the math model at certain points, would be a useful in testing a series of hypothetical scenarios in a cost-effective manner.

We propose a system of equations that will be paired with experimental data detailed in the studies of the previous chapter to validate the system of equations. In addition, the mathematical model will be used to assess different variations of the experiments in order to explore operating conditions.

4.1.2 HYPOTHESIS

The focus of this phase of the project was to establish a system of equations that could be used to model critical culture parameters in a proof-of-concept model without sensors. We hypothesize that stem cells do not divide symmetrically, and a math model should reflect that. Additionally, the concentration of nutrients such as glucose, lactate and oxygen, should be modeled by Michaelis-Menten kinetics but also be directly related to cell number. If the system of equations can be assembled, a programming language will be used to model hypothetical scenarios that could optimize the design of future experiments.

4.1.3 OBJECTIVES

The objectives for this work were as follows:

1. Design mathematical model with a system of equations that can evaluate key parameters of monolayer cell culture in the bioreactor, including:
    a. Cell number/yield
    b. Glucose consumption
    c. Lactate production
    d. Oxygen consumption
2. Model the system of equations in MATLAB to evaluate hypothetical experiment

4.2 METHODS

4.2.1 MODEL DESCRIPTION

A mathematical model was designed to evaluate culture parameters that would typically be difficult to determine through experiment, without tedious reiteration. The bioreactor is a

continuous flow system with a cylindrical vessel that supports a monolayer culture insert for anchorage-dependent cell culture. It is assumed that the cells have the ability to be distributed uniformly along the surface of the insert due to its plasma treatment and additional protonation via an ethanol wash, making the surface comparable to that of industry-standard culture vessels currently available.

The volume is held constant with equivalent inlet and outlet volumetric flow rates. This leads to the assumption of the nature of the fluid properties of the cell growth medium in the bioreactor system. The liquid is assumed to be viscous with the presence of fetal bovine serum (FBS) in the medium and therefore, also Newtonian, like water. The medium contains cell nutrients to aid the cells in expansion such as glucose, nitrogen, oxygen, phosphates and FBS; the cells will output waste products such as lactate, carbon dioxide and water. The presence of FBS in the medium will contribute a small amount of lactate at the beginning of the model but will increase in concentration as culture time proceeds and not from media replenishment.

The model was derived from continuous stirred tank reactor (CSTR) design equations as the base for the conservation equations [67]. The bioreactor system is modular and can be altered, but this form was closest related to that of continuous flow systems. The model was used to predict the cell growth in the bioreactor system and the concentrations of glucose, lactate and oxygen; varying different parameters of the cell growth equation; and evaluating experimental data in comparison to the model.

4.2.2 DEVELOPMENT OF MODEL EQUATIONS

The mathematical model to describe parameters of the previously described bioreactor is a system of four ordinary differential equations (ODEs). There are three nutrient conservation

equations: the consumption of glucose (C_G) and oxygen (C_O) by the mesenchymal stromal cells (MSCs), and the production of lactate as a waste product in cell metabolism (C_L). The fourth equation describes cell density (C_N) and predicts cell growth and migration along the growth area in the bioreactor.

4.2.3 DEVELOPMENT OF NUTRIENT CONSERVATION EQUATIONS

The MSCs in the bioreactor vessel were cultured in low-glucose DMEM growth medium supplemented with 10% FBS. The media contains glucose and other additives previously mentioned to facilitate cell expansion in an *in vitro* environment. The equations for the conservation of glucose (C_G) and lactate (C_L) are derived from the base form of a general mass balance to describe the mass transport with design equations applied for continuous bioreactor systems for inlet and outlet flow (Figure 24).

[Rate of inlet flow of species A into the system] − [Rate of outlet flow of species A into the system] ± [**Generation** or **Consumption** of species A in the system] = [Rate of accumulation of A in the system]

Figure 24. A general mass balance [67].

The equations describing glucose uptake and lactate production are similar because lactate is produced as a result of glucose consumption and has been related with the multiplication of lactate yield from glucose metabolism ($Y_{L/G}$). The conservation of glucose and lactate are as follows:

$$\frac{dC_G}{dt} = (Q \times C_G) - \left(Q \times \frac{C_G}{1 + \frac{k \times C_G \times Vol}{U \times C_G}} \right) - \frac{V_{max,G} \times N \times C_G}{K_{m,G} + C_G}$$

and,

$$\frac{dC_L}{dt} = (Q \times C_L) - \left(Q \times \frac{C_L}{1 + \frac{k \times C_L \times Vol}{U \times C_L}} \right) - \left(Y_{L/G} \times \left(\frac{V_{max,G} \times N \times C_G}{K_{m,G} + C_G} \right) \right)$$

The glucose conservation equation begins with the inlet flow of glucose ($C_{G,in}$) introduced into the system by the pump at a constant flow rate (Q). The outlet flow is at the same numerical value flow rate (Q) as the inlet, but the concentration of glucose is modified to account for the consumption of glucose. The lactate conservation equation is similar. Both conservation equations have a consumption of glucose modeled by Michaelis-Menten kinetics as the model represents a way to describe the rate of enzymatic equations and the relationship between the substrate concentration and product formation [146]. Michaelis-Menten kinetics depend on the concentration of the desired substrate (C_G or C_L); maximum reaction rate (V_{max}) at the maximum amount of substrate concentration; the Michaelis-Menten constant (K_m) representing the concentration of substrate when the V_{max} is halved [146]. In both equations, the Michaelis-Menten kinetics are modified by the cell number (N) as the glucose consumption and the lactate production are directly proportional to the density of cells present.

The development of the oxygen conservation equation that describes the concentration of oxygen in the system from the air diffusing into the media. The inlet flow of the oxygen into the system has an additional source as the silicone material the system tubing is made from is permeable and allows for gas exchange. Below is the conservation of oxygen equation:

$$\frac{dC_O}{dt} = \left(D_{m,O} \times C_O\right) - \left(D_{m,O} \times \frac{C_O}{1 + \frac{k \times C_O \times Vol}{U \times C_O}} \right) - \frac{V_{max,O} \times N \times C_O}{K_{m,O} + C_O}$$

Where the rate constant, k, can be defined as using Michaelis-Menten variables:

$$k = K_{max} \left(\frac{C_G}{K_G + C_G} \times \frac{K_L}{C_L + K_L} \times \frac{C_O}{C_O + K_O} \right)$$

4.2.4 DEVELOPMENT OF CELL NUMBER EQUATION

There are several equations that can be used to predict the specific growth rates of micro-organisms but the most common is the exponential growth equation: $N = N_0e^{t/DT}$ where the number of cells (N) at a specific time, t, can be determined by the initial cell number (N_0), and the division time (DT) [147]. This equation assumes that all cells in culture are actively dividing and the daughter cells also actively divide; however, that is often not the case. Stem cell division is asymmetric where a daughter cell may remain dormant or differentiate into a specialized cell type [148]. Therefore, it is important to apply the appropriate growth kinetic model to stem cell expansion or else there will be an overestimation of population. The equation for the conservation of cell number is described by the *Sherley* model, which incorporates a parameter for the population of dividing cells and a parameter for the population of non-dividing cells. There are three assumptions: 1) the doubling time of cells is constant, 2) the daughter cells can give divide to create both populations and 3) the nondividing cells remain dormant and do not divide again [147, 148].

Sherley describes the derivation of the model from a general cell division progression while considering the populations of dividing and non-dividing cells as seen below where N_0 = initial number of cells; N = number of cells at a specific time, t; DT = doubling time; F_d = dividing cells and $1 – F_d$ = the fraction of non-dividing cells [148]. After the first cell cycle, the number of cells should be double the initial population of cells that double plus the remaining fraction that did not divide. After a second cycle, the cell division progression should read as follows: the fraction of cells from the initial population that did not divide, plus the new population of cells that do not divide, plus the new number of cells that will divide. Table 9 below will show the progression:

Table 9. Cell division progression derivation example [148].

t/DT	Cell Number (C)
0	N_0
1	$(1 - F_d)\, N_0 + 2\, F_d N_0$
2	$(1 - F_d)\, N_0 + (1 - F_d)\, (2\, F_d N_0) + 2\, F_d\, (2\, F_d\, N_0)$

Taking the sum of the cell division progression of the dividing and non-dividing cell populations, the cell proliferation can be modeled more generally as:

$$\frac{1}{2}\sum_{i=-}^{(t/DT)-1} x^i = \frac{1}{2}\left[\frac{1 - {F_d}^{t/DT}}{1 - F_d}\right]$$

And then, rewritten to express as:

$$N = N_0\left(0.5 + \frac{1 - (2 \times F_d)^{(t/DT)+1}}{2(1 - 2 \times F_d)}\right)$$

When the initial cell number and the doubling time of the cell line are known, then the fraction of dividing cells (F_d) can be determined with population growth data. If doubling time is not known, it can be calculated using the following equation with population growth data where, N_0 is the initial cell number at the initial time, t_0, N is the cell number at particular time, t, and $(t - t_0)$ is the period of time in days [119]:

$$DT = (t - t_0) \times \frac{\log(2)}{(\log(N) - \log(N_0))}$$

4.2.5 DETERMINATION OF VARIABLES

The system of equations required that several variables be determined experimentally for the specific cell line used in the bioreactor experiments. Others were retrieved from literature. All variables required for the solution of the system were compiled in the Table 10 below.

Table 10. List of variables for the mathematical model.

Parameter	Description	Value	Units	Reference
Media Properties				
S_m	Solubility of oxygen in media	2e-4	M	[100]
$C_{in,G}$	Initial glucose concentration	0.0051155892	M	Measured*
$C_{in,L}$	Initial lactate concentration	0.0016924366	M	Measured*
$D_{m,O}$	Oxygen diffusion coefficient in media	0.11844	cm^2/h	[149]
Cell Characteristics				
N_i	Initial cell number	4,000,000	$cells/cm^2$	*
N_{max}	Maximum cell number	7,500,000	$cells/cm^2$	*
$V_{max,O}$	Maximum oxygen uptake	1e-13	mol/h/cell	[150]
$V_{max,G}$	Maximum glucose uptake	2.72e-13	mol/h/cell	[150]
$Y_{L/G}$	Yield of lactate	2.0	-	[151]
$K_{m,O}$	Michaelis-Menten constant for oxygen uptake	4.05E-09	mol/cm^3	[152]
$K_{m,G}$	Michaelis-Menten constant for glucose uptake	3.50E-07	mol/cm^3	[153]
K_{max}	Max growth rate	0.02631	hr^{-1}	[100]
K_O	Oxygen Michaelis-Menten growth constant	1e-6	M	[154]
K_G	Glucose Michaelis-Menten growth constant	6e-6	M	[154]
K_L	Lactate Michaelis-Menten growth constant	0.043	M	[151]

4.2.6 SOLUTION METHOD

Mathematical modeling was conducted using MATLAB (The MathWorks Inc.). Experimental data used for validation was described in the previous chapter.

4.3 RESULTS

4.3.1 MATHEMATICAL MODEL PROOF OF CONCEPT

The mathematical model is a system of ordinary differential equations that required an ordinary differential equation (ODE) solver to solve. The ode15s was selected, and the MATLAB codes for each of the ode15s solvers and their respective call codes can be found in Appendix B – Appendix I. There are four different MATLAB codes for the system of equations and each model one of the specific parameters.

4.3.2 PROOF- OF-CONCEPT SYSTEM VALIDATION

Four graphs were produced by the system of equations: cell number, consumption of glucose, production of lactate and consumption of oxygen. The MSC monolayer growth model plotted a straight line unlike the expected trajectory of a growth curve (Figure 25). This indicates that there are parameters that need to be adjusted for accuracy. The model trajectories for glucose consumption, lactate production and oxygen consumption were as expected (Figure 26, 27 and 28); however, the values were higher than those obtained experimentally. The glucose consumption trend was similar to the lactate production. The oxygen concentration decreased very slowly due to the oxygen bubble in the vessel, as well as the gas exchange that occurs due to the gas permeable properties of the silicone tubing.

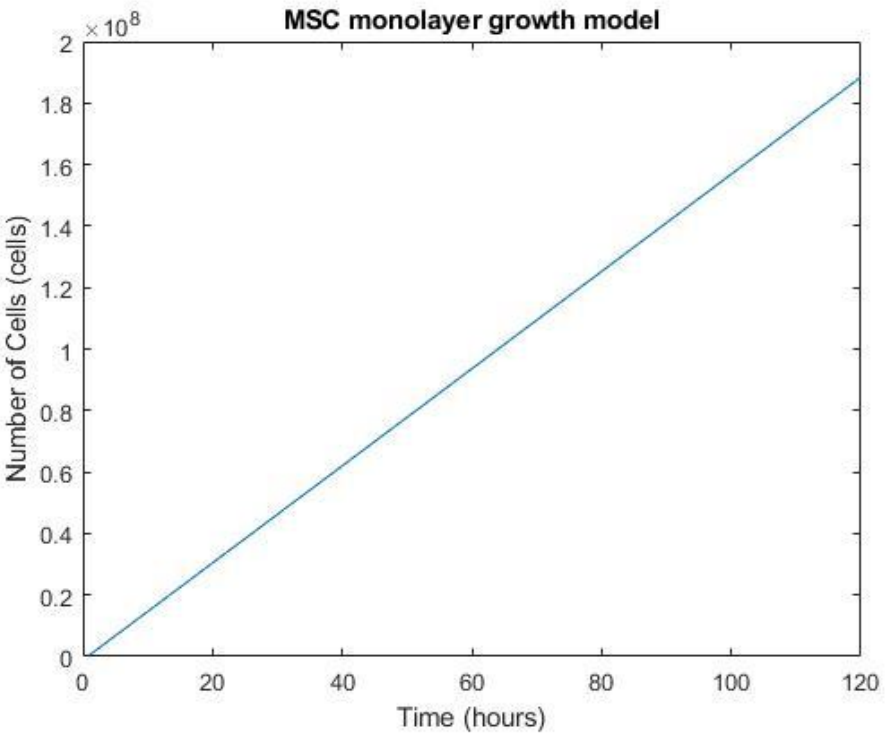

Figure 25: MSC monolayer growth model plotted by MATLAB.

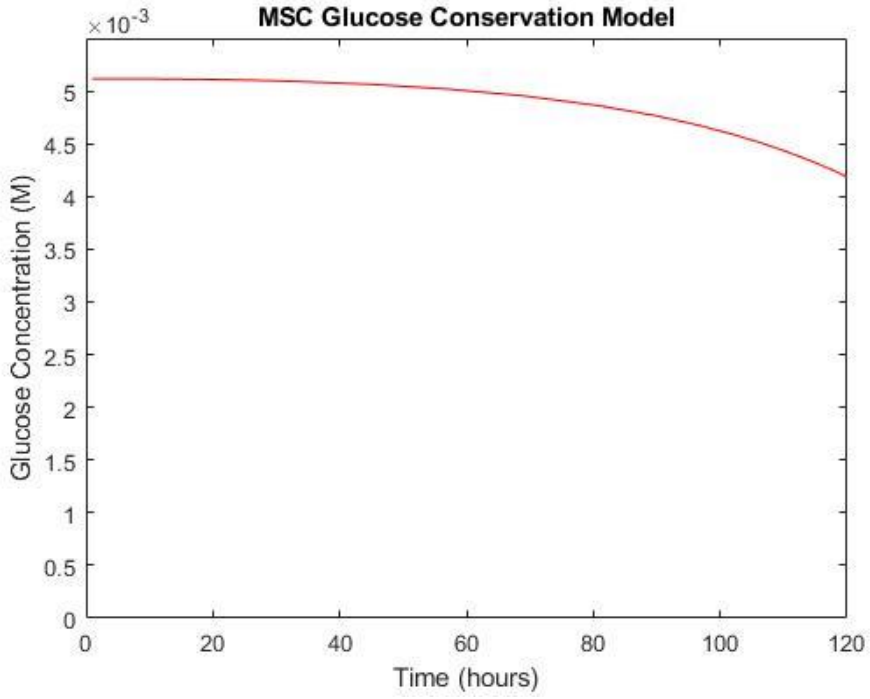

Figure 26: Glucose consumption model plotted by MATLAB.

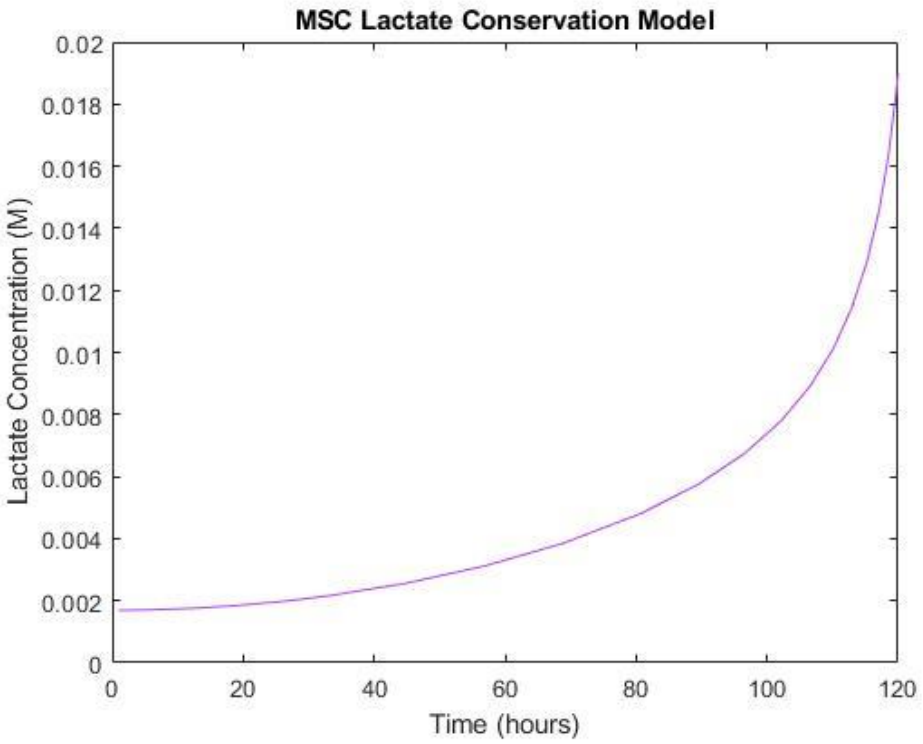

Figure 27: Lactate production model plotted by MATLAB.

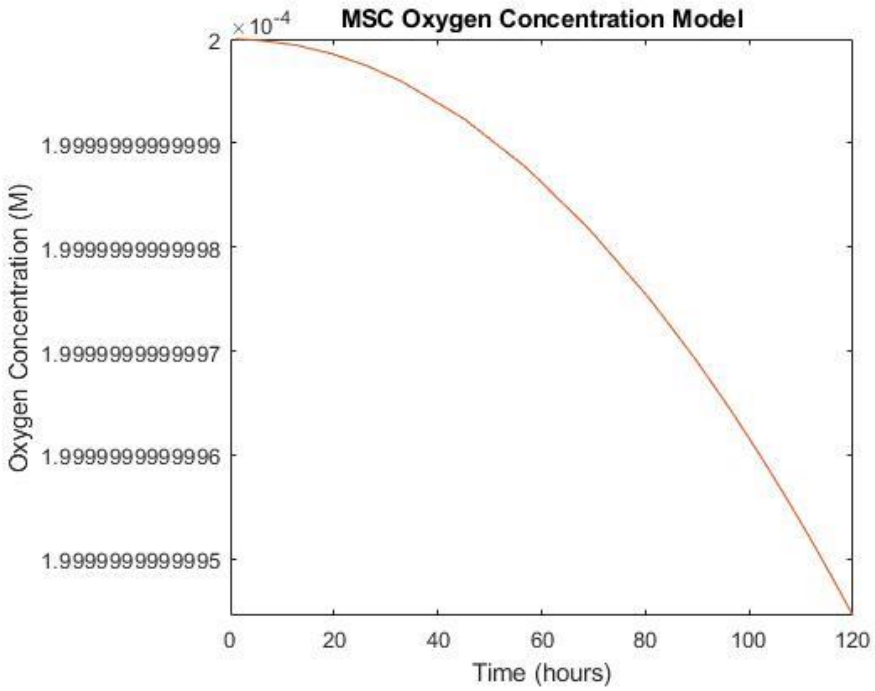

Figure 28: Oxygen consumption model plotted by MATLAB.

4.3.3 HYPOTHETICAL SCENARIO ANALYSIS

A second math model MATLAB code was developed to more accurately model the expansion of MSCs as a stand-alone ordinary differential equation solved with a general ODE solver instead of ode15s (Appendix J). This model was compared to the stand MSC monolayer growth model (Appendix H). Both models can be varied by changing the known dividing fraction of the cells in the population and the initial seeding density of cells. In the MSC monolayer growth model (Figure 28) and the new cell model (Figure 29), the variation of the dividing fraction revealed that the lower the dividing fraction, the decrease in the number of cells yielded over a certain time which is realistic (Figure 29). The seeding density variation produced graphs with similar trends, the lower the seeding density, a lower cell yield (Figure 30 and Figure 31).

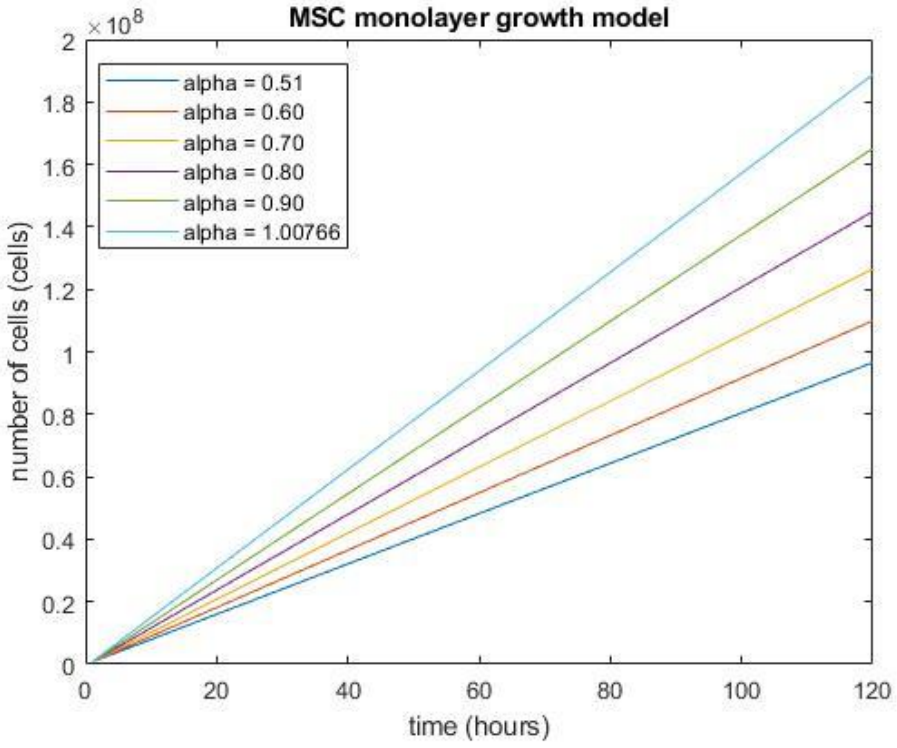

Figure 29: Plot of the variation of the dividing fraction of cells in the original MSC cell growth model.

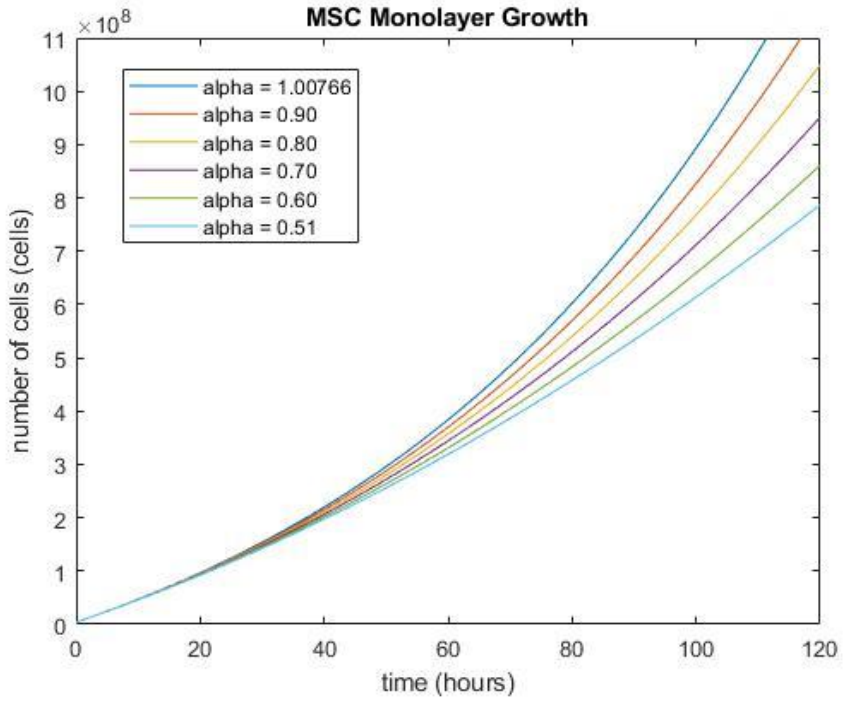

Figure 30: Plot of the variation of the dividing fraction of cells in the new MSC cell growth model.

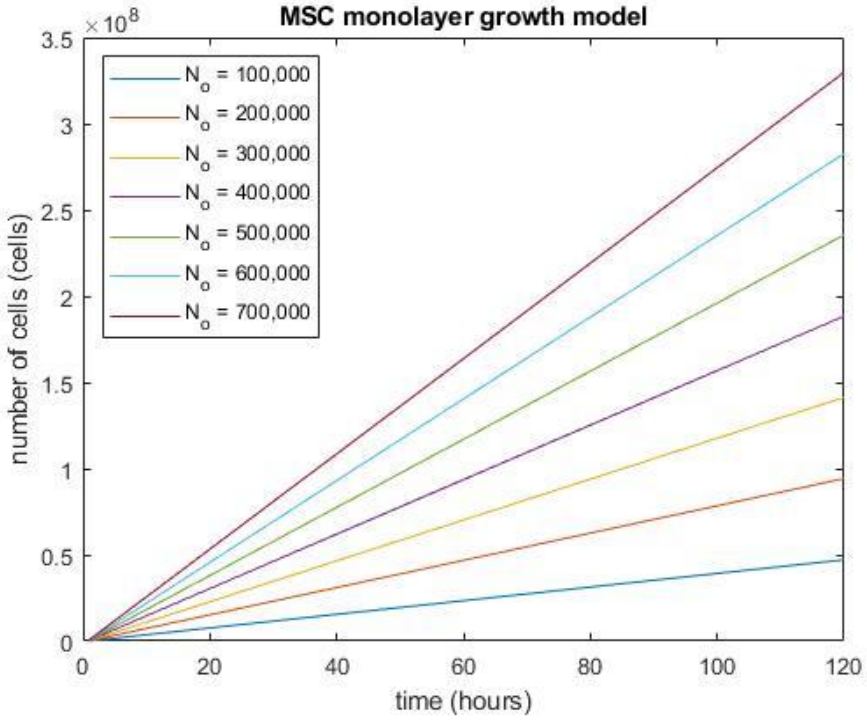

Figure 31: Plot of the variation of the seeding number of cells in the original MSC cell growth model.

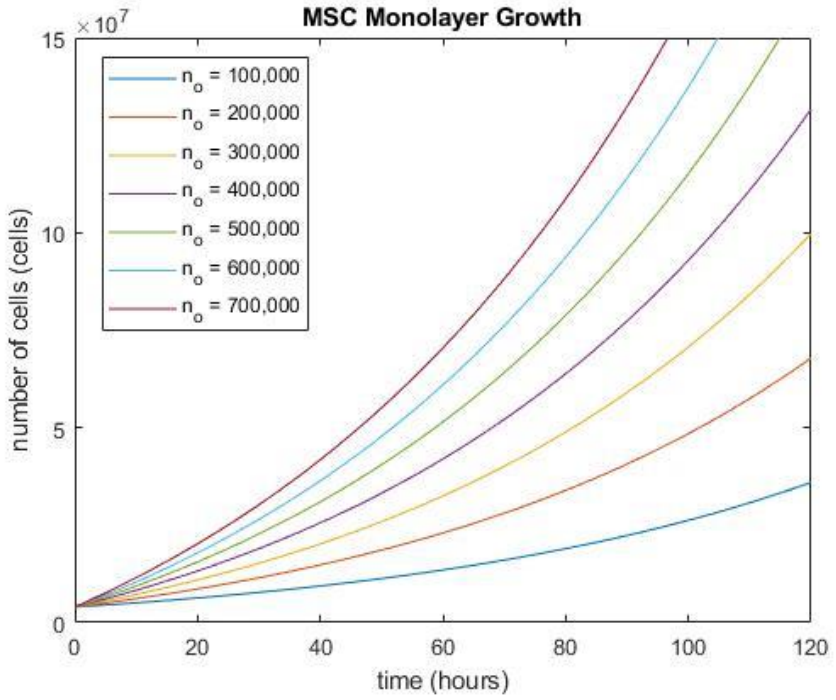

Figure 32: Plot of the variation of the seeding number of cells in the new MSC cell growth model.

4.4 DISCUSSION

The mathematical model previously described was successful in generating a series of models that could be used to validate the data obtained in the previous chapter. Mathematical model development has been briefly described and this section will focus more-in-depth look at the troubleshooting. The cell number equation was difficult to code with the ode15s solver unlike the nutrient conservation equations due to the presence of the time, t, variable in the equation. The ode15s solver would not accept the variable due to the use of the tspan variable used to represent time; it was not possible to represent time twice in an equation. There was the need to replace the t with a known value in order for the ode solver to compile without errors. At that point, it was necessary to pursue other ordinary differential equation solvers that would allow for the time input to remain and that was how the revised cell number model was developed (Appendix J). In

addition, the nutrient conservation equations are slightly skewed due to the inconsistency of the cell number. The trends, either positive or negative respectively, are realistic but the consumption or production component is skewed because the cell number that multiplies that factor is incorrect. At 96 hours, 4 days, of culturing within the vessel, the cell number averaged 14.8 million cells, an average glucose concentration of approximately 0.55 g/L (0.003 M) and an average lactate concentration of approximately 0.5 g/L (0.0055 M). The values in the math model around this time point for the cell number is vastly overestimated, 150 million cells instead of approximately 15 million cells, and therefore, over-estimates the rest of the parameters with the exception of oxygen because there was no measurement of oxygen concentration during the experiment series (Figure 32).

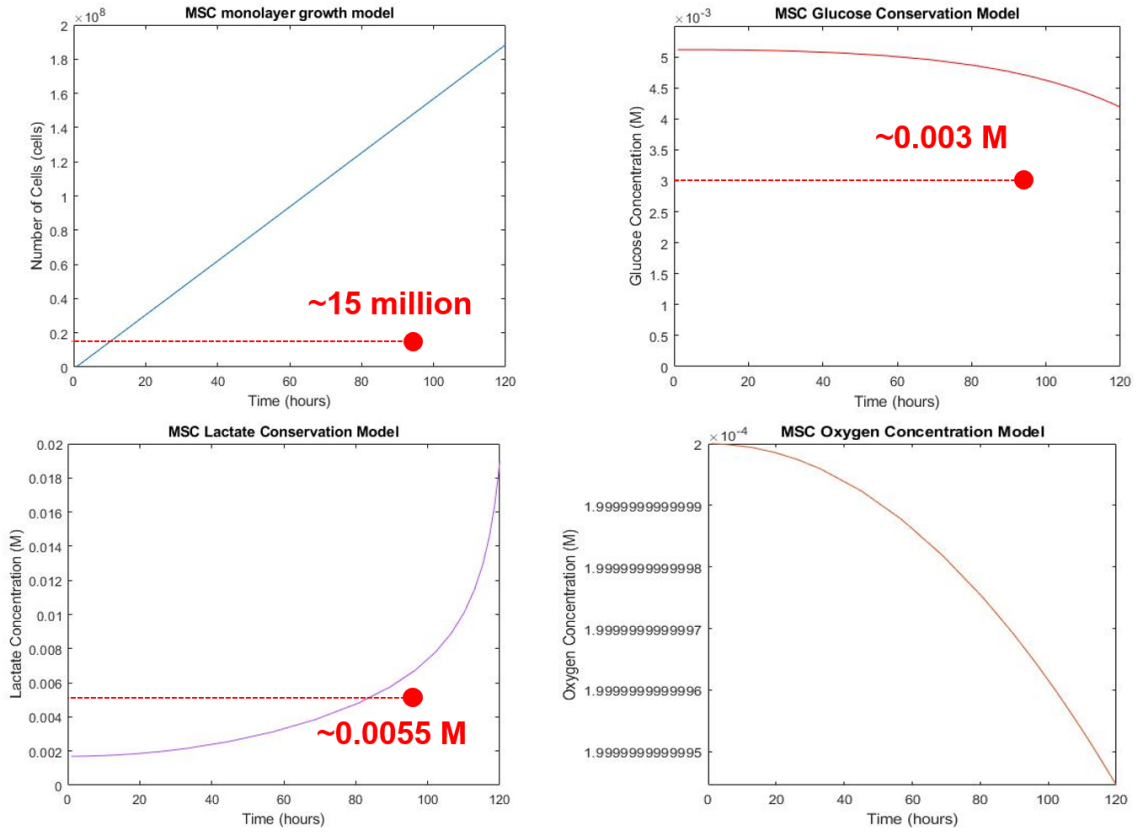

Figure 33: Comparison of monolayer growth, glucose consumption, lactate production and oxygen consumption with experimentally obtained data.

The revised cell model (Appendix J) generated a more realistic growth curve plot instead of a straight line. A comparison of hypothetical scenarios comparing the initial cell seeding density and the dividing fraction was made to compare the accuracy of the two models (Figure 34 and Figure 35). When varying the initial cell seeding density, the original cell model predicted the cell yield to be approximately 1.5 billion cells at 96 hours, whereas the revised cell model predicted the cell yield to be approximately 800 million. The lowest seeding density, 1×10^6 cells, 1 million cells, yielded approximately 20 million cells which was the closest value to the experimental data obtained in the previous chapter. When varying the dividing fraction, both the original cell model and the revised cell model produced higher cell yields than the experimental data; however, the revised cell model was only off by a factor of 10 and the curve trend was much more realistic. The cell yield generated by the revised cell growth model is still extremely high, which led to an evaluation of the three experimentally derived inputs required for the *Sherley* model: the doubling time of the cell population (DT), the dividing fraction of cells (F_d) and the cell number (N) at a given time point. The experimental values used to determine these are from time points over 24 hours and this longer time point is not a precise measurement of the true DT and cell number because larger step sizes have a wider margin of error. Thus, additional data is required from multiple sample counts over a longer period of time.

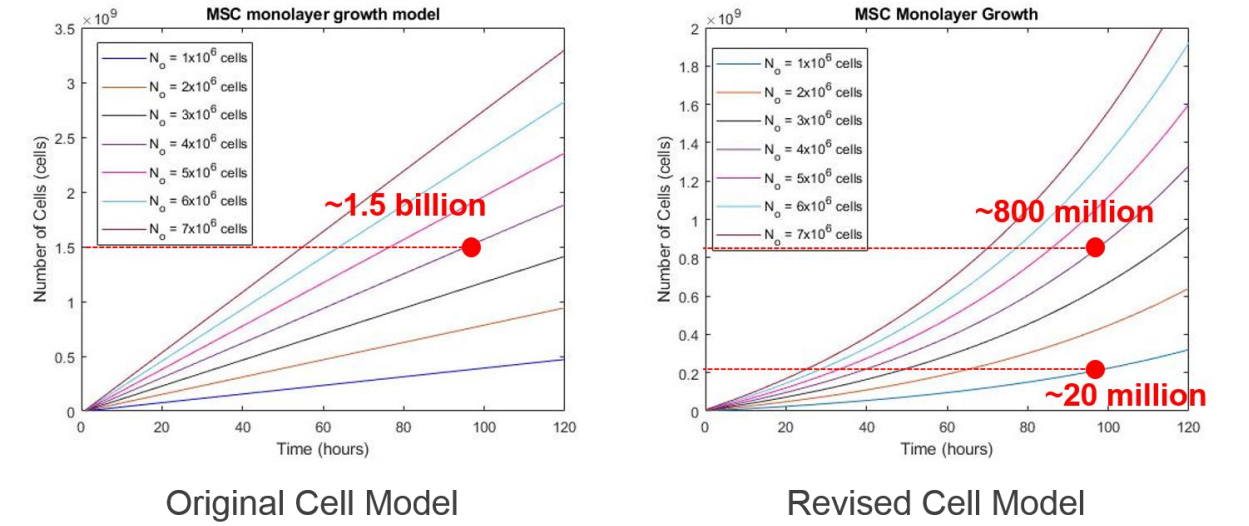

Figure 34: Comparison of hypothetical seeding densities with the original cell model and the revised cell model.

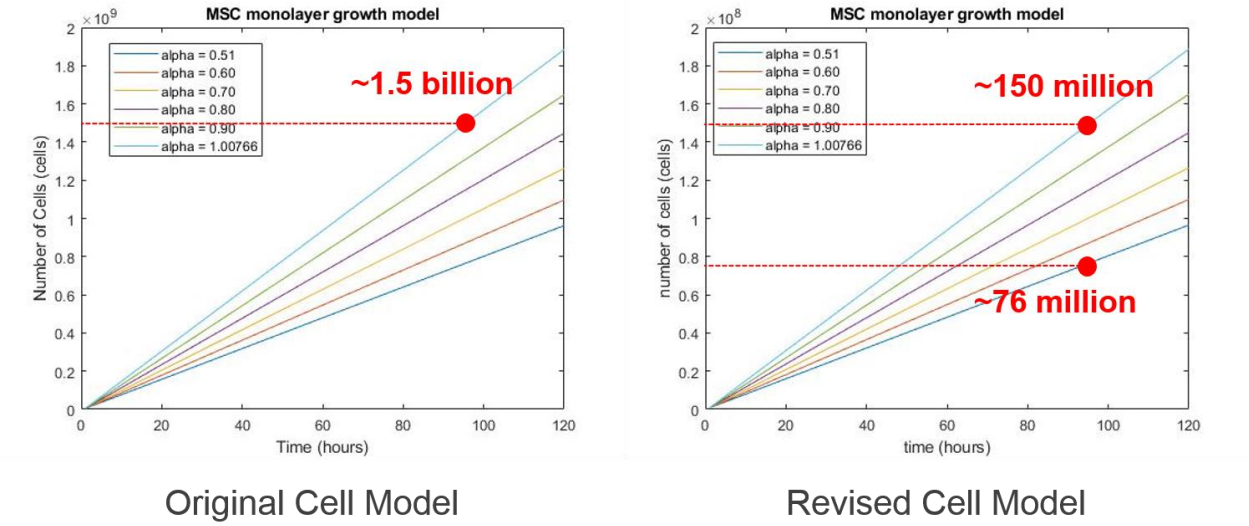

Figure 35: Comparison of hypothetical dividing fraction with the original cell model and the revised cell model.

4.5 CONCLUSION

Overall, this math model is solid foundation for a more complex modeling system that can more accurately estimate mesenchymal stromal cell culture parameters. In the beginning, ode15s

was selected to create the system of ordinary differential equations but the use of the ode15s solver was not adequate to model the growth of the cells due to the way time was represented within the function. The dsolve function was used to build the revised cell model (Appendix J) which incorporated time as a variable "t" within the equation instead of using tspan for the entire system. This revised cell model produced trends that were more realistic than the original cell model despite being inaccurate like the original cell model. With the variation of cell culture parameters such as initial cell seeding density and dividing fraction of cells (Figure 34 and Figure 35), the revised cell model did produce less inaccurate cell yields which indicates that the model is more accurate but requires some refinement. A series of experiments to experimentally determine the doubling time and dividing fraction of a specific cell line would improve the accuracy of the model and help tailor it to specific cell line growth kinetics.

CHAPTER 5

SUMMARY AND RECOMMENDATIONS

In this work, we successfully designed and fabricated a bioreactor vessel system for mesenchymal stromal cell expansion. The bioreactor was built to support both monolayer culture for anchorage-dependent cell culture with Lexan™ inserts and microcarrier culture with the cell culture colander. The bioreactor system was able to yield similar cell harvests comparable to the T-75 flask control, and cells from both culturing conditions underwent bone differentiation, mineralization, after 14 days of exposure to bone differentiation media. Media samples were analyzed for glucose, lactate, and hydrogen peroxide concentrations to compare the metabolic activity of the culturing conditions. When assessing the hydrogen peroxide metabolic activity, there was little difference between the culturing conditions because the cells had similar growth rates, but the bioreactor vessel displayed a greater dilution of lactate and a higher concentration of glucose because it is designed for longer-term culturing. Additionally, the math model was successful in identifying key parameters of cell culture that we wanted to predict. The cell number equation evolved over time to be more accurate with a simpler solver, and the nutrient conservation equations follow the correct trends expected.

Recommendations for future work would be to explore the effects of dynamic culture on a human mesenchymal stromal cell line and to evaluate the osteogenic potential. In addition, a note would be to seed the cells at a lower density in future trials using cells grown in the bioreactor system to reduce the chances of retraction from the edges of the well plate. Several other aspects

that have yet to be fully explored include the effects on differentiation culturing in the dynamic environment compared to static culture; a secretome analysis with xeno-free media to compare the protein secretion between the different culturing conditions; and evaluating the potential three-dimensional culture with microcarriers for scale-up.

Further studies will be needed to refine the mathematical model with a series of experiments to determine the actual doubling time of the cell lines used; a more accurate fraction of the population doubling; and the length of the cell cycle. Incorporating this into the cell number math model will improve the accuracy of prediction and help normalize the nutrient conservation model outputs. This can be done by monitoring and counting mesenchymal cell culture in well-plates at specific time intervals such as 12 hours, 24 hours, and 48 hours. Additionally, a camera could be used to visualize the wells and more accurately label the actively dividing population within the well-plate. Determining the cell culture growth kinetics experimentally will improve the math model and advance the future research design with this bioreactor.

REFERENCES

1. *Stem Cell Basics I*. **Stem Cell Information** 2016.
2. Cowan, C.A., I. Klimanskaya, J. McMahon, J. Atienza, J. Witmyer, J.P. Zucker, S. Wang, C.C. Morton, A.P. McMahon, and D. Powers, *Derivation of embryonic stem-cell lines from human blastocysts.* New England Journal of Medicine, 2004. **350**(13): p. 1353-1356.
3. van der Kooy, D. and S. Weiss, *Why stem cells?* Science, 2000. **287**(5457): p. 1439-1441.
4. Chamberlain, G., J. Fox, B. Ashton, and J. Middleton, *Concise review: mesenchymal stem cells: their phenotype, differentiation capacity, immunological features, and potential for homing.* Stem cells, 2007. **25**(11): p. 2739-2749.
5. Sheng, G., *The developmental basis of mesenchymal stem/stromal cells (MSCs).* BMC developmental biology, 2015. **15**(1): p. 44.
6. Phinney, D.G. and D.J. Prockop, *Concise review: mesenchymal stem/multipotent stromal cells: the state of transdifferentiation and modes of tissue repair—current views.* Stem cells, 2007. **25**(11): p. 2896-2902.
7. Wang, G., B.A. Bunnell, R.G. Painter, B.C. Quiniones, S. Tom, N.A. Lanson, J.L. Spees, D. Bertucci, A. Peister, and D.J. Weiss, *Adult stem cells from bone marrow stroma differentiate into airway epithelial cells: potential therapy for cystic fibrosis.* Proceedings of the National Academy of Sciences, 2005. **102**(1): p. 186-191.

8. Chen, S., W. Zhang, J.-M. Wang, H.-T. Duan, J.-H. Kong, Y.-X. Wang, M. Dong, X. Bi, and J. Song, *Differentiation of isolated human umbilical cord mesenchymal stem cells into neural stem cells.* International journal of ophthalmology, 2016. **9**(1): p. 41.

9. Huebsch, N., P.R. Arany, A.S. Mao, D. Shvartsman, O.A. Ali, S.A. Bencherif, J. Rivera-Feliciano, and D.J. Mooney, *Harnessing traction-mediated manipulation of the cell/matrix interface to control stem-cell fate.* Nature Materials, 2010. **9**(6): p. 518.

10. Karnieli, O., Y. Izhar-Prato, S. Bulvik, and S. Efrat, *Generation of insulin-producing cells from human bone marrow mesenchymal stem cells by genetic manipulation.* Stem cells, 2007. **25**(11): p. 2837-2844.

11. Yin, X., B.E. Mead, H. Safaee, R. Langer, J.M. Karp, and O. Levy, *Engineering stem cell organoids.* Cell stem cell, 2016. **18**(1): p. 25-38.

12. Vining, K.H. and D.J. Mooney, *Mechanical forces direct stem cell behaviour in development and regeneration.* Nature Reviews Molecular Cell Biology, 2017. **18**(12): p. 728.

13. Zonari, E., G. Desantis, C. Petrillo, F.E. Boccalatte, M.R. Lidonnici, A. Kajaste-Rudnitski, A. Aiuti, G. Ferrari, L. Naldini, and B. Gentner, *Efficient ex vivo engineering and expansion of highly purified human hematopoietic stem and progenitor cell populations for gene therapy.* Stem Cell Reports, 2017. **8**(4): p. 977-990.

14. Pastrana, E., V. Silva-Vargas, and F. Doetsch, *Eyes wide open: a critical review of sphere-formation as an assay for stem cells.* Cell stem cell, 2011. **8**(5): p. 486-498.

15. Mescher, A.L., *Macrophages and fibroblasts during inflammation and tissue repair in models of organ regeneration.* Regeneration, 2017. **4**(2): p. 39-53.

16. Reinke, S., A. Dienelt, A. Blankenstein, G.N. Duda, and S. Geissler, *Qualifying stem cell sources: how to overcome potential pitfalls in regenerative medicine?* Journal of Tissue Engineering and Regenerative Medicine, 2016. **10**(1): p. 3-10.

17. Makris, E.A., A.H. Gomoll, K.N. Malizos, J.C. Hu, and K.A. Athanasiou, *Repair and tissue engineering techniques for articular cartilage.* Nature Reviews Rheumatology, 2015. **11**(1): p. 21.

18. Breton, A., R. Sharma, A.C. Diaz, A.G. Parham, A. Graham, C. Neil, C.B. Whitelaw, E. Milne, and F.X. Donadeu, *Derivation and characterization of induced pluripotent stem cells from equine fibroblasts.* Stem cells development, 2012. **22**(4): p. 611-621.

19. Liu, M., X. Zeng, C. Ma, H. Yi, Z. Ali, X. Mou, S. Li, Y. Deng, and N. He, *Injectable hydrogels for cartilage and bone tissue engineering.* Bone research, 2017. **5**: p. 17014.

20. Atala, A., R. Lanza, T. Mikos, and R. Nerem, *Principles of regenerative medicine*. 2018: Academic Press.

21. Schwartz, S.D., C.D. Regillo, B.L. Lam, D. Eliott, P.J. Rosenfeld, N.Z. Gregori, J.-P. Hubschman, J.L. Davis, G. Heilwell, and M. Spirn, *Human embryonic stem cell-derived retinal pigment epithelium in patients with age-related macular degeneration and Stargardt's macular dystrophy: follow-up of two open-label phase 1/2 studies.* The Lancet, 2015. **385**(9967): p. 509-516.

22. Yu, J. and J.A. Thomason. *Embryonic Stem Cells*. Stem Cell Information 2016.

23. Ilic, D. and C. Ogilvie, *Concise review: Human embryonic stem cells—what have we done? What are we doing? Where are we going?* Stem Cells, 2017. **35**(1): p. 17-25.

24. Gottweis, H., *The endless hESC controversy in the United States: history, context, and prospects.* Cell Stem Cell, 2010. **7**(5): p. 555-558.

25. Rabb, H.S., *Federal funding for research involving human pluripotent stem cells.* 1999.

26. Jiang, Y., B.N. Jahagirdar, R.L. Reinhardt, R.E. Schwartz, C.D. Keene, X.R. Ortiz-Gonzalez, M. Reyes, T. Lenvik, T. Lund, and M. Blackstad, *Pluripotency of mesenchymal stem cells derived from adult marrow.* Nature, 2002. **418**(6893): p. 41.

27. Turinetto, V., E. Vitale, and C. Giachino, *Senescence in human mesenchymal stem cells: functional changes and implications in stem cell-based therapy.* International journal of molecular sciences, 2016. **17**(7): p. 1164.

28. Hass, R., C. Kasper, S. Böhm, and R. Jacobs, *Different populations and sources of human mesenchymal stem cells (MSC): a comparison of adult and neonatal tissue-derived MSC.* Cell Communication Signaling, 2011. **9**(1): p. 12.

29. Wagner, W., F. Wein, A. Seckinger, M. Frankhauser, U. Wirkner, U. Krause, J. Blake, C. Schwager, V. Eckstein, and W. Ansorge, *Comparative characteristics of mesenchymal stem cells from human bone marrow, adipose tissue, and umbilical cord blood.* Experimental Hematology, 2005. **33**(11): p. 1402-1416.

30. Domen, J., A. Wagers, and I.L. Weissman. *Bone Marrow (Hematopoietic) Stem Cells*. Stem Cell Information 2016.

31. Takahashi, K. and S. Yamanaka, *Induction of pluripotent stem cells from mouse embryonic and adult fibroblast cultures by defined factors.* Cell, 2006. **126**(4): p. 663-676.

32. Park, I.-H., R. Zhao, J.A. West, A. Yabuuchi, H. Huo, T.A. Ince, P.H. Lerou, M.W. Lensch, and G.Q. Daley, *Reprogramming of human somatic cells to pluripotency with defined factors.* Nature, 2008. **451**(7175): p. 141.

33. Medvedev, S.P., A.I. Shevchenko, and S.M. Zakian, *Induced pluripotent stem cells: problems and advantages when applying them in regenerative medicine.* Acta Naturae, 2010. **2**(2): p. 18-27.

34. Borger, D.K., B. McMahon, T.R. Lal, J. Serra-Vinardell, E. Aflaki, and E. Sidransky, *Induced pluripotent stem cell models of lysosomal storage disorders.* Disease models & mechanisms, 2017. **10**(6): p. 691-704.

35. Evans, M.J. and M.H. Kaufman, *Establishment in culture of pluripotential cells from mouse embryos.* Nature, 1981. **292**(5819): p. 154.

36. Serra, M., C. Brito, C. Correia, and P.M. Alves, *Process engineering of human pluripotent stem cells for clinical application.* Trends in Biotechnology, 2012. **30**(6): p. 350-359.

37. Abbasi-Malati, Z., A.M. Roushandeh, Y. Kuwahara, and M.H. Roudkenar, *Mesenchymal stem cells on horizon: a new arsenal of therapeutic agents.* Stem Cell Reviews and Reports, 2018. **14**: p. 484-499.

38. Farini, A., C. Sitzia, S. Erratico, M. Meregalli, and Y. Torrente, *Clinical applications of mesenchymal stem cells in chronic diseases.* Stem cells international, 2014. **2014**.

39. Kim, N. and S.-G. Cho, *Clinical applications of mesenchymal stem cells.* The Korean journal of internal medicine, 2013. **28**(4): p. 387.

40. Castro-Manrreza, M.E. and J.J. Montesinos, *Immunoregulation by mesenchymal stem cells: biological aspects and clinical applications.* Journal of immunology research, 2015. **2015**.

41. Squillaro, T., G. Peluso, and U. Galderisi, *Clinical trials with mesenchymal stem cells: an update.* Cell transplantation, 2016. **25**(5): p. 829-848.

42. Wang, S., X. Qu, and R.C. Zhao, *Clinical applications of mesenchymal stem cells.* Journal of hematology and oncology, 2012. **5**(1): p. 19.

43. Yeatts, A.B., D.T. Choquette, and J.P. Fisher, *Bioreactors to influence stem cell fate: augmentation of mesenchymal stem cell signaling pathways via dynamic culture systems.* Biochimica et Biophysica Acta (BBA)-General Subjects, 2013. **1830**(2): p. 2470-2480.

44. Ma, T., A.-C. Tsai, and Y. Liu, *Biomanufacturing of human mesenchymal stem cells in cell therapy: influence of microenvironment on scalable expansion in bioreactors.* Biochemical Engineering Journal, 2016. **108**: p. 44-50.

45. Beşkardeş, I.G., R.S. Hayden, D.L. Glettig, D.L. Kaplan, and M. Gümüşderelioğlu, *Bone tissue engineering with scaffold-supported perfusion co-cultures of human stem cell-derived osteoblasts and cell line-derived osteoclasts.* Process Biochemistry, 2017. **59**: p. 303-311.

46. Olivares-Navarrete, R., E.M. Lee, K. Smith, S.L. Hyzy, M. Doroudi, J.K. Williams, K. Gall, B.D. Boyan, and Z. Schwartz, *Substrate stiffness controls osteoblastic and chondrocytic differentiation of mesenchymal stem cells without exogenous stimuli.* PloS one, 2017. **12**(1): p. e0170312.

47. Vidal, M.A., G.E. Kilroy, J.R. Johnson, M.J. Lopez, R.M. Moore, and J.M. Gimble, *Cell growth characteristics and differentiation frequency of adherent equine bone marrow–derived mesenchymal stromal cells: adipogenic and osteogenic capacity.* Veterinary Surgery, 2006. **35**(7): p. 601-610.

48. Hoch, A. and J.K. Leach, *Concise review: optimizing expansion of bone marrow mesenchymal stem/stromal cells for clinical applications.* Stem Cells Translational Medicine, 2014. **3**(5): p. 643-652.

49. Jung, S., K.M. Panchalingam, R.D. Wuerth, L. Rosenberg, and L.A. Behie, *Large-scale production of human mesenchymal stem cells for clinical applications.* Biotechnology applied biochemistry, 2012. **59**(2): p. 106-120.

50. Bunnell, B.A., M. Flaat, C. Gagliardi, B. Patel, and C. Ripoll, *Adipose-derived stem cells: isolation, expansion and differentiation.* Methods, 2008. **45**(2): p. 115-120.

51. Baer, P.C. and H. Geiger, *Adipose-derived mesenchymal stromal/stem cells: tissue localization, characterization, and heterogeneity.* Stem cells international, 2012. **2012**.

52. *Mesenchymal Stem Cells (MSCs) for Treatment of Acute Respiratory Distress Syndrome (ARD) in Patients With Malignancies*. Available from: https://ClinicalTrials.gov/show/NCT02804945.

53. Mazzini, L., I. Ferrero, V. Luparello, D. Rustichelli, M. Gunetti, K. Mareschi, L. Testa, A. Stecco, R. Tarletti, and M. Miglioretti, *Mesenchymal stem cell transplantation in amyotrophic lateral sclerosis: a phase I clinical trial.* Experimental neurology, 2010. **223**(1): p. 229-237.

54. Nabavi, S.M., L. Arab, N. Jarooghi, T. Bolurieh, F. Abbasi, S. Mardpour, V. Azimyian, F. Moeininia, S. Maroufizadeh, and L. Sanjari, *Safety, feasibility of intravenous and intrathecal injection of autologous bone marrow derived mesenchymal stromal cells in patients with amyotrophic lateral sclerosis: an open label phase I clinical trial.* Cell Journal, 2018. **20**(4): p. 592.

55. Carlsson, P.-O., E. Schwarcz, O. Korsgren, and K. Le Blanc, *Preserved β-cell function in type 1 diabetes by mesenchymal stromal cells.* Diabetes, 2015. **64**(2): p. 587-592.

56. Connick, P., M. Kolappan, C. Crawley, D.J. Webber, R. Patani, A.W. Michell, M.-Q. Du, S.-L. Luan, D.R. Altmann, and A.J. Thompson, *Autologous mesenchymal stem cells for*

the treatment of secondary progressive multiple sclerosis: an open-label phase 2a proof-of-concept study. The Lancet Neurology, 2012. **11**(2): p. 150-156.

57. Connick, P., M. Kolappan, R. Patani, M.A. Scott, C. Crawley, X.-L. He, K. Richardson, K. Barber, D.J. Webber, and C.A. Wheeler-Kingshott, *The mesenchymal stem cells in multiple sclerosis (MSCIMS) trial protocol and baseline cohort characteristics: an open-label pre-test: post-test study with blinded outcome assessments.* Trials, 2011. **12**(1): p. 62.

58. Jarocha, D., O. Milczarek, A. Wedrychowicz, S. Kwiatkowski, and M. Majka, *Continuous improvement after multiple mesenchymal stem cell transplantations in a patient with complete spinal cord injury.* Cell transplantation, 2015. **24**(4): p. 661-672.

59. Merten, O.-W., *Advances in cell culture: anchorage dependence.* Philosophical Transactions of the Royal Society B: Biological Sciences, 2015. **370**(1661).

60. Abbasalizadeh, S. and H. Baharvand, *Technological progress and challenges towards cGMP manufacturing of human pluripotent stem cells based therapeutic products for allogeneic and autologous cell therapies.* Biotechnology advances, 2013. **31**(8): p. 1600-1623.

61. Chen, A.K.-L., S. Reuveny, and S.K.W. Oh, *Application of human mesenchymal and pluripotent stem cell microcarrier cultures in cellular therapy: achievements and future direction.* Biotechnology advances, 2013. **31**(7): p. 1032-1046.

62. Vacanti, J.P. and R. Langer, *Tissue engineering: the design and fabrication of living replacement devices for surgical reconstruction and transplantation.* The Lancet, 1999. **354**: p. S32-S34.

63. Zhao, J., M. Griffin, J. Cai, S. Li, P.E. Bulter, and D.M. Kalaskar, *Bioreactors for tissue engineering: An update.* Biochemical engineering journal, 2016. **109**: p. 268-281.

64. Martin, I., D. Wendt, and M. Heberer, *The role of bioreactors in tissue engineering.* Trends in biotechnology, 2004. **22**(2): p. 80-86.

65. Spier, M.R., L. Vandenberghe, A.B.P. Medeiros, and C.R. Soccol, *Application of different types of bioreactors in bioprocesses.* Bioreactors: Design, Properties and Applications, 2011: p. 53-87.

66. Konstantinov, K.B. and C.L. Cooney, *White Paper on Continuous Bioprocessing May 20–21 2014 Continuous Manufacturing Symposium.* Journal of Pharmaceutical Sciences, 2015. **104**(3): p. 813-820.

67. Fogler, H.S., *Elements of chemical reaction engineering.* 1999.

68. King, J.A. and W.M. Miller, *Bioreactor development for stem cell expansion and controlled differentiation.* Current Opinion in Chemical Biology, 2007. **11**(4): p. 394-398.

69. Le, H., H. Chen, and C.T. Goudar, *Continuous Processing in Upstream Operations.* Chemical Engineering Progress, 2015. **111**(12): p. 32-37.

70. Warnock, J.N. and M. Al-Rubeai, *Bioreactor systems for the production of biopharmaceuticals from animal cells.* Biotechnology and Applied Biochemistry, 2006. **45**(1): p. 1-12.

71. Riboldi, S.A., S. Bertoldi, and S. Mantero, *In vitro dynamic culture of cell-biomaterial constructs*, in *Characterization of Polymeric Biomaterials*. 2017, Elsevier. p. 339-363.

72. Borys, B.S., E.L. Roberts, A. Le, and M.S. Kallos, *Scale-up of embryonic stem cell aggregate stirred suspension bioreactor culture enabled by computational fluid dynamics modeling.* Biochemical engineering journal, 2018. **133**: p. 157-167.

73. Hookway, T.A., J.C. Butts, E. Lee, H. Tang, and T.C. McDevitt, *Aggregate formation and suspension culture of human pluripotent stem cells and differentiated progeny.* Methods, 2016. **101**: p. 11-20.

74. Kehoe, D.E., D. Jing, L.T. Lock, and E.S. Tzanakakis, *Scalable stirred-suspension bioreactor culture of human pluripotent stem cells.* Tissue Engineering Part A, 2009. **16**(2): p. 405-421.

75. Lam, A.T.-L., A.K.-L. Chen, S.Q.-P. Ting, S. Reuveny, and S.K.-W. Oh, *Integrated processes for expansion and differentiation of human pluripotent stem cells in suspended microcarriers cultures.* Biochemical biophysical research communications, 2016. **473**(3): p. 764-768.

76. Oh, S.K., A.K. Chen, Y. Mok, X. Chen, U.-M. Lim, A. Chin, A.B. Choo, and S. Reuveny, *Long-term microcarrier suspension cultures of human embryonic stem cells.* Stem cell research, 2009. **2**(3): p. 219-230.

77. Ashok, P., Y. Fan, M.R. Rostami, and E.S. Tzanakakis, *Aggregate and microcarrier cultures of human pluripotent stem cells in stirred-suspension systems*, in *Bioreactors in Stem Cell Biology*. 2015, Springer. p. 35-52.

78. McKee, C. and G.R. Chaudhry, *Advances and challenges in stem cell culture.* Colloids Surfaces B: Biointerfaces, 2017. **159**: p. 62-77.

79. Eibes, G., F. dos Santos, P.Z. Andrade, J.S. Boura, M.M. Abecasis, C.L. da Silva, and J.M. Cabral, *Maximizing the ex vivo expansion of human mesenchymal stem cells using a*

microcarrier-based stirred culture system. Journal of biotechnology, 2010. **146**(4): p. 194-197.

80. Badenes, S., A. Fernandes-Platzgummer, C. Rodrigues, M. Diogo, C. da Silva, and J. Cabral, *Microcarrier Culture Systems for Stem Cell Manufacturing*, in *Stem Cell Manufacturing*. 2016, Elsevier. p. 77-104.

81. Li, B., X. Wang, Y. Wang, W. Gou, X. Yuan, J. Peng, Q. Guo, and S. Lu, *Past, present, and future of microcarrier-based tissue engineering.* Journal of orthopaedic translation, 2015. **3**(2): p. 51-57.

82. Hossain, K.M.Z., U. Patel, and I. Ahmed, *Development of microspheres for biomedical applications: a review.* Progress in biomaterials, 2015. **4**(1): p. 1-19.

83. Hervy, M., J.L. Weber, M. Pecheul, P. Dolley-Sonneville, D. Henry, Y. Zhou, and Z. Melkoumian, *Long term expansion of bone marrow-derived hMSCs on novel synthetic microcarriers in xeno-free, defined conditions.* PloS one, 2014. **9**(3): p. e92120.

84. Dias, A.D., J.M. Elicson, and W.L. Murphy, *Microcarriers with synthetic hydrogel surfaces for stem cell expansion.* Advanced healthcare materials, 2017. **6**(16): p. 1700072.

85. Atala, A., R. Lanza, T. Mikos, and R. Nerem, *Principles of regenerative medicine*. 2008: Academic Press. 1473.

86. Tavassoli, H., S.N. Alhosseini, A. Tay, P.P. Chan, S.K.W. Oh, and M.E. Warkiani, *Large-scale production of stem cells utilizing microcarriers: a biomaterials engineering perspective from academic research to commercialized products.* Biomaterials, 2018.

87. Malda, J. and C.G. Frondoza, *Microcarriers in the engineering of cartilage and bone.* Trends in biotechnology, 2006. **24**(7): p. 299-304.

88. Yu, C., A. Kornmuller, C. Brown, T. Hoare, and L.E. Flynn, *Decellularized adipose tissue microcarriers as a dynamic culture platform for human adipose-derived stem/stromal cell expansion.* Biomaterials, 2017. **120**: p. 66-80.

89. Heathman, T.R., V.A. Glyn, A. Picken, Q.A. Rafiq, K. Coopman, A.W. Nienow, B. Kara, and C.J. Hewitt, *Expansion, harvest and cryopreservation of human mesenchymal stem cells in a serum-free microcarrier process.* Biotechnology bioengineering, 2015. **112**(8): p. 1696-1707.

90. Sonnaert, M., I. Papantoniou, V. Bloemen, G. Kerckhofs, F. Luyten, and J. Schrooten, *Human periosteal-derived cell expansion in a perfusion bioreactor system: proliferation, differentiation and extracellular matrix formation.* Journal of tissue engineering regenerative medicine, 2017. **11**(2): p. 519-530.

91. Hoch, A.I., R. Duhr, N. Di Maggio, A. Mehrkens, M. Jakob, and D. Wendt, *Expansion of bone marrow mesenchymal stromal cells in perfused 3D ceramic scaffolds enhances in vivo bone formation.* Biotechnology journal, 2017. **12**(12): p. 1700071.

92. Guyot, Y., F. Luyten, J. Schrooten, I. Papantoniou, and L. Geris, *A three-dimensional computational fluid dynamics model of shear stress distribution during neotissue growth in a perfusion bioreactor.* Biotechnology and bioengineering, 2015. **112**(12): p. 2591-2600.

93. Yeo, D., A. Kiparissides, J.M. Cha, C. Aguilar-Gallardo, J.M. Polak, E. Tsiridis, E.N. Pistikopoulos, and A. Mantalaris, *Improving embryonic stem cell expansion through the combination of perfusion and bioprocess model design.* PloS one, 2013. **8**(12): p. e81728.

94. Elder, B.D. and K.A. Athanasiou, *Hydrostatic pressure in articular cartilage tissue engineering: from chondrocytes to tissue regeneration.* Tissue Engineering Part B: Reviews, 2009. **15**(1): p. 43-53.

95. Schroeder, C., A. Hoelzer, G. Zhu, M. Woiczinski, O.B. Betz, H. Graf, S. Mayer-Wagner, and P.E. Mueller, *A closed loop perfusion bioreactor for dynamic hydrostatic pressure loading and cartilage tissue engineering.* Journal of Mechanics in Medicine and Biology, 2016. **16**(03): p. 1650025.

96. Manolagas, S.C. and R.L. Jilka, *Bone marrow, cytokines, and bone remodeling—emerging insights into the pathophysiology of osteoporosis.* New England journal of medicine, 1995. **332**(5): p. 305-311.

97. Mekala, N.K., R.R. Baadhe, and S.R. Parcha, *Review on bioreactors in tissue engineering.* 2011.

98. Guilak, F., D.M. Cohen, B.T. Estes, J.M. Gimble, W. Liedtke, and C.S. Chen, *Control of stem cell fate by physical interactions with the extracellular matrix.* Cell stem cell, 2009. **5**(1): p. 17-26.

99. Knippenberg, M., M.N. Helder, B. Zandieh Doulabi, C.M. Semeins, P.I. Wuisman, and J. Klein-Nulend, *Adipose tissue-derived mesenchymal stem cells acquire bone cell-like responsiveness to fluid shear stress on osteogenic stimulation.* Tissue engineering, 2005. **11**(11-12): p. 1780-1788.

100. Osiecki, M.J., S.D. McElwain, and W.B. Lott, *Modelling mesenchymal stromal cell growth in a packed bed bioreactor with a gas permeable wall.* PloS one, 2018. **13**(8): p. e0202079.

101. Li, D., T. Tang, J. Lu, and K. Dai, *Effects of flow shear stress and mass transport on the construction of a large-scale tissue-engineered bone in a perfusion bioreactor.* Tissue Engineering Part A, 2009. **15**(10): p. 2773-2783.

102. Lambrechts, T., I. Papantoniou, B. Rice, J. Schrooten, F.P. Luyten, and J.-M. Aerts, *Large-scale progenitor cell expansion for multiple donors in a monitored hollow fibre bioreactor.* Cytotherapy, 2016. **18**(9): p. 1219-1233.

103. Chapman, L.A., J.P. Whiteley, H.M. Byrne, S.L. Waters, and R.J. Shipley, *Mathematical modelling of cell layer growth in a hollow fibre bioreactor.* Journal of theoretical biology, 2017. **418**: p. 36-56.

104. Ahmed, H.M.M., S. Salerno, A. Piscioneri, S. Khakpour, L. Giorno, and L. De Bartolo, *Human liver microtissue spheroids in hollow fiber membrane bioreactor.* Colloids and Surfaces B: Biointerfaces, 2017. **160**: p. 272-280.

105. Knöspel, F., N. Freyer, M. Stecklum, J.C. Gerlach, and K. Zeilinger, *Periodic harvesting of embryonic stem cells from a hollow-fiber membrane based four-compartment bioreactor.* Biotechnology progress, 2016. **32**(1): p. 141-151.

106. Naghib, S.D., F.P. Di Maio, L. De Bartolo, E. Curcio, and A. Di Renzo, *Automation and control system for fluid dynamic stability in hollow-fiber membrane bioreactor for cell culture.* Journal of Chemical Technology & Biotechnology, 2018. **93**(3): p. 710-719.

107. Sheu, J., J. Beltzer, B. Fury, K. Wilczek, S. Tobin, D. Falconer, J. Nolta, and G. Bauer, *Large-scale production of lentiviral vector in a closed system hollow fiber bioreactor.* Molecular Therapy - Methods & Clinical Development, 2015. **2**: p. 15020.

108. Pihl, A.F., A.F. Offersgaard, C.K. Mathiesen, J. Prentoe, U. Fahnøe, H. Krarup, J. Bukh, and J.M. Gottwein, *High density Huh7. 5 cell hollow fiber bioreactor culture for high-*

yield production of hepatitis C virus and studies of antivirals. Scientific reports, 2018. **8**(1): p. 17505.

109. Yan, I.K., N. Shukla, D.A. Borrelli, and T. Patel, *Use of a hollow fiber bioreactor to collect extracellular vesicles from cells in culture*, in *Extracellular RNA*. 2018, Springer. p. 35-41.

110. Jones, M., B. Nankervis, N. Frank, B. Vang, T. DiLorenzo, D. Hill, and C. Coeshott, *CD146 expression, as a surrogate biomarker for human mesenchymal stromal cell multilineage differentiation, is preserved during cell expansion in an automated hollow-fiber membrane bioreactor.* Pharmaceutical Bioprocessing, 2018. **6**(3): p. 93-105.

111. Cipriano, M., N. Freyer, F. Knöspel, N.G. Oliveira, R. Barcia, P.E. Cruz, H. Cruz, M. Castro, J.M. Santos, and K. Zeilinger, *Self-assembled 3D spheroids and hollow-fibre bioreactors improve MSC-derived hepatocyte-like cell maturation in vitro.* Archives of toxicology, 2017. **91**(4): p. 1815-1832.

112. Godoy, P., N.J. Hewitt, U. Albrecht, M.E. Andersen, N. Ansari, S. Bhattacharya, J.G. Bode, J. Bolleyn, C. Borner, and J. Boettger, *Recent advances in 2D and 3D in vitro systems using primary hepatocytes, alternative hepatocyte sources and non-parenchymal liver cells and their use in investigating mechanisms of hepatotoxicity, cell signaling and ADME.* Archives of toxicology, 2013. **87**(8): p. 1315-1530.

113. Eghbali, H., M.M. Nava, D. Mohebbi-Kalhori, and M.T. Raimondi, *Hollow fiber bioreactor technology for tissue engineering applications.* The International journal of artificial organs, 2016. **39**(1): p. 1-15.

114. Jackson, L.R., L. Trudel, J. Fox, and N. Lipman, *Evaluation of hollow fiber bioreactors as an alternative to murine ascites production for small scale monoclonal antibody production.* Journal of immunological methods, 1996. **189**(2): p. 217-231.

115. Nold, P., C. Brendel, A. Neubauer, G. Bein, and H. Hackstein, *Good manufacturing practice-compliant animal-free expansion of human bone marrow derived mesenchymal stroma cells in a closed hollow-fiber-based bioreactor.* Biochemical and biophysical research communications, 2013. **430**(1): p. 325-330.

116. Godara, P., C.D. McFarland, and R.E. Nordon, *Design of bioreactors for mesenchymal stem cell tissue engineering.* Journal of Chemical Technology & Biotechnology: International Research in Process, Environmental & Clean Technology, 2008. **83**(4): p. 408-420.

117. Schop, D., F. Janssen, E. Borgart, J.D. de Bruijn, and R. van Dijkhuizen-Radersma, *Expansion of mesenchymal stem cells using a microcarrier-based cultivation system: growth and metabolism.* Journal of tissue engineering and regenerative medicine, 2008. **2**(2-3): p. 126-135.

118. Kirouac, D.C. and P.W. Zandstra, *The systematic production of cells for cell therapies.* Cell stem cell, 2008. **3**(4): p. 369-381.

119. Miyazawa, K., T. Hondo, T. Kanaya, S. Tanaka, I. Takakura, W. Itani, M.T. Rose, H. Kitazawa, T. Yamaguchi, and H. Aso, *Characterization of newly established bovine intestinal epithelial cell line.* Histochemistry and cell biology, 2010. **133**(1): p. 125-134.

120. Teixeira, F.G., K.M. Panchalingam, R. Assunção-Silva, S.C. Serra, B. Mendes-Pinheiro, P. Patrício, S. Jung, S.I. Anjo, B. Manadas, and L. Pinto, *Modulation of the mesenchymal*

stem cell secretome using computer-controlled bioreactors: impact on neuronal cell proliferation, survival and differentiation. Scientific reports, 2016. **6**: p. 27791.

121. Brindley, D., K. Moorthy, J.-H. Lee, C. Mason, H.-W. Kim, and I. Wall, *Bioprocess forces and their impact on cell behavior: implications for bone regeneration therapy.* Journal of tissue engineering, 2011. **2011**.

122. Mizukami, A. and K. Swiech, *Mesenchymal stromal cells: from discovery to manufacturing and commercialization.* Stem cells international, 2018. **2018**.

123. Petrenko, Y., E. Syková, and Š. Kubinová, *The therapeutic potential of three-dimensional multipotent mesenchymal stromal cell spheroids.* Stem cell research & therapy, 2017. **8**(1): p. 94.

124. Kitova, S., M. Minchev, and G. Danev, *RF plasma treatment of polycarbonate substrates.* Journal of Optoelectronics and Advanced Materials, 2005. **7**(5): p. 2607-2612.

125. Larsson, A. and H. Dérand, *Stability of polycarbonate and polystyrene surfaces after hydrophilization with high intensity oxygen RF plasma.* Journal of colloid and interface science, 2002. **246**(1): p. 214-221.

126. Jokinen, V., P. Suvanto, and S. Franssila, *Oxygen and nitrogen plasma hydrophilization and hydrophobic recovery of polymers.* Biomicrofluidics, 2012. **6**(1): p. 016501.

127. Lerman, M.J., J. Lembong, S. Muramoto, G. Gillen, and J.P. Fisher, *The evolution of polystyrene as a cell culture material.* Tissue Engineering Part B: Reviews, 2018. **24**(5): p. 359-372.

128. Dahir, G.A., Q. Cui, P. Anderson, C. Simon, C. Joyner, J.T. Triffitt, and G. Balian, *Pluripotential mesenchymal cells repopulate bone marrow and retain osteogenic properties.* Clinical Orthopaedics and Related Research®, 2000. **379**: p. S134-S145.

129. Diduch, D.R., M.R. Coe, C. Joyner, M.E. Owen, and G. Balian, *Two cell lines from bone marrow that differ in terms of collagen synthesis, osteogenic characteristics, and matrix mineralization.* JBJS, 1993. **75**(1): p. 92-105.

130. Banfi, A., A. Muraglia, B. Dozin, M. Mastrogiacomo, R. Cancedda, and R. Quarto, *Proliferation kinetics and differentiation potential of ex vivo expanded human bone marrow stromal cells: implications for their use in cell therapy.* Experimental hematology, 2000. **28**(6): p. 707-715.

131. Caroti, C.M., H. Ahn, H.F. Salazar, G. Joseph, S.B. Sankar, N.J. Willett, L.B. Wood, W.R. Taylor, and A.N. Lyle, *A novel technique for accelerated culture of murine mesenchymal stem cells that allows for sustained multipotency.* Scientific reports, 2017. **7**(1): p. 13334.

132. Schinköthe, T., W. Bloch, and A. Schmidt, *In vitro secreting profile of human mesenchymal stem cells.* Stem cells and development, 2008. **17**(1): p. 199-206.

133. Caplan, A.I. and D. Correa, *The MSC: an injury drugstore.* Cell stem cell, 2011. **9**(1): p. 11-15.

134. Osugi, M., W. Katagiri, R. Yoshimi, T. Inukai, H. Hibi, and M. Ueda, *Conditioned media from mesenchymal stem cells enhanced bone regeneration in rat calvarial bone defects.* Tissue engineering part A, 2012. **18**(13-14): p. 1479-1489.

135. Tsao, Y.-S., A. Cardoso, R. Condon, M. Voloch, P. Lio, J. Lagos, B. Kearns, and Z. Liu, *Monitoring Chinese hamster ovary cell culture by the analysis of glucose and lactate metabolism.* Journal of biotechnology, 2005. **118**(3): p. 316-327.

136. Michl, J., K.C. Park, and P. Swietach, *Evidence-based guidelines for controlling pH in mammalian live-cell culture systems.* Communications biology, 2019. **2**(1): p. 144.

137. Rhee, S.G., T.-S. Chang, W. Jeong, and D. Kang, *Methods for detection and measurement of hydrogen peroxide inside and outside of cells.* Molecules and cells, 2010. **29**(6): p. 539-549.

138. Gille, J. and H. Joenje, *Cell culture models for oxidative stress: superoxide and hydrogen peroxide versus normobaric hyperoxia.* Mutation Research/DNAging, 1992. **275**(3-6): p. 405-414.

139. Zmijewski, J.W., S. Banerjee, H. Bae, A. Friggeri, E.R. Lazarowski, and E. Abraham, *Exposure to hydrogen peroxide induces oxidation and activation of AMP-activated protein kinase.* Journal of Biological Chemistry, 2010. **285**(43): p. 33154-33164.

140. Gunawardena, D., R. Raju, and G. Münch, *Hydrogen peroxide mediates pro-inflammatory cell-to-cell signaling: a new therapeutic target for inflammation?* Neural regeneration research, 2019. **14**(8): p. 1430.

141. Nindl, G., N.R. Peterson, E.F. Hughes, L.R. Waite, and M.T. Johnson, *Effect of hydrogen peroxide on proliferation, apoptosis and interleukin-2 production of Jurkat T cells.* Biomedical sciences instrumentation, 2004. **40**: p. 123-128.

142. Murphy, M.B., K. Moncivais, and A.I. Caplan, *Mesenchymal stem cells: environmentally responsive therapeutics for regenerative medicine.* Experimental & molecular medicine, 2013. **45**(11): p. e54.

143. Pavel, M., M. Renna, S.J. Park, F.M. Menzies, T. Ricketts, J. Füllgrabe, A. Ashkenazi, R.A. Frake, A.C. Lombarte, and C.F. Bento, *Contact inhibition controls cell survival and proliferation via YAP/TAZ-autophagy axis.* Nature communications, 2018. **9**(1): p. 2961.

144. Atkins, G.J., D.M. Findlay, P.H. Anderson, and H.A. Morris, *Target genes: bone proteins*, in *Vitamin D*. 2011, Elsevier. p. 411-424.

145. Christenson, R.H., *Biochemical markers of bone metabolism: an overview.* Clinical biochemistry, 1997. **30**(8): p. 573-593.

146. Michaelis, L. and M.L. Menten, *Die kinetik der invertinwirkung*. 2007: Universitätsbibliothek Johann Christian Senckenberg.

147. Deasy, B., R. Jankowski, T. Payne, B. Cao, J. Goff, J. Greenberger, and J. Huard, *Modeling stem cell population growth: incorporating terms for proliferative heterogeneity.* Stem Cells, 2003. **21**(5): p. 536-545.

148. Sherley, J., P. Stadler, and J.S. Stadler, *A quantitative method for the analysis of mammalian cell proliferation in culture in terms of dividing and non-dividing cells.* Cell proliferation, 1995. **28**(3): p. 137-144.

149. Zhao, F., P. Pathi, W. Grayson, Q. Xing, B.R. Locke, and T. Ma, *Effects of oxygen transport on 3-d human mesenchymal stem cell metabolic activity in perfusion and static cultures: Experiments and mathematical model.* Biotechnology progress, 2005. **21**(4): p. 1269-1280.

150. Pattappa, G., H.K. Heywood, J.D. De Bruijn, and D.A. Lee, *The metabolism of human mesenchymal stem cells during proliferation and differentiation.* Journal of cellular physiology, 2011. **226**(10): p. 2562-2570.

151. Schop, D., F.W. Janssen, L.D. van Rijn, H. Fernandes, R.M. Bloem, J.D. de Bruijn, and R. van Dijkhuizen-Radersma, *Growth, metabolism, and growth inhibitors of mesenchymal stem cells.* Tissue Engineering Part A, 2009. **15**(8): p. 1877-1886.

152. Donato, D., I. Napoli, and G. Catapano, *Model-based optimization of scaffold geometry and operating conditions of radial flow packed-bed bioreactors for therapeutic applications.* Processes, 2014. **2**(1): p. 34-57.

153. Mohebbi-Kalhori, D., A. Behzadmehr, C.J. Doillon, and A. Hadjizadeh, *Computational modeling of adherent cell growth in a hollow-fiber membrane bioreactor for large-scale 3-D bone tissue engineering.* Journal of Artificial Organs, 2012. **15**(3): p. 250-265.

154. Campolo, M., F. Curcio, and A. Soldati, *Minimal perfusion flow for osteogenic growth of mesenchymal stem cells on lattice scaffolds.* AIChE Journal, 2013. **59**(8): p. 3131-3144.

APPENDICES

APPENDIX A: PREVIOUS BIOREACTOR DESIGNS

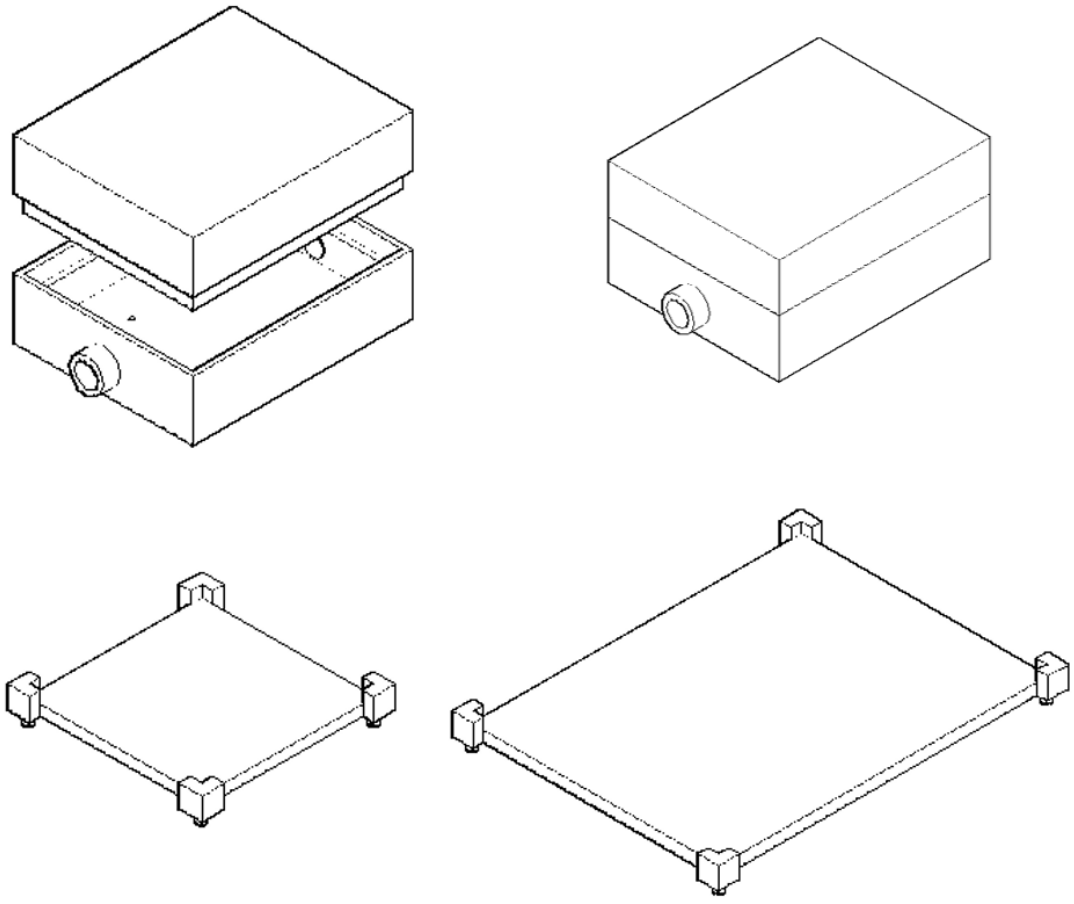

APPENDIX A1: AutoCAD schematics of initial bioreactor vessel design.

APPENDIX B: MATLAB CODE FOR GLUCOSE CONSERVATION CALCULATIONS

```
% This code is executed using an ode15s solver which is used for systems
% of equations. There are two codes needed:
% (1) the code with the system of equations and variables
% (2) the "call" code which summons up the system of equations and states
%     the initial conditions
function dcdt = glucoseconservation2D(~, c) % the input for ~ is t and y but it was recommended
to change it
dcdt = zeros (5,1); % this generates a 5 X 1 matrix
%%%%% Parameters of Interest:
% dcdt(1) = C_g; the concentration of glucose in media
% dcdt(2) = C_l; the concentration of lactate in the media
% dcdt(3) = N;   the concentration of hMSCs (cell number)
% dcdt(4) = C_o; the concentration of oxygen in media
% dcdt(5) = K; the growth rate of the cells
%%%%% Known Variables:
U = 60;            % inlet flow, ml/h
Vmax_g = 2.72e-13;  % maximum uptake of glucose by hMSCs, 272 fmol/h/cell converted to
mol/h/cell
Vmax_o = 1e-13;     % maximum uptake of oxygen by hMSCs, 100 fmol/h/cell converted to
mol/h/cell
Y_lg = 2.0;         % ratio of lactate produced from glucose consumption
Km_g = 3.5e-7;      % michaelis-menten constant for glucose consumption, mol/cm^3
```

```
Km_o = 4.05e09;     % michaelis-menten constant for oxygen consumption, mol/cm^3

N_o = 400000;       % initial number of cells

DT = 48.76672;      % doubling time of bioreactor cells, experimental data + calculated

alpha = 1.00766;

Vol = 110;          % volume of media present in the bioreactor, in ml

Kmax = 0.02631;     % maximum growth rate for hmscs, hr^-1

K_g = 6e-6;         % michaelis-menten glucose growth constant, 0.006 mM to M

K_l = 0.043;        % michaelis-menten lactate growth constant, 43 mM converted to M

K_o = 1e-6;         %michaelis-menten oxygen growth constant, 0.001 mM converted to M

%%%%% Conservation Equations:

dcdt(1) = U * c(1) - U*(c(1) /(1 + ((c(5) * c(1)* Vol)/U*c(1)))) - ((Vmax_g * c(1) * c(3))/(Km_g
+ c(1)));          % glucose conservation

dcdt(2) = U * c(2) - U*(c(2) /(1 + ((c(5) * c(2)* Vol)/U*c(2)))) + (Y_lg * ((Vmax_g * c(1) *
c(3))/(Km_g + c(1))));  %  lactate conservation

dcdt(3) = N_o *((0.5)+((1-((2*alpha).^((96/(DT))+1)))/(2*(1-(2*alpha)))));      % cell number

dcdt(4) = -((Vmax_o * c(3) * c(4))/(Km_o + c(4)));     % oxygen conservation

dcdt(5) =  Kmax * (((c(4))/(K_o + c(4))) * ((K_l)/(c(2) + K_l)) * ((c(1))/(c(1) + K_g))); %
growth constant

end
```

APPENDIX C: MATLAB CALL CODE FOR GLUCOSE CONSERVATION CALCULATIONS

```
% This is a call code. It will summon up a code that contains a system of
```

```
% ODEs (ordinary differential equations)and will apply a solver method and
% initial conditions. They cannot be combined into one equation if you want
% to apply the solver system in matlab.
function [T,C] = call_glucoseconservation2D()
tspan = [1 120];    % this is the range for t, time, in the system, hours
c1_0 = 0.005115589; % initial concentration of glucose in media, measured in M
c2_0 = 0.0016924366;  % initial concentration of lactate in media, measured in M
c3_0 = 400000;      % this is the initial cell density, cells/ml
c4_0 = 2e-4;        % solubility of oxygen in media, 0.2 mM converted to M
c5_0 = 0.0251915537; % initial starting k from calculation k =
Kmax*(((Cg)/(Kg+Cg))*(((Kl)/(Kl+Cl))*(((Co)/(Ko+Co)))
[T,C] = ode15s(@glucoseconservation2D, tspan, [c1_0 c2_0 c3_0 c4_0 c5_0]); % this is how to
set up the ode15s solver system
plot(T,C(:,1),'-r')                    % code to generate a graph
title('MSC Glucose Conservation Model');  % title of plot
xlabel ('Time (hours)');                % label of x axis
ylabel ('Glucose Concentration (M)');     % label of y axis
end
```

APPENDIX D: MATLAB CODE FOR LACTATE PRODUCTION CALCULATIONS

```
% This code is executed using an ode15s solver which is used for systems
% of equations. There are two codes needed:
% (1) the code with the system of equations and variables
```

```
% (2) the "call" code which summons up the system of equations and states
%     the initial conditions


function dcdt = lactateconservation2D(~, c) % the input for ~ is t and y but it was recommended
to change it
dcdt = zeros (5,1); % this generates a 5 X 1 matrix
%%%%% Parameters of Interest:
% dcdt(1) = C_l; the concentration of lactate in the media
% dcdt(2) = N;   the concentration of hMSCs (cell number)
% dcdt(3) = C_g; the concentration of glucose in media
% dcdt(4) = C_o; the concentration of oxygen in media
% dcdt(5) = K; the growth rate of the cells
%%%%% Known Variables:
U = 60;            % inlet flow, ml/h
Vmax_g = 2.72e-13;  % maximum uptake of glucose by hMSCs, 272 fmol/h/cell converted to
mol/h/cell
Vmax_o = 1e-13;     % maximum uptake of oxygen by hMSCs, 100 fmol/h/cell converted to
mol/h/cell
Y_lg = 2.0;            % ratio of lactate produced from glucose consumption
Km_g = 3.5e-7;      % michaelis-menten constant for glucose consumption, mol/cm^3
Km_o = 4.05e09;   % michaelis-menten constant for oxygen consumption, mol/cm^3
N_o = 400000;       % initial number of cells
DT = 48.76672;      % doubling time of bioreactor cells, experimental data + calculated
```

```
alpha = 1.00766;    % dividing fraction of hMSCs cells
Vol = 110;          % volume of media present in the bioreactor, in ml
Kmax = 0.02631;     % maximum growth rate for hmscs, hr^-1
K_g = 6e-6;         % michaelis-menten glucose growth constant, 0.006 mM to M
K_l = 0.043;        % michaelis-menten lactate growth constant, 43 mM converted to M
K_o = 1e-6;         %michaelis-menten oxygen growth constant, 0.001 mM converted to M
%%%%% Conservation Equations:
dcdt(1) = U * c(1) - U*(c(1) /(1 + ((c(5) * c(1)* Vol)/U*c(1)))) + (Y_lg * ((Vmax_g * c(2) *
c(3))/(Km_g + c(3))));   % lactate conservation
dcdt(2) = N_o *((0.5)+((1-((2*alpha).^((96/(DT))+1)))/(2*(1-(2*alpha)))));      % cell number

dcdt(3) = U * c(3) - U*(c(3) /(1 + ((c(5) * c(3)* Vol)/U*c(3)))) - ((Vmax_g * c(2) * c(3))/(Km_g
+ c(3)));          % glucose conservation
dcdt(4) =  -((Vmax_o * c(2) * c(4))/(Km_o + c(4)));      % oxygen conservation
dcdt(5) =  Kmax * (((c(4))/(K_o + c(4))) * ((K_l)/(c(1) + K_l)) * ((c(3))/(c(3) + K_g))); %
growth constant
end
```

APPENDIX E: MATLAB CALL CODE FOR LACTATE PRODUCTION CALCULATIONS

```
% This is a call code. It will summon up a code that contains a system of
% ODEs (ordinary differential equations)and will apply a solver method and
% initial conditions. They cannot be combined into one equation if you want
% to apply the solver system in matlab.
```

```
function [T,C] = call_lactateconservation2D()
tspan = [1 120];     % this is the range for t, time, in the system, hours
c1_0 = 0.0016924366;   % initial concentration of lactate in media, measured in M
c2_0 = 400000;       % initial cell density, cells/ml
c3_0 = 0.0051155892;  % initial concentration of glucose, measured in M
c4_0 = 2e-4;         % solubility of oxygen in media, 0.2 mM converted to M
c5_0 = 0.0251915537; % initial starting k from calculation k =
Kmax*(((Cg)/(Kg+Cg))*(((Kl)/(Kl+Cl))*(((Co)/(Ko+Co)))
[T,C] = ode15s(@lactateconservation2D, tspan, [c1_0 c2_0 c3_0 c4_0 c5_0]); % this is how to
set up the ode15s solver system
plot(T,C(:,1),'-m')                    % code to generate a graph
title('MSC Lactate Conservation Model');    % title of plot
xlabel ('Time (hours)');                % label of x axis
ylabel ('Lactate Concentration (M)');      % label of y axis
end
```

APPENDIX F: MATLAB CODE FOR OXYGEN CONSERVATION CALCULATIONS

```
% This code is executed using an ode15s solver which is used for systems
% of equations. There are two codes needed:
% (1) the code with the system of equations and variables
% (2) the "call" code which summons up the system of equations and states
%     the initial conditions
```

```
function dcdt = oxygenconservation2D(~, c) % the input for ~ is t and y but it was recommended
to change it
dcdt = zeros (5,1); % this generates a 5 X 1 matrix
%%%%% Parameters of Interest:
% dcdt(1) = C_o; the concentration of oxygen in media
% dcdt(2) = C_l; the concentration of lactate in the media
% dcdt(3) = C_g; the concentration of glucose in media
% dcdt(4) = N;   the number of hMSCs (cell number)
% dcdt(5) = K;   the growth rate of the cells
%%%%% Known Variables:
U = 60;            % inlet flow, ml/h
Vmax_g = 2.72e-13;  % maximum uptake of glucose by hMSCs, 272 fmol/h/cell converted to
mol/h/cell
Vmax_o = 1e-13;     % maximum uptake of oxygen by hMSCs, 100 fmol/h/cell converted to
mol/h/cell
Y_lg = 2.0;         % ratio of lactate produced from glucose consumption
Km_g = 3.5e-7;      % michaelis-menten constant for glucose consumption, mol/cm^3
Km_o = 4.05e09;     % michaelis-menten constant for oxygen consumption, mol/cm^3
N_o = 400000;       % initial number of cells, cell
DT = 48.76672;      % doubling time of bioreactor cells, experimental data + calculated
alpha = 1.00766;
Vol = 110;          % volume of media present in the bioreactor, in ml
Kmax = 0.02631;     % maximum growth rate for hmscs, hr^-1
```

```
K_g = 6e-6;        % michaelis-menten glucose growth constant, 0.006 mM to M
K_l = 0.043;       % michaelis-menten lactate growth constant, 43 mM converted to M
K_o = 1e-6;        %michaelis-menten oxygen growth constant, 0.001 mM converted to M
%%%%% Conservation Equations:
dcdt(1) =  - ((Vmax_o * c(1) * c(4))/(Km_o + c(1)));     % oxygen conservation
dcdt(2) = U * c(2) - U*(c(2) /(1 + ((c(5) * c(2)* Vol)/U*c(2)))) + (Y_lg * ((Vmax_g * c(4) *
c(3))/(Km_g + c(3))));  % lactate conservation
dcdt(3) = U * c(3) - U*(c(3) /(1 + ((c(5) * c(3)* Vol)/U*c(3)))) - ((Vmax_g * c(4) * c(3))/(Km_g
+ c(3)));          % glucose conservation
dcdt(4) = N_o *((0.5)+((1-((2*alpha).^((96/(DT))+1)))/(2*(1-(2*alpha)))));      % cell number
dcdt(5) =  Kmax * (((c(1))/(K_o + c(1))) * ((K_l)/(c(2) + K_l)) * ((c(3))/(c(3) + K_g))); %
growth constant
end
```

APPENDIX G: MATLAB CALL CODE FOR OXYGEN CONSERVATION CALCULATIONS

```
% This is a call code. It will summon up a code that contains a system of
% ODEs (ordinary differential equations)and will apply a solver method and
% initial conditions. They cannot be combined into one equation if you want
% to apply the solver system in matlab.
function [T,C] = call_oxygenconservation2D()
tspan = [1 120];     % this is the range for t, time, in the system, hours
c1_0 = 2e-4;         % solubility of oxygen in media, 0.2 mM converted to M
```

```
c2_0 = 0.0016924366;   % initial concentration of lactate in media, measured in M
c3_0 = 0.0051155892;  % initial concentration of glucose, measured in M
c4_0 = 400000;       % this is the initial cell number, cells
c5_0 = 0.0251915537; % initial starting k from calculation k =
Kmax*(((Cg)/(Kg+Cg))*(((Kl)/(Kl+Cl))*(((Co)/(Ko+Co)))
[T,C] = ode15s(@oxygenconservation2D, tspan, [c1_0 c2_0 c3_0 c4_0 c5_0]); % this is how to
set up the ode15s solver system
plot(T,C(:,1),'-g')                    % code to generate a graph
title('MSC Oxygen Concentration Model');    % title of plot
xlabel ('Time (hours)');                % label of x axis
ylabel ('Oxygen Concentration (M)');       % label of y axis
end
```

APPENDIX H: MATLAB CODE FOR CELL NUMBER CONSERVATION

```
% This code is executed using an ode15s solver which is used for systems
% of equations. There are two codes needed:
% (1) the code with the system of equations and variables
% (2) the "call" code which summons up the system of equations and states
%     the initial conditions
function dcdt = cellnumber2D(~, c) % the input for ~ is t and y but it was recommended to
change it
dcdt = zeros (5,1); % this generates a 5 X 1 matrix
%%%%% Parameters of Interest:
```

```
% dcdt(1) = N;   the concentration of hMSCs (cell number)
% dcdt(2) = C_l; the concentration of lactate in the media
% dcdt(3) = C_g; the concentration of glucose in media
% dcdt(4) = C_o; the concentration of oxygen in media
% dcdt(5) = K; the growth rate of the cells
%%%%% Known Variables:
 U = 60;            % inlet flow, ml/h
Vmax_g = 2.72e-13;  % maximum uptake of glucose by hmscs, 272 fmol/h/cell converted to
mol/h/cell
Vmax_o = 1e-13;     % maximum uptake of oxygen by hmscs, 100 fmol/h/cell converted to
mol/h/cell
Y_lg = 2.0;         % ratio of lactate produced from glucose consumption
Km_g = 3.5e-7;      % michaelis-menten constant for glucose consumption, mol/cm^3
Km_o = 4.05e09;     % michaelis-menten constant for oxygen consumption, mol/cm^3
N_o = 400000;       % initial number of cells
DT = 48.76672;      % doubling time of bioreactor cells, experimental data + calculated
alpha = 1.00766;
Vol = 110;          % volume of media present in the bioreactor, in ml
Kmax = 0.02631;     % maximum growth rate for hmscs, hr^-1
K_g = 6e-6;         % michaelis-menten glucose growth constant, 0.006 mM to M
K_l = 0.043;        % michaelis-menten lactate growth constant, 43 mM converted to M
K_o = 1e-6;         %michaelis-menten oxygen growth constant, 0.001 mM converted to M
%%%%% Conservation Equations:
```

```
dcdt(1) = (N_o *((0.5)+((1-((2*alpha)^((96/(DT))+1)))/(2*(1-(2*alpha))))));      % cell number
dcdt(2) = U * c(2) - U * (c(2) /(1 + ((c(5) * c(2) * Vol)/U * c(2)))) + (Y_lg * ((Vmax_g * c(1) *
c(3))/(Km_g + c(3))));  % lactate conservation
dcdt(3) = U * c(3) - U * (c(3) /(1 + ((c(5) * c(3) * Vol)/U * c(3)))) - ((Vmax_g * c(1) *
c(3))/(Km_g + c(3)));          % glucose conservation
dcdt(4) = - ((Vmax_o * c(1) * c(4))/(Km_o + c(4)));     % oxygen conservation
dcdt(5) =  Kmax * (((c(4))/(K_o + c(4))) * ((K_l)/(c(2) + K_l)) * ((c(3))/(c(3) + K_g))); %
growth constant
end
```

APPENDIX I: MATLAB CALL CODE FOR CELL NUMBER CONSERVATION

```
% This is a call code. It will summon up a code that contains a system of
% ODEs (ordinary differential equations)and will apply a solver method and
% initial conditions. They cannot be combined into one equation if you want
% to apply the solver system in matlab.
function [T,C] = call_cellnumber2D()
tspan = [1 120];    % this is the range for t, time, in the system, hours
c1_0 = 400000;     % this is the initial cell density, cells/ml
c2_0 = 0.0016924366;  % initial concentration of lactate in media, measured in M
c3_0 = 0.0051155892; % initial concentration of glucose in media, measured in M
c4_0 = 2e-4;        % solubility of oxygen in media, 0.2 mM converted to M
c5_0 = 0.0251915537; % initial starting k from calculation k =
Kmax*(((Cg)/(Kg+Cg))*(((Kl)/(Kl+Cl))*(((Co)/(Ko+Co)))
```

```
[T,C] = ode15s(@cellnumber2D, tspan, [ c1_0 c2_0 c3_0 c4_0 c5_0]); % this is how to set up
the ode15s solver system
plot(T,C(:,1),'-')                % code to generate a graph
title('MSC monolayer growth model'); % title of plot
xlabel ('Time (hours)');          % label of x axis
ylabel ('Number of Cells (cells)');  % label of y axis
end
```

APPENDIX J: MATLAB CODE FOR REVISED CELL NUMBER CONSERVATION

```
syms n(t)
%%%%%% Important Variables:
n_o = 4000000;
DT =48.7667219;
alpha = 1.00766;
%%%%%% The ODE Solver:
ode = diff(n,t) == n_o * ((0.5)+((1-(2*alpha).^((t/DT)+1))/(2*(1-(2*alpha)))));
cond = n(0) == 4000000;
nSol(t) = dsolve(ode,cond);
fplot(nSol,'-')                   % generates a graph of the data
title('MSC Monolayer Growth');    % title of plot
xlabel ('Time (hours)');          % label for x axis
ylabel ('Number of Cells (cells)'); % label for y axis
axis ([0 120 0 150000000]);       % sets limitations for each axis
```